Single-cell analysis reveals divergent responses of human dendritic cells to the MVA vaccine

Marius Döring, Kevin de Azevedo, Guillermo Blanco-Rodriguez, Francesca Nadalin, Takeshi Satoh, Matteo Gentili, Xavier Lahaye, Nilushi S de Silva, Cécile Conrad, Mabel Jouve, et al.

Single-cell analysis reveals divergent responses of human dendritic cells to the MVA vaccine

Marius Döring[1,2], Kevin De Azevedo[1], Guillermo Blanco-Rodriguez[1], Francesca Nadalin[1], Takeshi Satoh[1,2], Matteo Gentili[1], Xavier Lahaye[1], Nilushi S De Silva[1], Cécile Conrad[1], Mabel Jouve[1], Mireille Centlivre[2,3], Yves Lévy[2,3,4], and Nicolas Manel[l,2]*

Affiliations:

[1] Immunity and Cancer Department, Institut Curie, PSL Research University, INSERM U932, 75005 Paris, France

[2] Vaccine Research Institute (VRI), Créteil, Paris, France

[3] INSERM U955, Université Paris Est Créteil, Créteil, France

[4] AP-HP, Hôpital Henri-Mondor Albert-Chenevier, Service d'Immunologie Clinique et Maladies Infectieuses, Créteil, France.

*Corresponding author. Email : nicolas.manel@curie.fr.

Abstract

Modified vaccinia Ankara (MVA) is a live, attenuated human smallpox vaccine and a vector for the development of new vaccines against infectious diseases and cancer. Efficient activation of the immune system by MVA relies in part on its encounter with dendritic cells (DCs). MVA infection of DCs leads to multiple outcomes, including cytokine production, activation of co-stimulatory molecules for T cell stimulation, and cell death. Here, we examined how these diverse responses are orchestrated in human DCs at the single-cell level. Single-cell analyses revealed that MVA infection in DCs was limited to early gene expression. In response to the early events in the viral cycle, we found that DCs group into three distinct clusters. A cluster of infected cells senses the incoming MVA genome by the intracellular innate immunity pathway mediated by cGAS, STING, TBK1, and IRF3 and subsequently produces inflammatory cytokines. In response to these

cytokines, a cluster of non-infected bystander cells increases co-stimulatory molecule expression. A separate cluster of infected cells undergoes non-redundant apoptosis. Unexpectedly, induction of apoptosis remained intact after inhibition of innate immunity pathway mediators (specifically cGAS, STING, MAVS, TBK1, IRF3 or IRF7). Instead, cell death was a response to early MVA gene expression. Thus, apoptosis induction by human DCs upon MVA infection is distinct from previously described IRF-dependent or replication-dependent pathways. Altogether, our study identified distinct mechanisms that underlie the complex interactions of MVA with human DCs.

Introduction

Understanding the mechanisms by which vaccines elicit protective immunity is essential for improving their development and effectively preventing disease. Modified vaccinia Ankara (MVA) is a safe, immunogenic, and efficacious third-generation live smallpox vaccine (1). It is considered a promising vector for heterologous antigens to protect against relatively long-established diseases (such as AIDS, tuberculosis, and malaria) and emerging diseases [such as Covid-19 (2, 3)] and for use in cancer immunotherapy (4).

Organismal-level studies of vaccination in mice revealed that MVA induces a localized immune response, with presence of the virus at the infected site and in draining lymph nodes, leading to activation and systemic dissemination of MVA-specific T cells (5). After inoculation, MVA interacts with dendritic cells (DCs), leading to MVA-derived antigen presentation in lymph nodes (6, 7). DCs are important sentinels of the immune system that detect microbes and pathogens through pattern recognition receptors (PRR). In turn, they translate innate immune activation into adaptive immune responses.

Upon MVA detection, DCs acquire an activated phenotype. This is characterized by an induction of co-stimulatory molecules for T cell stimulation, and the production of inflammatory cytokines including antiviral interferons and tumor necrosis factor α (TNF-α) (8, 9). The PRR implicated in MVA detection have been analyzed in several cell types. In leukemia-derived THP-1 cells, interferon induction by MVA was shown to require the lipoprotein sensor and toll-like receptor heterodimer TLR2-TLR6 as well as the cytosolic RNA sensing pathway (MDA5-MAVS-IRF3) for production of interferon (IFN)-β (10). In in vitro-differentiated mouse DCs, the cytosolic DNA sensing axis mediated by cyclic GMP-AMP synthase (cGAS), stimulator of IFN signaling (STING), and IFN regulatory factor 3 (IRF3) was found to be essential for IFN-α and IFN-β production (11). A parallel and important outcome of MVA infection in DCs is their rapid death (8, 12-14). In in vitro-differentiated mouse macrophages, cell death induction by MVA was shown to require signaling through the retinoic acid-inducible gene I (RIG-I), melanoma differentiation-associated protein 5 (MDA5), mitochondrial antiviral signaling protein (MAVS), IRF3, and phorbol-12-myristate-13-acetate–induced protein 1 (NOXA) axis (15). Collectively, these studies placed nucleic acid sensing of MVA upstream of signaling events that all converge on the activation of IRF3, resulting in concomitant induction of antiviral interferons and NOXA-mediated cell death. However, while DCs are generally conserved between mice and humans, innate sensors

have extensively evolved between the two species, with crucial signaling differences (16, 17). Thus, the molecular mechanisms that orchestrate the human DCs responses to MVA are not known. It is notable that the rapid DC responses to MVA comprise diverse and potentially incompatible outcomes within a given single cell, such as cytokine biosynthesis and cell death. We previously demonstrated that for viruses, this contradiction could be resolved by a "division of labor" within the population of DCs (18). Single-cell RNA-sequencing (scRNA-seq) has emerged as an attractive approach to unambiguously identify infected cells and to decompose virus-host interactions that otherwise appear merged at the population level (19). Here, using single-cell approaches, we dissected the interactions between MVA and human DCs that control infection, innate immune activation, and cell death.

Results

MVA infection of DCs leads to inflammatory cytokine production but only bystander cells induce activation markers

In humans, blood monocyte-derived DCs (MDDCs) constitute an abundant and experimentally tractable model to study interaction with MVA (**fig. S1A**). We first characterized infection and activation of MDDCs by MVA coding green fluorescent protein (MVAGFP) **(Fig. 1A)**. Upon infection, only GFP-negative MDDCs expressed CD86, a costimulatory molecule induced by innate sensors and inflammatory cytokines, and Siglec-1 (sialic acid-binding Ig-like lectin 1), an interferon-stimulated gene (ISG) product. GFP-positive MDDCs expressed significantly lower levels of CD86 and Siglec-1 compared to GFP-negative cells **(Fig. 1B)**. The fraction of GFP-positive cells increased with the multiplicity of infection (MOI), as expected **(Fig. 1C)**. Similar populations were observed after infection of primary type-2 conventional DCs (cDC2) isolated from donor blood (**fig. S1B**). These results are in agreement with previous work (13, 20) and indicate that GFP-positive cells are productively infected cells, while GFP-negative cells are bystander cells that are uninfected or carry abortive infection. They also suggest that bystanders induce CD86 and Siglec-1 in response to inflammatory mediators produced by infected cells.

Next, we examined the induction of cytokines, which is a hallmark of DC activation upon viral infection and might alter the state of bystanders. It has been reported that MDDCs express IFN-β, TNF-α and interleukin 6 (IL-6) upon MVA infection (8). We confirmed and extended these results by additionally showing that IFN-λ1 expression was induced 100-fold, compared to 5-fold for IFN-

β. IFN-α2 expression was variable between donors and the absolute concentration was low **(Fig. 1D)**.

scRNA-seq analysis of MVA-infected MDDCs reveals a limited source of inflammatory cytokines that mediate activation of bystander cells

To understand the source of cytokines relative to productive infection by MVA, we performed scRNA-seq. Here we used MVA coding for mCherry instead of GFP. The analysis was done with two independent donors that were uniformly distributed on uniform manifold approximation and projection (UMAP) plots after dataset integration **(fig. S1C)**. Infected cells were located on UMAP plots using mCherry expression and the ratio of viral unique molecular identifiers (UMIs) over total UMI (vUMI/tUMI) **(Fig. 1E)**. mCherry expression correlated with the ratio of vUMI/tUMI, indicating that both values were indicative of productive MVA gene expression in MDDCs **(Fig. 1F and fig. S1D)**. We plotted the expression of *IFNB*, *IFNL1*, *TNFA* and *IL6* as well as bystander activation markers *CD86*, *SIGLEC1* and the inflammatory cytokine *CXCL10* (**Fig. 1G and fig. S1E**). It was apparent that *CD86*, *SIGLEC1* and *CXCL10*, a gene that can be induced by inflammatory cytokines, were preferentially expressed in bystanders, while *IFNB*, and *IFNL1* were mainly expressed in a subset of infected cells. This was confirmed by a correlation analysis (**fig. S1F**, Pearson correlation coefficients: -0.22 for *CD86*, -0.25 for *SIGLEC1*, -0.3 for *CXCL10*, 0.31 for *IFNB*, 0.22 for *IFNL1*, 0.05 for *TNFA*). Taken together, we conclude that MVA infection induces expression of inflammatory cytokines in a fraction of infected MDDCs. In contrast, uninfected bystanders demonstrate an activated state suggestive of paracrine mediators.

Next, we investigated the nature of the signals that mediate bystander activation. Filtered supernatant from MVA-infected MDDCs induced CD86 and Siglec-1 expression in uninfected MDDCs, indicating the presence of soluble mediators (**fig S1G**). We infected MDDCs in the presence of antibody cocktails neutralizing type I IFN, TNF-α or inhibited Janus kinase–signal transducer and activator of transcription (JAK-STAT) signaling with ruxolitinib (RUXO). Inhibiting type I IFN and JAK-STAT signaling decreased CD86 and Siglec-1 expression on bystanders, while neutralization of TNF-α only inhibited the CD86 expression of bystanders **(Fig. 1H)**. Of note, ruxolitinib exhibited a positive effect on MVAGFP expression in MDDCs in addition to abrogating bystander activation. Combined neutralization of both type I IFN and TNF-α further reduced CD86 expression **(fig. S1, H and I)**. Reciprocally, we tested the ability of recombinant of

IFN-α2 and TNF-α to induce CD86 and Siglec-1 expression. A low dose of 1 U/ml of IFN-α2 was sufficient to fully induce Siglec-1, indicating that this is a highly responsive ISG (**fig S2, A and B**). In contrast, full CD86 induction required the combination of IFN-α2 and TNF-α, and either cytokine alone could not fully induce CD86 expression at the highest doses tested. These results are in line with the hypothesis that both type I IFN and TNF-α are produced by MVA infected MDDCs and act synergistically to mediate activation (CD86 induction) of bystanders.

Inflammatory cytokines are induced by the cGAS-STING-IRF3 axis in MVA-infected MDDCs

These results suggest that innate sensors detect MVA in infected cells, leading to production of soluble cytokines that activate bystanders. The nature of MVA implies the involvement of a cytosolic DNA sensor in its detection, however additional sensors such as RNA sensors or TLR have been proposed (9-11, 21). We investigated the involvement of the cGAS/STING/IRF3 axis using RNA interference (RNAi) of cGAS, inhibition of STING, and expression of a dominant-negative mutant of IRF3 (IRF3DN) (23) in MDDCs. Upon cGAS knockdown (KD) (**fig. S3A**), MVA-infected MDDCs expressed significantly lower levels of CD86 and Siglec-1 compared with control MDDCs, similar to the results seen upon transfection with the cGAS-agonist HTDNA **(Fig. 2A)**. IFN-β and IFN-λ1 secretion by cGAS KD MDDCs was abrogated in response to MVA infection **(Fig. 2A)**. In contrast, cGAS KD did not affect the MDDC response to stimulation with cyclic GMP–AMP (cGAMP) **(fig. S3, B and C)**, confirming the functionality of the STING-IRF3 pathway downstream of cGAS in cGAS KD MDDCs. STING inhibition with H-151 (STINGi; (22)) decreased CD86, IFN-β, and IFN-λ1 secretion upon MVA infection or stimulation with cGAMP **(Fig. 2B and fig. S3E)**. Siglec-1 induction was not affected by STING inhibition, which is likely due to the high responsiveness of this ISG to low amounts of IFN. Expression of IRF3DN essentially abrogated induction of CD86, Siglec-1, IFN-β, and IFN-λ1 upon MVA infection and HTDNA stimulation **(Fig. 2C)**. Of note, MVAGFP expression was not affected in cGAS KD, STINGi-treated, or IRF3DN-expressing MDDCs **(fig. S3D)**. Similarly, CD86 induction by the TLR7/8 agonist R848 was unaffected in cGAS KD, STINGi-treated, and IRF3DN-expressing MDDCs, indicating that other PRR pathways were not interrupted in these cells (**fig. S3F**). We conclude that MDDCs sense MVA through the cGAS-STING-IRF3 axis to produce inflammatory mediators that activate bystanders.

Because TANK-binding kinase 1 (TBK1) mediates IRF3 activation downstream of STING (24), we also expressed a dominant-negative mutant of TBK1 (TBK1DN) (25) in MDDCs. In addition, to determine the potential contribution of the TLR system to MDDC activation upon MVA infection, we expressed dominant-negative mutants of TNF receptor-associated factor 6 [TRAF6 (TRAF6DN), downstream of the TLR adaptor molecule MYD88 (26)] and of TIR-domain-containing adapter-inducing interferon-β [TRIF (TRIFDN), downstream of TLR3/4 (27)]. In line with our previous results, only TBK1DN expressing MDDCs exhibited decreased CD86 expression and abrogated IFN-β, and IFN-λ1 secretion upon MVA infection or cGAMP stimulation **(fig. S4)**. Siglec-1 expression was not affected by TBK1DN expression, which again could be the result of high responsiveness of this ISG to low amounts of IFN. As control, TRAF6DN, and TRIFDN inhibited CD86 induction in response to R848 and poly(I:C), respectively **(fig. S4, A to D)**. TRAF6DN also inhibited expression of TNF-α and IL-6 in response to R848 **(fig. S4C)** and TRIFDN inhibited IFN-λ1 secretion in response to poly(I:C) (**fig. S4D**). This established that the TLR pathways were functionally inhibited in these experiments. The MVAGFP expression at MOI 0.3 was reduced in MDDCs expressing TBK1DN and TRAF6DN , but not to a degree that would explain the reduced expression of CD86 in the former **(fig. S4C)**.

Finally, we sought to confirm these results using a genetic knock-out (KO). Using murine bone marrow-derived dendritic cells (BMDCs), we found that the ablation of cGAS abrogated type I IFN secretion and the induction of CD80 and CD86 in bystander cells in response to MVA infection **(fig. S5, A to C)**. As expected, *Cgas*$^{-/-}$ BMDCs were not activated by HTDNA while the activation by R848 or cGAMP stimulation was not affected **(fig. S5, A and B)**. In summary, the induction of inflammatory cytokines by MVA-infected MDDCs, leading to activation of bystander cells, relies on the cGAS-STING-TBK1-IRF3 axis without the contribution of TLR pathway.

DCs respond to incoming MVA infection in the absence of viral DNA replication

The involvement of cGAS raised the question of the role of viral DNA replication in MVA infection and sensing of DCs. MVA is defective for productive replication in human cells due to an assembly defect. However, in HeLa cells, MVA still replicates its DNA (28). Additionally, SAMHD1 (SAM and HD domain-containing dNTP triphosphohydrolase 1) was found to be a restriction factor for vaccinia virus replication in myeloid cells (29). Subsequently, it was shown that MVA expressing viral protein X (Vpx), a lentiviral protein that degrades several host

proteins—including SAMHD1 and human silencing hub (HUSH) complex components (30), expressed late genes in MDDCs (31). Thus, we hypothesized that in MDDCs, MVA does not replicate its DNA due to SAMDH1 restriction and that cGAS may recognize the incoming genome. The scRNA-seq data showed that the proportions of early, intermediate and late gene expression were 85, 10 and 5 percent of all annotated and detected MVA transcripts, respectively **(Fig. 3A)**. This ratio was independent of the expression level of mCherry **(Fig. 3A)**. This suggested that MVA gene expression is largely restricted to early genes in MDDCs. To test whether we could restore MVA late gene expression and replication in MDDCs, we depleted MDDCs of SAMHD1 using Vpx **(Fig. 3B)**. We made use of the simian immunodeficiency virus (SIVmac) accessory protein Vpx that has been shown to alleviate SAMHD1 restriction in myeloid cells for human immunodeficiency virus (HIV) infection (32-35). Treatment of MDDCs with Vpx-containing SIV virus-like particles (SIVVLP VPX^{+}) but not empty SIVVLPs (SIVVLP VPX^{-}) induced SAMHD1 depletion as assessed by intranuclear staining **(Fig. 3B and fig. S6A)**. In SAMHD1-negative cells, a second MVAGFP population—herein termed $MVAGFP_{hi}$—was detected **(Fig. 3C)**. To determine if the $MVAGFP_{hi}$ population resulted from viral replication, we used the inhibitor cytosine arabinoside (AraC) (36, 37). The $MVAGFP_{hi}$ population was no longer detected in SIVVLP VPX^{+} treated MDDCs in the presence of AraC **(Fig. 3D)**. To confirm that the small fraction of $MVAGFP_{hi}$ cells contained replicated DNA, we measured the relative MVA genome content by qPCR. We detected more MVA genome in SIVVLP VPX^{+} treated MDDCs compared to SIVVLP VPX^{-} after MVA infection **(Fig. 3E)**. As previously reported (38), SIVVLP VPX^{+} treated MDDCs expressed less interferon upon MVA infection (**fig. S6B**). Next, we examined if antigen production by the MVA-based HIV (MVA HIV-B) vaccine is increased in SIVVLP VPX^{+} treated MDDCs. Indeed, significantly more HIV antigen p24 was found in SIVVLP VPX^{+} treated MDDCs compared to SIVVLP VPX^{-} **(Fig 3F)**. Because Vpx degrades proteins besides SAMHD1, we used an RNAi approach to knock down (KD) SAMHD1 **(Fig. 3G)**. The $MVAGFP_{hi}$ population was detected in SAMHD1-depleted cells but not control cells. As a control for successful SAMHD1 KD, we infected MDDCs with a HIV-1–derived vector **(fig. S6C)**. In conclusion, SAMHD1 restricts MVA late gene expression and replication in MDDCs. This implies that the cGAS response to the incoming virus, in the absence of new viral DNA synthesis, is sufficient to activate the sensor.

The incoming viral genome is sensed by cGAS to induce inflammatory cytokines

Next, we aimed to determine the role of early gene expression, which coincides with viral uncoating (39), in the cGAS dependent response to MVA infection. We infected MDDCs with UV-irradiated MVA (MVAUV), to cross-link nucleic acids and prevent viral gene expression, or added adenosine N_1-oxide (ANO) during MVA infection, which preserves early mRNA expression but blocks early gene translation (40). MVAGFP expression was completely abrogated upon MVAUV infection, while residual MVAGFP expression was detected with ANO **(fig. S7A)**. Upon MDDC infection with MVAUV MOI 0.3, we found a decreased CD86 expression and decreased secretion of IFN-β and TNF-α (**Fig. 4, A and B**). A caveat of ANO treatment was the induction of non-specific CD86 induction in the absence of infection. Despite this baseline, induction of CD86 and secretion of TNF-α by MVA was inhibited by ANO **(Fig. 4, A and B)**. This effect was specific to MVA since induction of CD86 and Siglec-1 by HTDNA, cGAMP or R848 was not inhibited by ANO **(fig. S7B)**. In contrast, Siglec-1 induction was maintained, and IFN-β secretion was largely normal **(Fig. 4, A and B)**. These data suggest that the incoming viral genome is sufficient to induce IFN-β secretion by the cGAS axis, while the translation of early MVA proteins is a prerequisite to increase TNF-α secretion, ultimately leading to full activation of bystander cells, as inferred from CD86 expression. To determine if TNF-α was the missing factor for bystander activation (CD86 expression), we complemented MVAUV and MVA+ANO infected MDDCs with TNF-α and/or IFN-α2 **(fig. S7, C and D; and fig. S8, A to D)**. TNF-α, but not IFN-α2, rescued CD86 expression of bystander MDDC upon infection with MVAUV **(fig. S7, C and D)** and MVA+ANO **(fig. S8, A and B)**. Together, our results point toward a two-step recognition of MVA infection in MDDCs, whereby the incoming genome is detected by cGAS and early viral gene expression enhances this process, collectively resulting in full activation of bystander cells.

MVA-infected MDDCs die of non-redundant apoptosis

Having characterized the inflammatory cytokine response to MVA infection, we next turned our attention to a seemingly simultaneous cellular event in MVA infection: the rapid death of infected cells. A decline in the expression of mitochondrial membrane protein and apoptosis inhibitor BCL2 was previously reported in MVA-infected MDDCs (12), but the mechanism of cell death remains elusive. Live imaging of MVA-infected MDDCs revealed GFP expression 4 hours after infection (hpi), blebbing of MVA infected MDDCs between 6-8 hpi, and cell death from 10 hpi on **(Fig.**

5A). Further, MVA-infected MDDCs became Annexin V-positive, indicative of apoptosis **(Fig. 5B)**. MVA-induced cell death was also observed after infection of primary cDC2 (**fig. S1B**). Of the caspase inhibitors tested, the pan-caspase inhibitors Q-VD-Oph and BocD effectively inhibited death induced by low concentrations actinomycin D (ActD) **(fig. S9, A and B)**, a compound that is considered to be apoptotic (41), as well as that induced by MVA **(Fig. 5, C and D)**. Caspase inhibition did not prevent the induction of CD86 or Siglec-1 in bystander cells, but it increased the fraction of live, infected cells thereby leading to an apparent decrease of CD86 or Siglec-1 at the whole-population level **(fig. S9, C and D)**. This result shows that MVA potently induces caspase-dependent death of infected of MDDCs.

Caspases are involved in numerous cell death pathways, including apoptosis and necroptosis. We optimized conditions of necroptosis inhibition by necrostatin 1 (Nec-1) or receptor-interacting protein kinase (RIPK) inhibitors RIPK1i III and RIPK3i using a necroptosis-inducing signal that consisted of poly(I:C) in the presence of caspase inhibitor z-VAD-FMK (zVAD) (**fig. S10A**). Inhibitors of necroptotic cell death that targeted RIPK1 and RIPK3 did not rescue MVA-induced cell death **(fig. S10B)**. Expression of CD86 and Siglec-1 on bystander cells was most strongly inhibited by RIPK1 inhibition (**fig. S10B**). RIPK1 is reportedly required for TNF receptor signaling (42, 43). We confirmed this finding in MDDCs **(fig. S10, C and D)**, further substantiating the role of TNF in bystander cell activation**.** To specifically inhibit apoptosis, we overexpressed BCL2 in MDDCs (44). BCL2-expressing MDDCs were completely protected against MVA-induced apoptosis and showed enhanced MVAGFP expression but showed no change in CD86 and Siglec-1 induction **(Fig. 5E and fig. S11A)**. Electron micrographs revealed that MDDCs exhibited various morphological characteristics of apoptosis 24 hpi with MVA, including rounding up, retraction of pseudopods, reduction of cellular volume, chromatin condensation, plasma membrane blebbing, cytoplasm fragmentation with formation of apoptotic bodies **(Fig. 5F)**. BCL2-expressing MDDCs did not generally exhibit these features **(Fig. 5F)**. We conclude that MVA infection kills MDDCs by apoptosis and that this cell death mechanism is not redundant with secondary cell death pathways. This also indicates that anti-apoptotic factors that are expressed as early genes upon MVA infection (45) either are insufficiently expressed until the onset of apoptosis or are not functional in DCs.

scRNA-seq analysis reveals co-expression of NOXA and inflammatory genes in infected cells

MVA-associated apoptosis was proposed to be dependent on MAVS-IRF3 signaling in murine BMDCs and bone-marrow-derived macrophage (BMDMs), leading to expression of the pro-apoptotic BH3-only protein NOXA (15). We examined the distribution of *IFN* gene expression, which are targets of IRF3, and NOXA expression across single cells. Three distinct clusters of infected MDDCs were identified after MVA-infection **(Fig. 6A and fig. S11B)**. Cluster 0 contained uninfected bystander cells with high amounts of cellular UMIs, low viral UMIs (low ratio of vUMI/tUMI) and background levels of the MVA-encoded mCherry **(Fig. 6B and table S1)**. Cluster 1 contained infected dying cells characterized by high viral UMIs, low cellular UMIs (high ratio of vUMI/tUMI), and a high expression of mitochondrial genes, which is a signature of apoptotic cells in scRNA-seq experiments (46) **(Fig. 6C)**. Cluster 2 contained infected cells with both high viral UMIs and high cellular UMIs **(Fig. 6B)**. NOXA-coding gene (*PMAIP1*), type I/III IFN-coding genes, and *TNFA* genes were expressed in this cluster predominantly **(Fig. 6D)**.

Of note, a subset of viral transcripts such as *E3L*, *B13L*, *N1L* and *F1L* was detected in all clusters, suggesting that these transcripts were probably distributed between cells by incoming viral particles, extra cellular vesicles or apoptotic bodies **(fig. S11C)** (47-49). Moreover, induction of ISGs, *CD86* and *Siglec-1* was detected in all clusters, indicative of a transcriptional response to extracellular IFN and TNF in all cells **(Figs. 1D and 6E, and fig. S11D)**. This suggested that the lack of detection of these molecules at the protein level in infected cells (**Fig. 1A**) was likely due to protein translation inhibition by MVA.

Additional genes were differentially expressed between the clusters (**data file S1**). Gene set enrichment analysis confirmed the increased interferon response in cluster 2 and mitochondrial dysfunction in cluster 1 (**fig. S12A**). Additional differentially enriched annotated terms and pathways were identified, such as actin and migration-related pathways that were depleted in cluster 0 (**fig. S12, B to E**).

MVA-induced apoptosis and activation of the IRF3 are independent responses

We next asked if there was a relationship between activation of the cGAS axis and apoptosis induction through NOXA in MVA-infected human MDDCs. Notably, MVA-induced apoptosis was untouched in MDDCs where cGAS, IRF3, TBK1, TRAF6 or TRIF were functionally disabled by knock down or dominant-negative expression **(Fig. 7A)**. We also found that MVA-induced cell death was unaltered in *Cgas*$^{-/-}$ murine BMDCs **(Fig. 7B)**, and upon the neutralization of type I IFN

(Fig. 7C). We next addressed the role of the incoming genome and viral gene expression in MVA-induced cell death. We also found that MVAUV infection, which is sufficient to induce the cGAS-mediated IFN response in MDDCs **(Fig. 4A)**, did not induce any detectable cytotoxicity **(Fig. 7D)**. Accordingly, HTDNA stimulation induced activation of MDDCs but not cell death (**fig. S13A**). In HeLa cells, VACV-induced cell death was previously shown to be sensitive to AraC, which decreases the amount of dsRNA synthesized after viral DNA replication (50, 51). AraC treatment of MDDCs did not inhibit MVA-induced apoptosis **(fig S13B)**, even though it inhibited viral DNA synthesis (**Fig 3D**). Finally, we arrested protein translation with either actinomycin D (ActD) or cycloheximide (CHX) globally. ActD and CHX had the caveat of being toxic to cells on their own, but both ActD- and CHX-treated cells were resistant to additional MVA-induced cell death (**Fig. 7E**). Thus, the incoming genome is sufficient to activate cGAS, but insufficient to trigger apoptosis, which additionally requires early gene expression and protein translation. We next examined the induction of BH3-only gene expression upon MVA infection or stimulation with ligands of cGAS and STING. The only BH3-only gene induced upon MVA infection, cGAS or STING stimulation was NOXA **(Fig. 7F)**. To determine the role of IRF3 in NOXA induction, we included IRF3DN that shuts down expression of IFN genes in response to MVA infection or HTDNA stimulation **(Fig. 2C, fig. S14A).** Notably, NOXA was still induced in IRF3DN expressing MDDCs in response to MVA, cGAMP, or HTDNA **(Fig. 7, F and G)**. KD of IRF3 using shRNA in MDDCs similarly inhibited innate immune activation by MVA infection and had no impact on MVA-induced cell death (**fig. S14, B and C**). KD of the related IRF7 had only a minor effect on CD86 induction by MVA, and no effect on MVA-induced cell death (**fig. S14, B and C**). To test the role of MAVS in MVA-induced apoptosis, we generated BMDCs from *Mavs*$^{-/-}$ mice (**fig. S15**). MVAGFP expression, CD86 expression and cell death induction upon MVA infection were similar in WT and *Mavs*$^{-/-}$ cells. In contrast, CD86 induction by Sendai virus, an RNA virus that activates the MAVS pathway (52), was inhibited in *Mavs*$^{-/-}$ cells. Thus, MVA-induced apoptosis does not require the cGAS-MAVS-IRF3-IRF7 axis, but results from a parallel sensing pathway that is associated with IRF3-independent NOXA expression (**Fig. 7H**).

Discussion

Here, we have deconvoluted the response of DCs to the MVA vaccine. We find that a population of DCs is infected by the virus and expresses early genes. These cells express cytokines, but they

fail to induce activation markers at their cell surface. A separate population of DCs succumbs to the infection. A third population of bystander DCs does not get infected but responds to signals from the infected ones and successfully induces activation markers.

In live infected DCs, we find that viral DNA replication is blocked by SAMHD1. Alleviating SAMHD1 enables the emergence of a new sub-population of DCs that expresses high levels of the vaccine antigen. Despite the abrogation of SAMHD1 in all cells, MVA appears to replicate its DNA in only a small fraction of DCs. This suggests that other, yet to be defined restrictions factors mitigate MVA replication and late gene expression. Alleviating these restrictions factors, while preserving the assembly block that ensures the safety of this vaccine in human cells, may improve the effect of MVA based vaccines.

We also find that live MVA-infected DCs produce inflammatory cytokines as a result of sensing by the cGAS-STING-IRF3 axis. The incoming virus is sufficient to induce production of interferons, in the absence of viral expression. Early viral gene expression was important to reach sufficient level of cytokine production, notably TNF, to promote full activation of bystander cells. This suggests that during early viral gene expression, remodeling of the viral core may lead to enhanced recruitment or activation of cGAS onto the viral DNA.

Live MVA-infected DCs express activation markers at the RNA level, when they do not express activation markers at the cell surface. This suggests that MVA infection induces a paralyzed state in infected DCs. This is most likely due to MVA-induced protein translation shut-down (8). In contrast to activation markers, interferon and TNF-α were expressed at the protein level. These cytokines may be induced by the incoming DNA early enough, before translation shut-down, or even benefit from such arrest (53).

We also describe a population of dead DCs, with a low amount of cellular RNA, and high amounts of viral RNA. Multiple lines of evidence converge on the idea that innate immune activation and induction of apoptotic cell death are independent responses in infected DCs. On the cellular side, inhibition of cGAS by shRNA, STING by inhibitor, TBK1 and IRF3 by dominant negative proteins, all inhibited innate immune activation, but had no impact on induction of cell death. Conversely, caspase inhibitors or expression of BCL2 inhibited MVA-induced cell death, but did not alter the level of innate immune activation by MVA. On the viral side, inhibition of viral RNA expression by UV irradiation preserved induction of interferon, but prevented induction of cell death. It is striking that MVA induces rapid, but targetable, apoptotic death of DCs despite the

presence of well-described anti-apoptotic early genes, such as *E3L, F1L, N1L, B13R, B22R* (7, 45, 54-56). In murine embryonic fibroblasts and HeLa cells, apoptosis induction by MVA has been shown to require deletion of the *F1L* gene (56). MVA lacking *F1L* induces apoptosis in a NOXA-dependent manner (15). In DCs, we find that MVA induces NOXA and this is maintained when innate immune activation is blocked by IRF3DN. However, HTDNA also induced NOXA, but no cell death was detected, suggesting that NOXA induction is not sufficient. We have not tested the role of NOXA in MVA-induced apoptosis. Another study proposed that in HeLa cells, MVA induces apoptosis as a result of accumulation of dsRNA in infected cells (51). dsRNA accumulation after MVA infection is mainly confined to late gene expression (57). HeLa cells are cycling, hence do not have an active SAMHD1 restriction, enabling MVA to replicate its DNA and perform late gene expression. Accordingly, MVA-induced apoptosis of HeLa cells was inhibited by treatment with AraC, which prevents DNA replication, late gene expression and ensuing accumulation of dsRNA (50). We find that in DCs, MVA induces apoptosis in the absence of DNA replication. AraC has no effect on the MVA life cycle due to the SAMHD1 restriction, and consequently, AraC does not block MVA-induced apoptosis of DCs. A study showed that activated IRF3 can directly interact with Bax to trigger apoptosis in response to transfected dsRNA, even when IRF3DN, deleted for the DNA binding domain, is used (58). However, this apoptotic process was inhibited by TBK1DN, which is not the case in our study. Thus, MVA appears to induce an apoptotic pathway in DCs distinct from apoptosis previously associated with IRF3 activation or late gene expression. Low amounts of viral dsRNA can be detected after early gene expression (57), and we do not exclude that they contribute to the apoptotic trigger in DCs. It will be important to identify the signalling pathway that mediates MVA-induced apoptosis in DCs.

Finally, we find that a population of bystanders, exposed to the virus, does not express viral genes, but instead induces activation markers and co-stimulatory molecules. Presumably, this subset of DCs represents the fraction of cells that capture viral antigen from neighbouring infected cells (7, 20, 55), and has the ability to present antigens to lymphocytes, similar to the situation we previously described for blood DC subsets (18).

Our study has revealed the critical role of the cGAS-STING-TBK1-IRF3 axis for cytokine induction by MVA-infected human DCs, without apparent contribution from other PRR pathways, while MVA-induced apoptosis proceeds through a distinct, IRF3-independent, sensing of MVA early gene expression. These events occur in the absence of viral DNA replication due to SAMHD1

restriction. Manipulation of MVA-induced apoptosis and the extent of viral replication in DCs offer the potential to ultimately enhance immunogenic properties of the vaccine vector in vivo.

Materials and Methods

Reagents and Resources are listed in **table S2**.

Human subjects
This study and protocols applied during this study are conform with the 1975 Declaration of Helsinki and were approved by the *Comité de protection des personnes Ile de France II*, the French advisory committee on data processing in medical research and the *Institut National de la Santé et de la Recherche Médicale* ethics committee. Healthy individuals from Paris and *Ile de France* donated venous blood for research. Gender identity and age from anonymous healthy donors was available partially, from the end of 2018 onward.

Cell lines
HEK 293FT cells were obtained from Thermo Fisher Scientific, and HeLa cells were obtained from the Littman lab (New York University). Cell line validation was performed by STR and POWERPLEX 16HS analysis for both cell lines. All cell lines were routinely screened for the presence of mycoplasma (Eurofins).

Plasmids and constructs
CMV-VSVG, psPAX2, pLKO.1puro, pSIV3^{+} were previously reported in the literature (59). shRNA targeting LacZ, cGAS, SAMHD1, IRF3 and IRF7 were in the pLKO.1puro vector. IRF3DN (deletion of amino acids 7 to 132) and BCL2, were cloned from pTRIP-GFP-IRF3 (60) and HDV-BCL2-IRES-dsRED (61) into pTRIP-SFFV-mtagBFP-2A, resulting in pTRIP-SFFV-tagBFP-2A-IRF3DN-FLAG and pTRIP-SFFV-tagBFP-2A-BCL2, respectively. TBK1DN (mutation K38M), TRAF6DN (deletion of amino acids 1-286), and TRIFDN (deletion of amino acids 1-386 and 567-712) were cloned into pTRIP-CMV-puro2A, resulting in pTRIP-CMV-Puro2A-hTBK1 DN, pTRIP-CMV-puro-2A-FLAG-TRAF6 DN and pTRIP-CMV-puro-2A-TRIFDN-CFLAG, respectively. In all final constructs, the entire DNA fragments originating from PCR or synthesis and used for cloning were fully verified by sequencing encompassing the restriction sites. Plasmid DNA was purified using with the low endotoxin HiPure plasmid kit (Thermo Fisher Scientific).

Modified Vaccinia Virus Ankara
MVA was manufactured by Transgene (Illkirch-Graffenstaden, France) and provided by the ANRS. The fluorescent marker, eGFP or mCherry, was expressed under the control of the early promotor p11K7.5 and viral preparations were purified tangential flow filtration. MVA clone is based on the one described in (62).

Mice
All animal procedures were in accordance with the guidelines and regulations of the French Veterinary Department in an accredited animal facility. The animal protocol was approved by the

Animal Ethical Committee of Paris Centre (C2EA-59). C57BL/6J-Mb21d1tm1d(EUCOMM)Hmgu (*Cgas*$^{-/-}$) and C57BL/6J were obtained from The Jackson Laboratory. B6.STOCK-Mavs(tm1Tsc) (*Mavs*$^{-/-}$) mice (63) were bred under specific pathogen-free conditions in the central mouse facility of the Helmholtz Centre for Infection Research, Brunswick, and at TWINCORE, Centre for Experimental and Clinical Infection Research, Hanover, Germany.

Cell line cultivation and isolation of monocytes

HEK 293FT and HeLa cells were cultured in DMEM, 10% fetal bovine serum (FBS) (Eurobio), Penicillin-Streptomycin (Gibco). Human peripheral blood mononuclear cells (hPBMCs) were isolated from blood obtained from Leukocyte Reduction System Chamber (LRSC) including the tubing from healthy human donors (approved by the *Institut National de la Santé et de la Recherche Médicale* ethics committee) using Ficoll-Paque PLUS (GE) in SepMate^{TM} tubes and taken up in RPMI medium supplemented with 10% FBS (Corning), Penicillin-Streptomycin, Gentamicin (50 µg/ml, Gibco), HEPES (Gibco) (DC medium) and stored at 4°C until further processing. CD14^{+} cells were isolated by positive selection with anti-human CD14 magnetic beads (Miltenyi) in LS columns on the manual QuadroMACS^{TM} separator from PBMCs. Purity was checked by flow cytometry using an anti-CD14 (eBioscience), anti-DC-SIGN (R&D Systems) antibody and purity was superior to 97%. To obtain monocyte-derived dendritic cells (MDDCs), CD14^{+} cells were cultured in DC medium supplemented with human GM-CSF (Miltenyi) at 10 ng/ml, and IL-4 (Miltenyi) at 50 ng/ml for 5 days. Total blood DCs were enriched with EasySep human pan-DC pre-enrichment kit (Stemcell Technologies). DC-enriched fractions were stained with antibodies specific for HLA-DR APCeFluor780, CD1c PerCPeFluor710 (eBioscience), CD123 Viogreen, CD45RA Vioblue (Miltenyi), CD33 PE-CF594, Clec-9A PE (BD), AXL PE (Bio-Techne) and with a mixture of antibodies against lineage markers CD19 (Miltenyi), CD3, CD14, CD16, and CD34 (BD) in the FITC channel. cDC2s were sorted as Lin^{-} HLADR^{+}CD33^{+}CD45RA^{-}CD1c^{+}CD123^{-}. Cells were sorted on a FACSAria (BD) using Diva software (BD) in 5 mL polypropylene round-bottom tubes containing 1 mL X-VIVO-15 medium (Lonza BE04-418F). Post-sort cell purity after gating on live cells by FCS/SSC was routinely between 90 and 99%. Absence of mycoplasma contamination during the course of the study was confirmed regularly (Eurofins).

Lentiviral vector production

Lentiviral vectors were produced by transfection of 0.8 million HEK 293FT cells (passage 3-22) per 6-well with 3 µg DNA and 8 µl TransIT-293 (Mirus Bio) per well; for SIVmac VLPs (SIVVLPs) 0.4 µg CMV-VSVG and 2.6 µg pSIV3^{+} were transfected; for shRNA or dominant negative mutant containing vectors 0.4 µg CMV-VSVG, 1 µg psPAX2 and 1.6 µg lentiviral vector plasmid were transfected. The morning after transfection medium was replaced with fresh DC medium. Viral supernatants were harvested after 24 hours, filtered at 0.45 µm, and used directly for transduction of monocytes. Of note, lentivirus-containing supernatants did not alter dendritic cell differentiation or lead to their activation in the absence infection/stimulation.

Transduction of monocytes

Blood was received the day of donation and obtained from LRSC plus tubing. Subsequently, PBMCs were isolated the same day and stored in DC medium at 4°C overnight. After CD14^{+} isolation, monocytes were seeded in 10 cm perti dishes at 1 million per ml in DC medium supplemented with human GM-CSF (Miltenyi) at 10 ng/ml, and IL-4 (Miltenyi) at 50 ng/ml for 5

days to obtain MDDCs. For targeted knockdown by RNAi or overexpression of dominant negative mutants, 2 million monocytes in 2 ml DC medium supplemented with 3X GM-CSF and IL-4 were transduced with 2 ml of SIVVLPs (containing VPX) and 2 ml lentiviral vectors encoding for the shRNA or the dominant negative mutants as previously described (59, 64) in 6 well plates. The transduction mix was supplemented with 8 µg/ml protamine to mask the hindering charges between lentiviral vectors and monocytes. Upon transduction with lentiviral vectors containing a puromycin resistance, medium change with medium containing puromycin (2 µg/ml) was done for at least 48 hours. KD efficiency was measured by western blotting at day 5 (for MDDCs at the time of infection). For the KD of IRF3 and IRF7, a mix of 5 shRNAs was used.

Infection and stimulation

At day 5 of MDDC differentiation, cells were harvested, counted and resuspended in fresh DC medium supplemented with GM-CSF (20 ng/ml) and IL-4 (100 ng/ml) at a concentration of 1 million per ml. Sorted cDC2s were resuspended at the same concentration in X-VIVO-15 medium supplemented with Penicillin-Streptomycin (Gibco) and 3 ng/ml human GM-CSF (Miltenyi). 100 µl of MDDCs were seeded in round-bottom 96-well plates and stimulated/infected with 100 µl of MVA dilutions or PRR ligand dilutions. MVA infection was performed with increasing MOIs at increments of 1/3 ranging from 0.01 to 1. For all experiments the MOIs 0.3 and 1 are shown as indicated in the figures. Stimulation with PRR ligands was equally performed with increasing concentrations at increments of 1/3 ranging from 0.03-3 µg/ml for HMW poly(I:C) (Invivogen), R848 (Invivogen), and HTDNA (Sigma), and at 0.04-4 µg/ml for 2'3'-cGAMP (Invivogen). R848 was directly added in the medium, while poly(I:C), HTDNA, and 2'3'-cGAMP were delivered complexed with Lipofectamine 2000 (Thermo Fisher Scientific) for transfection. For transfection, Lipofectamine + OPTIMEM and the PRR ligand + OPTIMEM were incubated for 5 min separately, before being mixed and incubated for another 15 min together at RT. Finally, the mix was filled up to 1.5 ml and 100 µl used for stimulation per well. 24 hours after infection/stimulation supernatants were analyzed for cytokine quantification and cells were immunolabeled and analyzed by flow cytometry or were used for RNA isolation and cDNA generation to run qPCR reactions.

Perturbations during MVA Infection of MDDCs

For type I IFN neutralization during MVA infection a cocktail containing 3 µg/ml recombinant B18R (eBioscience), 1.2 µg/ml monoclonal anti-IFN-α (Invitrogren), 2.5 mg/ml monoclonal anti-IFN-β (eBioscience), and 1.5 µg/ml monoclonal anti- IFNAR chain 2 (Millipore) was added before infection. For TNF-α neutralization 10 µg/ml anti-TNF RII, anti-TNF RI, and anti-TNF-α (R&D Systems) were added before infection. For JAK/STAT inhibition 1 µM ruxolitinib (Invivogen) was added before infection. For STING inhibition by H-151 (STINGi, ProbeChem) MDDCs were incubated with 20 µM of H-151 for 1 hour before infection. To specifically block MVA replication 10 µM cytarabine (AraC, Tocris) was added right before infection. To block translation of early MVA RNAs MDDCs were incubated with 3µg adenosine N_1-oxide (ANO, Afla Chemistry), to block translation and transcription globally cells were incubated with 0.3/1/3 µg/ml cycloheximde (CHX, Sigma) or 1.25/2.5/5 µM actinomycin D (ActD, Sigma), respectively, for 1 hour before infection with MVA. To inhibit the various forms of cell death MDDCs were incubated with 20 µM Q-VD-Oph, 22µM zVAD, 25 µM BocD, 40 µM Nec-1, 2 µM RIPK1 inhibitor III and 12 µM RIPK3 inhibitor for 30 min before infection. For the reconstitution experiments with IFN-α2 and TNF-α upon MDDC infection with MVA+ANO or MVAUV, IFN-α2 was supplemented 2 hpi, and TNF-α was supplemented 6 hpi.

Murine bone marrow derived dendritic cells (BMDCs) differentiation and infection.
BMDCs were obtained by culturing murine bone marrow cells (from both male and female mice) for 10-11 days in complete DC medium [IMDM medium supplemented with fetal calf serum (FCS, 10%), glutamine (20 mM), penicillin-streptomycin (100 U/mL), ß-mercaptoethanol (50 µM) and granulocyte-macrophage colony-stimulating factor (50 ng/mL)- containing supernatant obtained from transfected J558L cells(65)]. In brief, bone marrow was collected by flushing of tibia and femur, put in culture at 1 million cells / mL of complete DC medium, and on day 4, all cells were collected with PBS EDTA (5 mM), spun down and resuspended in fresh complete DC medium at $0.5x10^6$ cells / mL. On day 7, non-adherent cells were removed, semi-adherent and adherent cells were collected with PBS EDTA (5 mM), spun down and resuspended in fresh complete DC medium at $0.5x10^6$ cells / mL. At day 10 or 11, BMDCs were collected by gentle recovery of semi-adherent cells with PBS EDTA and used for infection experiments. The percentage of differentiated cells was analyzed by cytometry with antibodies against mouse CD11c and Cd11b (mean = 85, 62±5, 46% $CD11b^+CD11c^+$). 50,000 BMDCs cells were seeded in a 96 well plate and infected with MVAGFP (MOI 1 or 3) or Sendai virus (MOI 1) and incubated for 24 hours.

Flow cytometry
For immunolabeling cells were washed twice with PBS in the 96 well plates. Cell-surface immunolabeling of CD86 (eBioscience) or Siglec-1 (Miltenyi Biotec) was performed together with a fixable viability dye (eBiosience) in PBS for 20 min at 4°C, washed twice and fixed with 1% PFA. For intranuclear SAMHD1 staining 300,000 cells were transferred to a 1.5 ml Eppendorf reaction cups, resuspended in 100 µl 1% PFA/PBS, and fixed for 10 min at 37°C. Upon centrifugation at 0.4 rcf for 5 min 4°C pellet was resuspended in 100 µl Glycine/PBS (375 mg/50ml) for 10 min at RT. Cells were centrifuged as before, taken up in 100 µl of ice cold 80/20 methanol/H2O and incubated for 30 min on ice. Finally, cells were washed in 1mL of 5% BSA/PBS at 0.4 rcf 5 min 4°C and resuspended in 50 µl of 10% BSA/PBS for 10min at RT. Subsequently, 50 µl of 10% BSA/PBS with 1/100 (2x) SAMHD1 antibody (Sigma) were added and incubated for 1hr at RT. Cells were washed in 1ml of 5% BSA/PBS and resuspended in 100µl of 1/500 diluted anti-rabbit-Alexa488 (Invitrogen) in 5% BSA/PBS and incubated for 30min at RT. Cells were washed at 0.4 rcf 5 min 4°C with 1ml 5% BSA/PBS one more time, resuspended in 200 µl of PBS and analyzed by flowcytometry. For immunolabeling of Annexin V cells were washed once in PBS and once in Annexin V Binding Buffer, then incubated for 20 min at RT, washed twice with Binding Buffer and analyzed by flowcytometry. All samples were analyzed on a BD FACSVerse , or the MACSQuant flow cytometer using a 96 well plate reader.

CXCL10, IL-6 and TNF-α Protein Quantification
IL-6 and TNF-α concentration was measured in pure or for CXCL10 in 50-fold diluted supernatants from infected or stimulated MDDCs. CXCL10, IL-6 and TNF-α concentrations were measured using a cytometric bead assay (BD) according to manufacturer's protocol. Data was acquired on a BD FACSVerse (BD) and analyzed in FCAP Array (BD).

IFN-α2, IFN-β and IFN-λ1 Protein Quantifications
IFN-α2, IFN-β and IFN-λ1 concentrations were measured in undiluted supernatants from infected or stimulated DCs using a LEGENDplex Human Anti-Virus Response assay (BioLegend) according to manufacturer's protocol. Data were acquired on a BD FACSVerse (BD) and analyzed with LEGENDplex Software (BioLegend).

MVA UV Irradiation

For ultraviolet (UV) irradiation, MVA stock solution was irradiated (UV corsslinker CL-508 UVItec) on ice in an non-treated perti dish until 300 mJ/cm^2 was reached. Subsequently the UV-irradiated stock solution was diluted in increments of 1/3. The dose of UV irradiation needed to abrogate MVA gene expression was determined by infection of HeLa cells. 30 mJ/cm2 abolished MVA replication in HeLa cells and 300 mJ/cm2 abolished gene expression **(fig. S16A)**.

Gene Expression Quantification

Five days after lentiviral vector transduction of MDDCs, total RNA was extracted from 300 000 cells using Nucleospin RNA II kit (Macherey-Nagel). cDNA was synthesized with random hexamer from 0.1µg total RNA using SuperScript III Reverse Transcriptase (Thermo Fisher Scientific). Real-time qPCR was performed using SYBR Green I Master (Roche) and primers (**table S2**). Expression level of mRNA was calculated according to the housekeeper gene beta-actin for stimulation with PRR ligands, and the geometric mean between the two housekeepers HPRT and RPL34 for MVA infected samples.

MVA genome Real-time PCR

Real-time PCR analysis was performed as previously described (66). Each sample was measured in triplicate for all primers. 24 hpi with total DNA was extracted from 300 000 thousand MDDCs using NucleoSpin Tissue kit (Macherey-Nagel). Real-time qPCR was performed using SYBR Green I Master (Roche). The level of MVA genome was calculated relative to beta-globulin expression. The primer sequences for E9L, present in MVA and the parental strain, and the POX gene, present in most of the poxviruses are listed in the resources.

Western Blotting

0.5 to 2 million MDDCs were lysed in 50 µL of RIPA buffer (50mM Tris HCl, 150mM NaCl, 0.1% SDS, 0.5% DOC, 1% NP-40) to which protease inhibitor (Roche; 1187358001) was added each time before use. Lysis was performed on ice for 30 minutes. Lysates were cleared by centrifugation at 8000g for 8 minutes at 4°C, and 50 µl of Laemmli 2X (12% SDS, 30% Glycerol, 0.375M Tris-HCl pH6.8, 30% 2-mercaptoehtanol, 1% bromophenol blue) was added and samples were boiled at 95°C for 15min. Samples were migrated on Biorad precast SDS-PAGE gels and transferred on PVDF membranes. Membranes were saturated and proteins were blotted with antibodies in 5% non-fat dry milk, PBS, 0.1% Tween buffer. ECL signal was recorded on the ChemiDoc-XRS or ChemiDoc Touch Biorad Imager. Data was analyzed and quantified with the Image Lab software (Biorad).

Electron Microscopy

For electron microscopy MDDCs were infected for 24 hours in 96 well round-bottom plates and then transferred onto poly-L-lysin treated coverslips. Upon attachment for 30 min at 37°C, cells were fixed in 1 ml of fixative (2.5 % glutaraldehyde in 0.1 M cacoldylate buffer, pH 7.4) for 1 hour, post fixed for 1 hour with 2 % buffered osmium tetroxide, dehydrated in a graded series of ethanol solution, and then embedded in epoxy resin. Images were acquired with a digital camera Quemesa (SIS) mounted on a Tecnai Spirit transmission electron microscope (FEI Company) operated at 80kV.

Quantification and Statistical Analysis

Statistical parameters including the exact value of n, dispersion and precision measures (as mean ± SEM) and statistical significance are reported in the Figures. In all graphs, symbols represent single donors, and bars show mean + SEM, or geometric mean for logarithmic scales. In figures asterisks denote statistical significance: *p<0.05, **p<0.01, ***p<0.005, ****p<0.0001, "ns"=not significant. Comparisons between any 2 or more groups were analyzed by analysis of variance (RM two-way ANOVA with Geisser-Greenhouse and Sidak's correction for multiple comparison) or as indicated otherwise in figure legends. Statistical analysis was performed in GraphPad PRISM 7, 8 and 10 (Graph Pad Software Inc.).

scRNA-seq

24 hpi with MVA at MOI 0.5 MDDCs were sorted according to FSC/SSC characteristics, DAPI labeling, and subsequently loaded on a 10× Chromium instrument (10× Genomics) according to manufacturer's protocol based on the 10× GEMCode proprietary technology. Single-cell RNA-Seq libraries were prepared using Chromium Single Cell 3′ v2 Reagent Kit (10× Genomics) according to manufacturer's protocol. Briefly, the initial step consisted of performing an emulsion where individual cells were isolated into droplets together with gel beads coated with unique primers bearing 10× barcodes, unique molecular identifiers (UMI), and poly(dT) sequences. Reverse transcription reactions were performed to generate barcoded full-length cDNA followed by the disruption of emulsion droplets using the recovery agent. cDNA was cleaned up with DynaBeads MyOne Silane Beads (Thermo Fisher Scientific). Bulk cDNA was amplified using a GeneAmp PCR System 9700 with 96-Well Gold Sample Block Module (Applied Biosystems) (98 °C for 3 min; cycled 14×: 98 °C for 15 s, 67 °C for 20 s, and 72 °C for 1 min; held at 4 °C). Amplified cDNA product was cleaned up with the SPRI select Reagent Kit (Beckman Coulter). Indexed sequencing libraries were constructed using the reagents from the Chromium Single Cell 3′ v2 Reagent Kit, following these steps: (1) fragmentation, end repair, and A-tailing; (2) size selection with SPRI select; (3) adaptor ligation; (4) post ligation cleanup with SPRI select; (5) sample index PCR and cleanup with SPRI select beads. Library quantification and quality assessment was performed using Qubit fluorometric assay (Invitrogen) with dsDNA HS (High Sensitivity) Assay Kit and Bioanalyzer Agilent 2100 using a High Sensitivity DNA chip (Agilent Genomics). Indexed libraries were equimolarly pooled and sequenced on an NovaSeq6000 system PE26/8/91 bp as sequencing mode. Using a full Rapid flow cell, 600M clusters have been used with a targeted coverage of around 150M reads per sample.

scRNA-seq analysis, alignment

Data of a non-infected and an MVA-infected sample derived from two healthy donors was aligned to a concatenated genome consisting of hg38 (NCBI assembly: GCA_000001405.28, annotation: ENSEMBL release 101), the MVA genome (NCBI assembly: GCF_000860085.1) and mCherry sequence (AY678264.1) using CellRanger (v.4.0.0). The expected number of cells for the infected andthe uninfected replicates was set to 1000 and 2000, respectively. Viral and cellular feature count was also performed using CellRanger. A coverage just below 200 million reads per sample was obtained corresponding to 70,000 – 170,000 reads per cell (**fig. S16B**).

scRNA-seq analysis, cell calling

Cell calling was performed using two different algorithms: CellRanger (v.4.0.0) and EmptyDrops (67) from the DropletUtils package (v 1.6.1). Thereby, cells with an UMI count higher than a tenth of the 99th percentile of the total UMI count were selected. To recover MVA-infected cells that exhibited MVA-associated cell death with low cellular RNA counts and high viral RNA counts,

the EmptyDrops package was used with an FDR of 0.1 and a cutoff of 1000 total UMIs or 100 viral UMIs. The cells used for downstream analysis were the union of cells recovered by each algorithm (**fig. S16C**).

scRNA-seq analysis, normalization

The data was normalized to remove the technical bias based on sequencing depth. Viral and cellular features were normalized separately. To this end, the count table was split into two matrices, one with only viral genes (mCherry was considered a "viral gene") and one with only cellular genes. The function NormalizeData from the Seurat package (v.3.1.1) was used with the default parameters on these two matrices. Finally, the two matrices were concatenated into a single matrix in a new Seurat object. Of note, this normalization method will artificially inflate values for viral features when there are few viral UMIs in a cell, which has a strong impact in the uninfected samples in case of error in read assignment.

scRNA-seq analysis, removal or donor effect

To reduce the inter-donor variability and conserve changes in the gene expression in response to MVA infection the Mutual Nearest Neighbor (MNN) method (68) was used (69) **(fig. S16D)**. After normalization, the FindVariableFeatures function computed a set of 2000 variable features using the vst method separately on both the infected and non-infected samples. To minimize the impact of infection on integration, we intersected the two sets of features (958 variable features). The intersection was used to integrate the two replicates of the MVA condition with the unFastMNN Seurat wrapper with a number of nearest neighbors of k=20.

scRNA-seq analysis, descriptive analysis of infected samples

The descriptive analysis of the infected sample was done on the MNN reduction. The ratio of viral UMIs in a cell (a) divided by the total amount of UMIs (b) was log-transformed according to the formula $\log(\frac{a}{b} \times 10000 + 1)$. This ratio and mCherry expression normalized to total UMIs were used as proxy of infection.

scRNA-seq analysis, bar plots for MVA genes classes

The proportion of different classes of MVA genes (early, intermediate, and late) (70) expressed in MVA-infected samples was depicted in bar plots. In these, the x-axis is a discrete axis representing the cells, sorted by the normalized value of mCherry expression. Cells with MVA UMIs lower than 10 or with a normalized mCherry expression of 0 were filtered out. Upon filtering, 608 of 1235 cells remained for replicate 1 and 523 of 1035 cells for replicate 2. The y-axis represents the percentage of each class among all viral UMIs in a cell. The UMIs were grouped into the three classes based on literature annotations or discarded if no information was available (about half of the viral genes expressed) (70).

scRNA-seq analysis, feature plot with mCherry

MVA gene expression was visualized as normalized mCherry expression or the ratio of viral UMIs over total UMIs on a UMAP reduction of the MNN integration. Expression of cellule genes was plotted similarly. Additionally, the Pearson's correlation coefficient was computed between these genes and the ratio of viral UMIs over total UMIs.

scRNA-seq analysis, clustering

A clustering solution based on the MNN reduction was computed for infected samples only. First, shared nearest neighbors in this reduction were computed with the Seurat FindNeighbors function with a number of nearest neighbors k = 10. Second, the FindClusters function was applied, with a resolution of 0.05. Default parameters were used otherwise. The selection of the clustering solution was based on the average Silhouette score of the clusters, balanced sample composition of each cluster **(fig. S16D–E)**, and biological significance of the clusters.

scRNA-seq analysis, differential expression
The gene expression profiles of each cluster were compared. To this end, differential gene expression of each cluster against all remaining cells was computed separately. The version 1.12.0 of the MAST package (74) for the differential gene expression was used, and the information of which donor each cell derived from was added to the hurdle model. Only DEGs with an adjusted p-value ≤ 0.05, an absolute value of log fold change ($\log_2$(FC)) ≥ 0.5, and DEGs that were expressed in $\geq 30\%$ of the cells of the non-infected samples or the cluster were selected.

scRNA-seq analysis, pathway analysis
The DOSE package (v.3.12.0) (75) was used for pathway analysis. The GO database, the KEGG database, and the HallMark gene set (Molecular Signature Database) were used tocompute for each cluster differentially increased and decreased genes. For the GO database the simplify function was used in order to remove redundantly identified pathway, while for the othere databases used the differentially expressed pathways with an adjusted p-value ≤ 0.01 and containing at least 5 genes from differential gene set were selected.

Supplementary Materials

Figures S1 – S16
Tables S1 and S2
Data file S1

References and Notes

1. A. Volz, G. Sutter, in *Advances in virus research*. (Elsevier, 2017), vol. 97, pp. 187-243.

2. L. Sanchez-Sampedro, B. Perdiguero, E. Mejias-Perez, J. Garcia-Arriaza, M. Di Pilato, M. Esteban, The evolution of poxvirus vaccines. *Viruses* **7**, 1726 (2015); published online EpubApr 7 (10.3390/v7041726).

3. N. K. Routhu, S. Gangadhara, N. Cheedarla, A. Shiferaw, S. A. Rahman, A. Sahoo, P.-Y. Shi, V. D. Menachery, K. Floyd, S. Fischinger, C. Atyeo, G. Alter, M. S. Suthar, R. R. Amara, Modified Vaccinia Ankara Based SARS-CoV-2 Vaccine Expressing Full-Length Spike Induces Strong Neutralizing Antibody Response. *bioRxiv*, (2020); published online Epub2020-01-01 00:00:00 (

4. P. Dai, W. Wang, N. Yang, C. Serna-Tamayo, J. M. Ricca, D. Zamarin, S. Shuman, T. Merghoub, J. D. Wolchok, L. Deng, Intratumoral delivery of inactivated modified

vaccinia virus Ankara (iMVA) induces systemic antitumor immunity via STING and Batf3-dependent dendritic cells. *Sci Immunol* **2**, (2017); published online EpubMay 19 (10.1126/sciimmunol.aal1713).

5. M. Kadoki, A. Patil, C. C. Thaiss, D. J. Brooks, S. Pandey, D. Deep, D. Alvarez, U. H. von Andrian, A. J. Wagers, K. Nakai, T. S. Mikkelsen, M. Soumillon, N. Chevrier, Organism-Level Analysis of Vaccination Reveals Networks of Protection across Tissues. *Cell* **171**, 398 (2017); published online EpubOct 5 (10.1016/j.cell.2017.08.024).

6. A. F. Altenburg, C. E. van de Sandt, B. W. S. Li, R. J. MacLoughlin, R. A. M. Fouchier, G. van Amerongen, A. Volz, R. W. Hendriks, R. L. de Swart, G. Sutter, G. F. Rimmelzwaan, R. D. de Vries, Modified Vaccinia Virus Ankara Preferentially Targets Antigen Presenting Cells In Vitro, Ex Vivo and In Vivo. *Scientific reports* **7**, 8580 (2017); published online EpubAug 17 (10.1038/s41598-017-08719-y).

7. E. Guzman, C. Cubillos-Zapata, M. G. Cottingham, S. C. Gilbert, H. Prentice, B. Charleston, J. C. Hope, Modified vaccinia virus Ankara-based vaccine vectors induce apoptosis in dendritic cells draining from the skin via both the extrinsic and intrinsic caspase pathways, preventing efficient antigen presentation. *Journal of virology* **86**, 5452 (2012); published online EpubMay (10.1128/jvi.00264-12).

8. S. Guerra, J. L. Najera, J. M. Gonzalez, L. A. Lopez-Fernandez, N. Climent, J. M. Gatell, T. Gallart, M. Esteban, Distinct gene expression profiling after infection of immature human monocyte-derived dendritic cells by the attenuated poxvirus vectors MVA and NYVAC. *Journal of virology* **81**, 8707 (2007); published online EpubAug (10.1128/JVI.00444-07).

9. Z. Waibler, M. Anzaghe, H. Ludwig, S. Akira, S. Weiss, G. Sutter, U. Kalinke, Modified vaccinia virus Ankara induces Toll-like receptor-independent type I interferon responses. *Journal of virology* **81**, 12102 (2007); published online EpubNov (10.1128/JVI.01190-07).

10. J. Delaloye, T. Roger, Q. G. Steiner-Tardivel, D. Le Roy, M. Knaup Reymond, S. Akira, V. Petrilli, C. E. Gomez, B. Perdiguero, J. Tschopp, G. Pantaleo, M. Esteban, T. Calandra, Innate immune sensing of modified vaccinia virus Ankara (MVA) is mediated by TLR2-TLR6, MDA-5 and the NALP3 inflammasome. *PLoS Pathog* **5**, e1000480 (2009); published online EpubJun (10.1371/journal.ppat.1000480).

11. P. Dai, W. Wang, H. Cao, F. Avogadri, L. Dai, I. Drexler, J. A. Joyce, X. D. Li, Z. Chen, T. Merghoub, S. Shuman, L. Deng, Modified vaccinia virus Ankara triggers type I IFN production in murine conventional dendritic cells via a cGAS/STING-mediated cytosolic DNA-sensing pathway. *PLoS Pathog* **10**, e1003989 (2014); published online EpubApr (10.1371/journal.ppat.1003989).

12. A. Chahroudi, D. A. Garber, P. Reeves, L. Liu, D. Kalman, M. B. Feinberg, Differences and similarities in viral life cycle progression and host cell physiology after infection of human dendritic cells with modified vaccinia virus Ankara and vaccinia virus. *Journal of virology* **80**, 8469 (2006); published online EpubSep (10.1128/JVI.02749-05).

13. W. Kastenmuller, I. Drexler, H. Ludwig, V. Erfle, C. Peschel, H. Bernhard, G. Sutter, Infection of human dendritic cells with recombinant vaccinia virus MVA reveals general persistence of viral early transcription but distinct maturation-dependent cytopathogenicity. *Virology* **350**, 276 (2006); published online EpubJul 5 (10.1016/j.virol.2006.02.039).

14. S. Brandler, A. Lepelley, M. Desdouits, F. Guivel-Benhassine, P. E. Ceccaldi, Y. Levy, O. Schwartz, A. Moris, Preclinical studies of a modified vaccinia virus Ankara-based HIV candidate vaccine: antigen presentation and antiviral effect. *Journal of virology* **84**, 5314 (2010); published online EpubMay (10.1128/JVI.02329-09).

15. P. Eitz Ferrer, S. Potthoff, S. Kirschnek, G. Gasteiger, W. Kastenmuller, H. Ludwig, S. A. Paschen, A. Villunger, G. Sutter, I. Drexler, G. Hacker, Induction of Noxa-mediated apoptosis by modified vaccinia virus Ankara depends on viral recognition by cytosolic helicases, leading to IRF-3/IFN-beta-dependent induction of pro-apoptotic Noxa. *PLoS Pathog* **7**, e1002083 (2011); published online EpubJun (10.1371/journal.ppat.1002083).

16. M. M. Gaidt, T. S. Ebert, D. Chauhan, K. Ramshorn, F. Pinci, S. Zuber, F. O'Duill, J. L. Schmid-Burgk, F. Hoss, R. Buhmann, G. Wittmann, E. Latz, M. Subklewe, V. Hornung, The DNA Inflammasome in Human Myeloid Cells Is Initiated by a STING-Cell Death Program Upstream of NLRP3. *Cell* **171**, 1110 (2017); published online EpubNov 16 (10.1016/j.cell.2017.09.039).

17. R. L. Brunette, J. M. Young, D. G. Whitley, I. E. Brodsky, H. S. Malik, D. B. Stetson, Extensive evolutionary and functional diversity among mammalian AIM2-like receptors. *The Journal of experimental medicine* **209**, 1969 (2012); published online EpubOct 22 (10.1084/jem.20121960).

18. A. Silvin, C. I. Yu, X. Lahaye, F. Imperatore, J. B. Brault, S. Cardinaud, C. Becker, W. H. Kwan, C. Conrad, M. Maurin, C. Goudot, S. Marques-Ladeira, Y. Wang, V. Pascual, E. Anguiano, R. A. Albrecht, M. Iannacone, A. García-Sastre, B. Goud, M. Dalod, A. Moris, M. Merad, A. K. Palucka, N. Manel, Constitutive resistance to viral infection in human CD141(+) dendritic cells. *Sci Immunol* **2**, (2017); published online EpubJul 7 (10.1126/sciimmunol.aai8071).

19. S. Cristinelli, A. Ciuffi, The use of single-cell RNA-Seq to understand virus-host interactions. *Current opinion in virology* **29**, 39 (2018); published online EpubApr (10.1016/j.coviro.2018.03.001).

20. M. F. Pascutti, A. M. Rodriguez, J. Falivene, L. Giavedoni, I. Drexler, M. M. Gherardi, Interplay between modified vaccinia virus Ankara and dendritic cells: phenotypic and functional maturation of bystander dendritic cells. *Journal of virology* **85**, 5532 (2011); published online EpubJun (10.1128/JVI.02267-10).

21. K. J. Ishii, C. Coban, H. Kato, K. Takahashi, Y. Torii, F. Takeshita, H. Ludwig, G. Sutter, K. Suzuki, H. Hemmi, S. Sato, M. Yamamoto, S. Uematsu, T. Kawai, O. Takeuchi, S. Akira, A Toll-like receptor-independent antiviral response induced by double-stranded B-

form DNA. *Nature immunology* **7**, 40 (2006); published online EpubJan (10.1038/ni1282).

22. S. M. Haag, M. F. Gulen, L. Reymond, A. Gibelin, L. Abrami, A. Decout, M. Heymann, F. G. van der Goot, G. Turcatti, R. Behrendt, A. Ablasser, Targeting STING with covalent small-molecule inhibitors. *Nature* **559**, 269 (2018); published online EpubJul (10.1038/s41586-018-0287-8).

23. B. S. Parekh, T. Maniatis, Virus infection leads to localized hyperacetylation of histones H3 and H4 at the IFN-beta promoter. *Molecular cell* **3**, 125 (1999); published online EpubJan (10.1016/s1097-2765(00)80181-1).

24. V. Hornung, R. Hartmann, A. Ablasser, K. P. Hopfner, OAS proteins and cGAS: unifying concepts in sensing and responding to cytosolic nucleic acids. *Nature reviews. Immunology* **14**, 521 (2014); published online EpubAug (10.1038/nri3719).

25. Y. Tojima, A. Fujimoto, M. Delhase, Y. Chen, S. Hatakeyama, K. Nakayama, Y. Kaneko, Y. Nimura, N. Motoyama, K. Ikeda, M. Karin, M. Nakanishi, NAK is an IkappaB kinase-activating kinase. *Nature* **404**, 778 (2000); published online EpubApr 13 (10.1038/35008109).

26. K. Burns, F. Martinon, C. Esslinger, H. Pahl, P. Schneider, J. L. Bodmer, F. Di Marco, L. French, J. Tschopp, MyD88, an adapter protein involved in interleukin-1 signaling. *The Journal of biological chemistry* **273**, 12203 (1998); published online EpubMay 15 (10.1074/jbc.273.20.12203).

27. M. Yamamoto, S. Sato, K. Mori, K. Hoshino, O. Takeuchi, K. Takeda, S. Akira, Cutting edge: a novel Toll/IL-1 receptor domain-containing adapter that preferentially activates the IFN-beta promoter in the Toll-like receptor signaling. *Journal of immunology (Baltimore, Md. : 1950)* **169**, 6668 (2002); published online EpubDec 15 (10.4049/jimmunol.169.12.6668).

28. M. C. Sancho, S. Schleich, G. Griffiths, J. Krijnse-Locker, The block in assembly of modified vaccinia virus Ankara in HeLa cells reveals new insights into vaccinia virus morphogenesis. *Journal of virology* **76**, 8318 (2002); published online EpubAug (10.1128/jvi.76.16.8318-8334.2002).

29. J. A. Hollenbaugh, P. Gee, J. Baker, M. B. Daly, S. M. Amie, J. Tate, N. Kasai, Y. Kanemura, D. H. Kim, B. M. Ward, Y. Koyanagi, B. Kim, Host factor SAMHD1 restricts DNA viruses in non-dividing myeloid cells. *PLoS Pathog* **9**, e1003481 (2013)10.1371/journal.ppat.1003481).

30. G. Chougui, S. Munir-Matloob, R. Matkovic, M. M. Martin, M. Morel, H. Lahouassa, M. Leduc, B. C. Ramirez, L. Etienne, F. Margottin-Goguet, HIV-2/SIV viral protein X counteracts HUSH repressor complex. *Nature microbiology* **3**, 891 (2018).

31. K. Sliva, J. Martin, C. von Rhein, T. Herrmann, A. Weyrich, M. Toda, B. S. Schnierle, Interference with SAMHD1 Restores Late Gene Expression of Modified Vaccinia Virus

Ankara in Human Dendritic Cells and Abrogates Type I Interferon Expression. *Journal of virology* **93**, (2019); published online EpubNov 15 (10.1128/JVI.01097-19).

32. N. Laguette, B. Sobhian, N. Casartelli, M. Ringeard, C. Chable-Bessia, E. Segeral, A. Yatim, S. Emiliani, O. Schwartz, M. Benkirane, SAMHD1 is the dendritic- and myeloid-cell-specific HIV-1 restriction factor counteracted by Vpx. *Nature* **474**, 654 (2011); published online EpubMay 25 (10.1038/nature10117).

33. K. Hrecka, C. Hao, M. Gierszewska, S. K. Swanson, M. Kesik-Brodacka, S. Srivastava, L. Florens, M. P. Washburn, J. Skowronski, Vpx relieves inhibition of HIV-1 infection of macrophages mediated by the SAMHD1 protein. *Nature* **474**, 658 (2011); published online EpubJun 29 (10.1038/nature10195).

34. C. Goujon, V. Arfi, T. Pertel, J. Luban, J. Lienard, D. Rigal, J. L. Darlix, A. Cimarelli, Characterization of simian immunodeficiency virus SIVSM/human immunodeficiency virus type 2 Vpx function in human myeloid cells. *Journal of virology* **82**, 12335 (2008); published online EpubDec (10.1128/JVI.01181-08).

35. A. Bergamaschi, D. Ayinde, A. David, E. Le Rouzic, M. Morel, G. Collin, D. Descamps, F. Damond, F. Brun-Vezinet, S. Nisole, F. Margottin-Goguet, G. Pancino, C. Transy, The human immunodeficiency virus type 2 Vpx protein usurps the CUL4A-DDB1 DCAF1 ubiquitin ligase to overcome a postentry block in macrophage infection. *Journal of virology* **83**, 4854 (2009); published online EpubMay (10.1128/JVI.00187-09).

36. J. J. Furth, S. S. Cohen, Inhibition of mammalian DNA polymerase by the 5'-triphosphate of 1-beta-d-arabinofuranosylcytosine and the 5'-triphosphate of 9-beta-d-arabinofuranoxyladenine. *Cancer Res* **28**, 2061 (1968); published online EpubOct (

37. F. M. Schabel, Jr., The antiviral activity of 9-beta-D-arabinofuranosyladenine (ARA-A). *Chemotherapia (Basel)* **13**, 321 (1968).

38. K. Sliva, J. Martin, C. von Rhein, T. Herrmann, A. Weyrich, M. Toda, B. S. Schnierle, Interference with SAMHD1 restores late gene expression of modified vaccinia virus Ankara (MVA) in human dendritic cells and abrogates type I interferon expression. *Journal of virology*, (2019); published online EpubAug 28 (10.1128/JVI.01097-19).

39. S. S. Broyles, Vaccinia virus transcription. *The Journal of general virology* **84**, 2293 (2003); published online EpubSep (10.1099/vir.0.18942-0).

40. E. M. Kane, S. Shuman, Adenosine N1-oxide inhibits vaccinia virus replication by blocking translation of viral early mRNAs. *Journal of virology* **69**, 6352 (1995); published online EpubOct (

41. J. Kleeff, M. Kornmann, H. Sawhney, M. Korc, Actinomycin D induces apoptosis and inhibits growth of pancreatic cancer cells. *International journal of cancer* **86**, 399 (2000); published online EpubMay 1 (10.1002/(sici)1097-0215(20000501)86:3<399::aid-ijc15>3.0.co;2-g).

42. H. Hsu, J. Huang, H. B. Shu, V. Baichwal, D. V. Goeddel, TNF-dependent recruitment of the protein kinase RIP to the TNF receptor-1 signaling complex. *Immunity* **4**, 387 (1996); published online EpubApr (10.1016/s1074-7613(00)80252-6).

43. A. T. Ting, F. X. Pimentel-Muinos, B. Seed, RIP mediates tumor necrosis factor receptor 1 activation of NF-kappaB but not Fas/APO-1-initiated apoptosis. *The EMBO journal* **15**, 6189 (1996); published online EpubNov 15 (

44. S. F. Fischer, H. Ludwig, J. Holzapfel, M. Kvansakul, L. Chen, D. C. Huang, G. Sutter, M. Knese, G. Hacker, Modified vaccinia virus Ankara protein F1L is a novel BH3-domain-binding protein and acts together with the early viral protein E3L to block virus-associated apoptosis. *Cell Death Differ* **13**, 109 (2006); published online EpubJan (10.1038/sj.cdd.4401718).

45. D. L. Veyer, G. Carrara, C. Maluquer de Motes, G. L. Smith, Vaccinia virus evasion of regulated cell death. *Immunology letters* **186**, 68 (2017); published online EpubJun (10.1016/j.imlet.2017.03.015).

46. T. Ilicic, J. K. Kim, A. A. Kolodziejczyk, F. O. Bagger, D. J. McCarthy, J. C. Marioni, S. A. Teichmann, Classification of low quality cells from single-cell RNA-seq data. *Genome biology* **17**, 29 (2016); published online EpubFeb 17 (10.1186/s13059-016-0888-1).

47. A. Schwab, S. S. Meyering, B. Lepene, S. Iordanskiy, M. L. van Hoek, R. M. Hakami, F. Kashanchi, Extracellular vesicles from infected cells: potential for direct pathogenesis. *Frontiers in microbiology* **6**, 1132 (2015).

48. H. S. Chahar, X. Bao, A. Casola, Exosomes and their role in the life cycle and pathogenesis of RNA viruses. *Viruses* **7**, 3204 (2015).

49. S. R. Baglio, M. A. van Eijndhoven, D. Koppers-Lalic, J. Berenguer, S. M. Lougheed, S. Gibbs, N. Léveillé, R. N. Rinkel, E. S. Hopmans, S. Swaminathan, Sensing of latent EBV infection through exosomal transfer of 5′ pppRNA. *Proceedings of the National Academy of Sciences* **113**, E587 (2016).

50. C. Colby, C. Jurale, J. R. Kates, Mechanism of synthesis of vaccinia virus double-stranded ribonucleic acid in vivo and in vitro. *Journal of virology* **7**, 71 (1971); published online EpubJan (

51. K. V. Kibler, T. Shors, K. B. Perkins, C. C. Zeman, M. P. Banaszak, J. Biesterfeldt, J. O. Langland, B. L. Jacobs, Double-stranded RNA is a trigger for apoptosis in vaccinia virus-infected cells. *Journal of virology* **71**, 1992 (1997); published online EpubMar (

52. Q. Sun, L. Sun, H. H. Liu, X. Chen, R. B. Seth, J. Forman, Z. J. Chen, The specific and essential role of MAVS in antiviral innate immune responses. *Immunity* **24**, 633 (2006); published online EpubMay (10.1016/j.immuni.2006.04.004).

53. A. Dalet, R. J. Argüello, A. Combes, L. Spinelli, S. Jaeger, M. Fallet, T. P. Vu Manh, A. Mendes, J. Perego, M. Reverendo, V. Camosseto, M. Dalod, T. Weil, M. A. Santos, E.

Gatti, P. Pierre, Protein synthesis inhibition and GADD34 control IFN-β heterogeneous expression in response to dsRNA. *The EMBO journal* **36**, 761 (2017); published online EpubMar 15 (10.15252/embj.201695000).

54. J. L. Najera, C. E. Gomez, E. Domingo-Gil, M. M. Gherardi, M. Esteban, Cellular and biochemical differences between two attenuated poxvirus vaccine candidates (MVA and NYVAC) and role of the C7L gene. *Journal of virology* **80**, 6033 (2006); published online EpubJun (10.1128/JVI.02108-05).

55. S. Greiner, J. Y. Humrich, P. Thuman, B. Sauter, G. Schuler, L. Jenne, The highly attenuated vaccinia virus strain modified virus Ankara induces apoptosis in melanoma cells and allows bystander dendritic cells to generate a potent anti-tumoral immunity. *Clin Exp Immunol* **146**, 344 (2006); published online EpubNov (10.1111/j.1365-2249.2006.03177.x).

56. M. Ohmer, A. Weber, G. Sutter, K. Ehrhardt, A. Zimmermann, G. Hacker, Anti-apoptotic Bcl-XL but not Mcl-1 contributes to protection against virus-induced apoptosis. *Cell Death Dis* **7**, e2340 (2016); published online EpubAug 18 (10.1038/cddis.2016.242).

57. M. Wolferstätter, M. Schweneker, M. Späth, S. Lukassen, M. Klingenberg, K. Brinkmann, U. Wielert, H. Lauterbach, H. Hochrein, P. Chaplin, M. Suter, J. Hausmann, Recombinant modified vaccinia virus Ankara generating excess early double-stranded RNA transiently activates protein kinase R and triggers enhanced innate immune responses. *Journal of virology* **88**, 14396 (2014); published online EpubDec (10.1128/jvi.02082-14).

58. S. Chattopadhyay, J. T. Marques, M. Yamashita, K. L. Peters, K. Smith, A. Desai, B. R. Williams, G. C. Sen, Viral apoptosis is induced by IRF-3-mediated activation of Bax. *The EMBO journal* **29**, 1762 (2010); published online EpubMay 19 (10.1038/emboj.2010.50).

59. N. Manel, B. Hogstad, Y. Wang, D. E. Levy, D. Unutmaz, D. R. Littman, A cryptic sensor for HIV-1 activates antiviral innate immunity in dendritic cells. *Nature* **467**, 214 (2010); published online EpubSep 9 (10.1038/nature09337).

60. M. Gentili, X. Lahaye, F. Nadalin, G. P. F. Nader, E. Puig Lombardi, S. Herve, N. S. De Silva, D. C. Rookhuizen, E. Zueva, C. Goudot, M. Maurin, A. Bochnakian, S. Amigorena, M. Piel, D. Fachinetti, A. Londoño-Vallejo, N. Manel, The N-Terminal Domain of cGAS Determines Preferential Association with Centromeric DNA and Innate Immune Activation in the Nucleus. *Cell reports* **26**, 2377 (2019); published online EpubFeb 26 (10.1016/j.celrep.2019.01.105).

61. S. A. Rawlings, F. Alonzo, 3rd, L. Kozhaya, V. J. Torres, D. Unutmaz, Elimination of HIV-1-Infected Primary T Cell Reservoirs in an In Vitro Model of Latency. *PloS one* **10**, e0126917 (2015)10.1371/journal.pone.0126917).

62. H. Meyer, G. Sutter, A. Mayr, Mapping of deletions in the genome of the highly attenuated vaccinia virus MVA and their influence on virulence. *The Journal of general*

virology **72 (Pt 5)**, 1031 (1991); published online EpubMay (10.1099/0022-1317-72-5-1031).

63. M.-C. Michallet, E. Meylan, M. A. Ermolaeva, J. Vazquez, M. Rebsamen, J. Curran, H. Poeck, M. Bscheider, G. Hartmann, M. König, TRADD protein is an essential component of the RIG-like helicase antiviral pathway. *Immunity* **28**, 651 (2008).

64. T. Satoh, N. Manel, Gene transduction in human monocyte-derived dendritic cells using lentiviral vectors. *Methods Mol Biol* **960**, 401 (2013)10.1007/978-1-62703-218-6_30).

65. B. C. Gil-Torregrosa, A. M. Lennon-Dumenil, B. Kessler, P. Guermonprez, H. L. Ploegh, D. Fruci, P. van Endert, S. Amigorena, Control of cross-presentation during dendritic cell maturation. *European journal of immunology* **34**, 398 (2004); published online EpubFeb (10.1002/eji.200324508).

66. X. Lahaye, T. Satoh, M. Gentili, S. Cerboni, C. Conrad, I. Hurbain, A. El Marjou, C. Lacabaratz, J. D. Lelievre, N. Manel, The capsids of HIV-1 and HIV-2 determine immune detection of the viral cDNA by the innate sensor cGAS in dendritic cells. *Immunity* **39**, 1132 (2013); published online EpubDec 12 (10.1016/j.immuni.2013.11.002).

67. A. T. L. Lun, S. Riesenfeld, T. Andrews, T. P. Dao, T. Gomes, J. participants in the 1st Human Cell Atlas, J. C. Marioni, EmptyDrops: distinguishing cells from empty droplets in droplet-based single-cell RNA sequencing data. *Genome biology* **20**, 63 (2019); published online EpubMar 22 (10.1186/s13059-019-1662-y).

68. L. Haghverdi, A. T. L. Lun, M. D. Morgan, J. C. Marioni, Batch effects in single-cell RNA-sequencing data are corrected by matching mutual nearest neighbors. *Nature biotechnology* **36**, 421 (2018); published online EpubJun (10.1038/nbt.4091).

69. L. Lovmar, A. Ahlford, M. Jonsson, A. C. Syvanen, Silhouette scores for assessment of SNP genotype clusters. *BMC genomics* **6**, 35 (2005); published online EpubMar 10 (10.1186/1471-2164-6-35).

70. Z. Yang, S. Cao, C. A. Martens, S. F. Porcella, Z. Xie, M. Ma, B. Shen, B. Moss, Deciphering poxvirus gene expression by RNA sequencing and ribosome profiling. *Journal of virology* **89**, 6874 (2015); published online EpubJul (10.1128/JVI.00528-15).

71. G. Antoine, F. Scheiflinger, F. Dorner, F. G. Falkner, The complete genomic sequence of the modified vaccinia Ankara strain: comparison with other orthopoxviruses. *Virology* **244**, 365 (1998); published online EpubMay 10 (10.1006/viro.1998.9123).

72. Z. Yang, D. P. Bruno, C. A. Martens, S. F. Porcella, B. Moss, Genome-wide analysis of the 5' and 3' ends of vaccinia virus early mRNAs delineates regulatory sequences of annotated and anomalous transcripts. *Journal of virology* **85**, 5897 (2011); published online EpubJun (10.1128/JVI.00428-11).

73. Z. Yang, C. A. Martens, D. P. Bruno, S. F. Porcella, B. Moss, Pervasive initiation and 3'-end formation of poxvirus postreplicative RNAs. *The Journal of biological chemistry* **287**, 31050 (2012); published online EpubSep 7 (10.1074/jbc.M112.390054).

74. G. Finak, A. McDavid, M. Yajima, J. Deng, V. Gersuk, A. K. Shalek, C. K. Slichter, H. W. Miller, M. J. McElrath, M. Prlic, P. S. Linsley, R. Gottardo, MAST: a flexible statistical framework for assessing transcriptional changes and characterizing heterogeneity in single-cell RNA sequencing data. *Genome biology* **16**, 278 (2015); published online EpubDec 10 (10.1186/s13059-015-0844-5).

75. G. Yu, L. G. Wang, G. R. Yan, Q. Y. He, DOSE: an R/Bioconductor package for disease ontology semantic and enrichment analysis. *Bioinformatics* **31**, 608 (2015); published online EpubFeb 15 (10.1093/bioinformatics/btu684).

Acknowledgments: We thank the Genomics Facility, the Bioinformatics Facility, the Cytometry Facility, the Electron Microscopy platform (PICT-IBiSA, France-BioImaging, Labex CelTisPhyBio ANR-10-LBX-0038 and ANR-10-INSB-04) at Institut Curie, Francesca Ruscetti, Tarek Gharsalli, Derya Unutmaz for providing the BCL2 plasmid, Christine Lacabaratz for providing MVA stocks, Ulrich Kalinke and Annett Ziegler for providing *Mavs*$^{-/-}$ bone marrow, Philippe Benaroch and Clotilde Théry for scientific discussions, Flavien Brouiller for cDC2s sorting, Pierre Gestraud for expertise on statistical analysis. **Funding**: This work was supported by LABEX VRI (ANR-10-LABX-77), LABEX DCBIOL (ANR-10-IDEX-0001-02 PSL* and ANR-11-LABX-0043), ANRS (France Re-cherche Nord & Sud Sida-hiv Hépatites; ECTZ25472, ECTZ36691, ECTZ71745), Sidaction (VIH2016126002, 17-1-AAE-11097-2), ANR (ANR-17-CE15-0025-01, ANR-14-CE14-0004-02, ANR-19-CE15-0018-01, ANR-18-CE92-0022-01), ITMO (19CS007-00), DIM1HEALTH to N.M.. M.D. was supported with a fellowship from the German Research Foundation (DFG, DO 2152/1-1). NS was supported with a fellowship from the EMBO (1298_2016) and from the European Commission (H2020-MSCA-IF-2016 DCBIO) **Author contributions**: MD and NM designed the study and wrote the manuscript. MD conducted most experiments. TS performed preliminary experiments. MG contributed to molecular cloning. XL performed parts of some experiments. NS contributed to experiment with murine primary cells. GB performed experiments with cDC2s and *Mavs*$^{-/-}$ BMDCs. CC provided technical help. KA and FN performed computational analyses. MJ did electron microscopy experiments. MC contributed to scientific project management. YL contributed to design and supervision of the project. **Competing Interests:** The authors declare no competing interests. **Data and materials availability**: The accession number for the raw sequencing data files is NCBI GEO: GSE153835. The scripts used for analysis are available at https://github.com/Manel-Lab/MVA_DC_scRNAseq. MVAGFP and MVAmCherry must be obtained through an MTA with ANRS. All other data needed to evaluate the conclusions in the paper are present in the paper or the Supplementary Materials.

Figure legends

Fig. 1. MVA infection of MDDCs induces type I IFN and TNF-α that activate uninfected bystanders.

(A to C) CD86, Siglec-1 and MVAGFP expression of MDDCs 24 hours after infection (hpi) with MVA (at 0.3 or 1 MOI). NI = non-infected. Data from n=10 donors from five independent experiments. **(D)** Secretion of type I (IFN-β and IFN-α2) and type III IFN (IFN-λ1), TNF-α, and IL-6 by MDDCs 24 hpi with MVA. Data are from n=6 donors from three independent experiments. **(E to G)** Single-cell RNA sequencing analysis of MVA-infected MDDCs. (E) Feature plots depicting log-normalized gene expression of mCherry and vUMI/tUMI in UMAPs of the MNN reduction. vUMI/tUMI represents the ratio of viral UMIs (vUMI) over total UMI (tUMI) and is a proxy for MVA gene expression. mCherry was normalized to tUMI. (F) Comparison of the normalized mCherry gene expression (red line) and the polynomial smoothing of vUMI/tUMI (black line) across cells sorted by increasing normalized value of mCherry. (G) Feature plots depicting log-normalized gene expression of the indicated markers in UMAPs of the MNN reduction. **(H)** CD86, Siglec-1 and MVAGFP expression of MDDCs infected with MVA in the presence of neutralizing antibodies for type I IFN, TNF-α, or JAK/STAT inhibitor ruxolitinib (Ruxo). Data from n=8 donors from four independent experiments. Left, representative flow cytometry from the 0.3 MVA condition. In all graphs, bars indicate mean + SEM, *p<0.05, **p<0.01, ***p<0.005, ****p<0.0001, by (B and I) two-way ANOVA with Geisser-Greenhouse and Sidak's correction or (C and D) Kruskal-Wallis test with Dunn's correction for multiple comparison.

Fig. 2. Inflammatory cytokines and activation markers are induced by the cGAS-STING-IRF3 axis in MVA-infected MDDCs.

(A) CD86 and Siglec-1 expression by flow cytometry (middle, n=12 donors from six independent experiments), and secretion of IFN-β and IFN-λ1 measured by ELISA (right, n=8 donors in four independent experiments) in MDDCs transduced at day 0 with a control shRNA against LacZ or an shRNA against cGAS, combined with Vpx-containing VLPs, 24 hpi with MVA (0.3 or 1 MOI) or upon stimulation with HTDNA (1 or 3 µg/ml). NI = non-infected; NT = non-treated. Left, representative flow cytometry from the 0.3 MVA condition. **(B)** As described in (A), in MDDCs pretreated for 1 hour with STINGi (H-151, 20µM) or a comparable concentration of DMSO 24 hpi with MVA or upon stimulation with cGAMP (1.2 or 4 µg/ml). n=6 donors from three independent experiments. **(C)** As described in (A), in MDDCs expressing BFP or of dominant-negative IRF3 (IRF3DN). Flow cytometry, n=12 donors from 6 independent experiments; ELISA, n=6 donors from three independent experiments. In all graphs, bars indicate mean + SEM, *p<0.05, **p<0.01, ***p<0.005, ****p<0.0001, by two-way ANOVA with Geisser-Greenhouse and Sidak's correction.

Fig. 3. SAMHD1 prevents MVA replication and limits antigen expression in MDDCs.

(A) Proportion of MVA gene classes (early, intermediate, and late) of the viral UMIs per cell. Cells were sorted by increasing value of mCherry (normalized to total UMIs, black line); cells with less than 10 viral UMIs and no mCherry gene expression were filtered out. Total cells combined from both donors are shown (donor 1 562 cells and donor 2 578 cells). **(B)** SAMHD1 expression in MDDCs treated with empty or VPX-containing VLPs. Data from n=6 donors from 3 independent experiments. Left, representative flow cytometry. **(C)** MVAGFP expression (MVA_{med} and MVA_{hi} gates) on SAMHD1-positive or SAMHD1-negative MDDCs treated with VPX-containing VLPs, 24 hpi with MVA (0.3 or 1 MOI). NI = non-infected. Left, representative flow cytometry from NI and 1 MVA. **(D)** MVAGFP expression in MDDCs as described in (C), after treatment with cytarabine (10 µM, AraC) or no treatment. Left, representative flow cytometry from 1 MVA condition. **(E)** Abundance of MVA genes E9L and POX in MDDCs as described in (C). In (B to E) n=6 donors from three independent experiments. **(F)** p24 concentration in supernatants of MDDCs treated as in (C) and infected with with MVA-HIVB from . n=8 donors from four independent experiments. **(G)** MVAGFP expression in control (LacZ shRNA) and SAMHD1 KD (shRNA #1 and #5) MDDCs 24 hpi with MVA (0.3 or 1 MOI). Left, representative flow cytometry from 0.3 MVA conditions. n=6 donors from three independent experiments. In all graphs, bars indicate mean + SEM, *p<0.05, **p<0.01, ***p<0.005, ****p<0.0001, by (B) Wilcoxon matched-pairs signed rank test or by (C to F) two-way ANOVA with Geisser-Greenhouse and Sidak's correction.

Fig. 4. Inflammatory cytokines are induced by the incoming genome and enhanced by viral gene expression.

(A) CD86 and Siglec-1 expression in MDDCs 24 hpi with MVA (0.3 or 1 MOI), UV irradiated MVA and MVA in the presence of adenosine N_1-oxide. Left, representative flow cytometry from MVA 0.3 condition. NI = non-infected. **(B)** Concentrations of IFN-β and TNF-α in supernatants of MDDCs as described in (A). In all graphs, n=6 donors from three independent experiments, bars indicate mean + SEM, *p<0.05, **p<0.01, ***p<0.005, ****p<0.0001, by two-way ANOVA with Geisser-Greenhouse and Sidak's correction.

Fig. 5. MVA-infected MDDCs die of non-redundant apoptosis.

(A) Overlay montage of time lapse microscopy showing the bright field and GFP channel of MVA infected MDDCs from 0-14 hpi. Arrowheads indicate cells that first show MVA early gene expression (4 hpi), blebbing (6–8 hpi), and sign of apoptotic cell death (10–14 hpi). Scale bar 25 µm, representative donor from five in three independent experiments. **(B)** Annexin V and MVAmCherry expression in MDDCs 24 hpi with MVA (0.3 or 1 MOI) from n=5 donors from two independent experiments. Left, representative flow cytometry. NI = non-infected. **(C to D)** LIVE/DEAD labeling (upper panel) and FSC/SSC characteristics (lower panel) of MDDCs 24 hpi with MVA (0.3 or 1 MOI). (C) Treatment with DMSO or Q-VD-Oph (25 µM). (D) Treatment with DMSO or BoCD (25 µM). In (B to D), n=6 donors from three independent experiments. Left,

representative flow cytometry of the indicated conditions. **(E)** FSC/SSC characteristics, LIVE/DEAD labeling, expression of CD86, Siglec-1 and MVAGFP in MDDCs transduced with a control vector or with a BCL2-encoding vector 24 hpi with MVA (0.3 or 1 MOI). Left, representative flow cytometry of the 0.3 MVA condition. Right, graphs from n=8 donors from four independent experiments. **(F)** Electron micrographs of MDDCs as described in (E). NT = non-transduced. Scale bars from left to right at 10 µm, 2 µm and 5 µm. Representative images from 3 donors. C to E, *p<0.05, **p<0.01, ***p<0.005, ****p<0.0001, by two-way ANOVA with Geisser-Greenhouse and Sidak's correction.

Fig. 6. scRNA-seq identifies the transcriptional signature of infected, bystander and dead cells.

(A) UMAP colored by cell cluster number from scRNA-seq of MDDCs 24 hpi with MVA at 0.5 MOI. **(B)** mCherry gene expression, viral and cellular UMIs and the ratio thereof. **(C)** Expression levels of indicated mitochondrial genes. **(D)** Expression of *PMAIP1*, *IFNL1*, *IFNB1* and *TNFA*. **(E)** Expression of *CXCL10*, *ISG15*, *CD86* and *SIGLEC-1*. In (B-D) numbers indicate the cell cluster in the MVA-infected condition. NI = non-infected. In all graphs, ****p<0.0001, detailed adjusted p-values indicated in the table S1.

Fig. 7. MVA-induced cell death relies on early gene expression and is uncoupled from IRF3 activation.

(A to C) FSC/SSC characteristics of MDDCs infected with MVA (0.3 or 1 MOI). (A) MDDCs transduced with the indicated vectors as described in Fig. 2A, 2C, S4B and S4D. (B) WT and *Cgas*$^{-/-}$ BMDCs. n=3 mice. (C) Infection in the presence of neutralizing antibodies for type I IFN. n=6 donors from three independent experiments. **(D)** FSC/SSC characteristics and LIVE/DEAD labeling of MDDCs 24 hpi with MVA (0.3 or 1 MOI) or with UV irradiated MVA. n=6 donors from three independent experiments. **(E)** MVAGFP expression, LIVE/DEAD labeling and FSC/SSC characteristics of MDDCs 24 hpi with MVA (0.3 or 1 MOI) in the presence of cycloheximide (CHX) or actinomycin D (ActD). n=8 donors from 3 independent experiments. **(F)** Average fold change of BH3-only protein coding gene expression in BFP or IRF3DN expressing MDDCs 24 hpi with MVA (0.3 or 1 MOI) or after stimulation with HTDNA (1 µg/ml) or cGAMP (1.2 µg/ml) assessed by RT-qPCR. **(G)** NOXA expression in MDDCs as described in (F). Two-way ANOVA with Geisser-Greenhouse and Sidak's correction. In (F to G) n=6 donors from three independent experiments. **(H)** Working model of interactions between the MVA vaccine vector and human MDDCs. NI = non-infected.

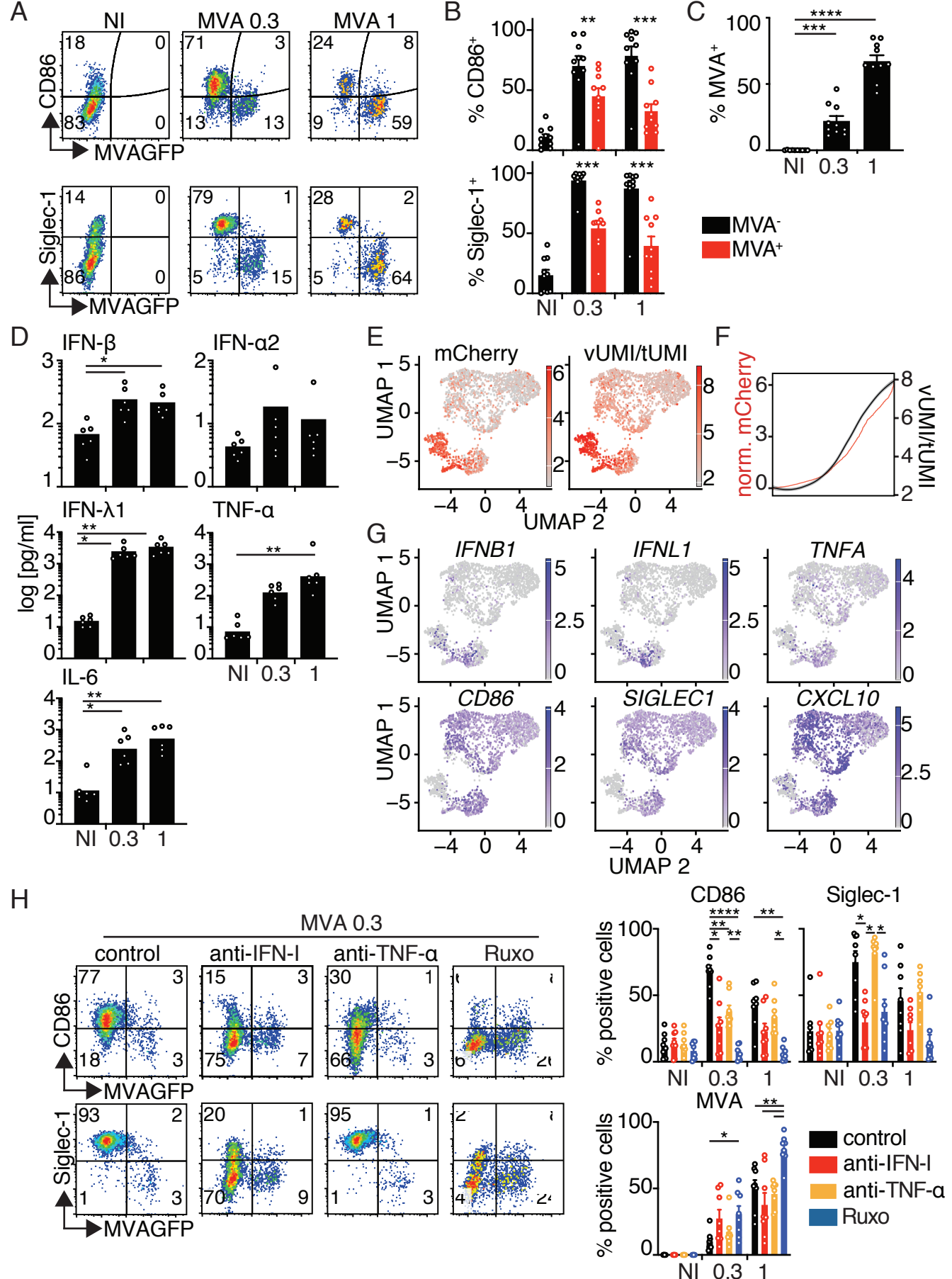
A
NI
MVA 0.3
MVA 1
CD86
MVAGFP
Siglec-1
B
% CD86+
% Siglec-1+
NI
0.3
1
C
% MVA+
MVA-
MVA+
D
IFN-β
IFN-α2
IFN-λ1
TNF-α
IL-6
log [pg/ml]
E
mCherry
vUMI/tUMI
UMAP 1
UMAP 2
F
norm. mCherry
vUMI/tUMI
G
IFNB1
IFNL1
TNFA
CD86
SIGLEC1
CXCL10
H
MVA 0.3
control
anti-IFN-I
anti-TNF-α
Ruxo
CD86
Siglec-1
% positive cells
MVA
control
anti-IFN-I
anti-TNF-α
Ruxo

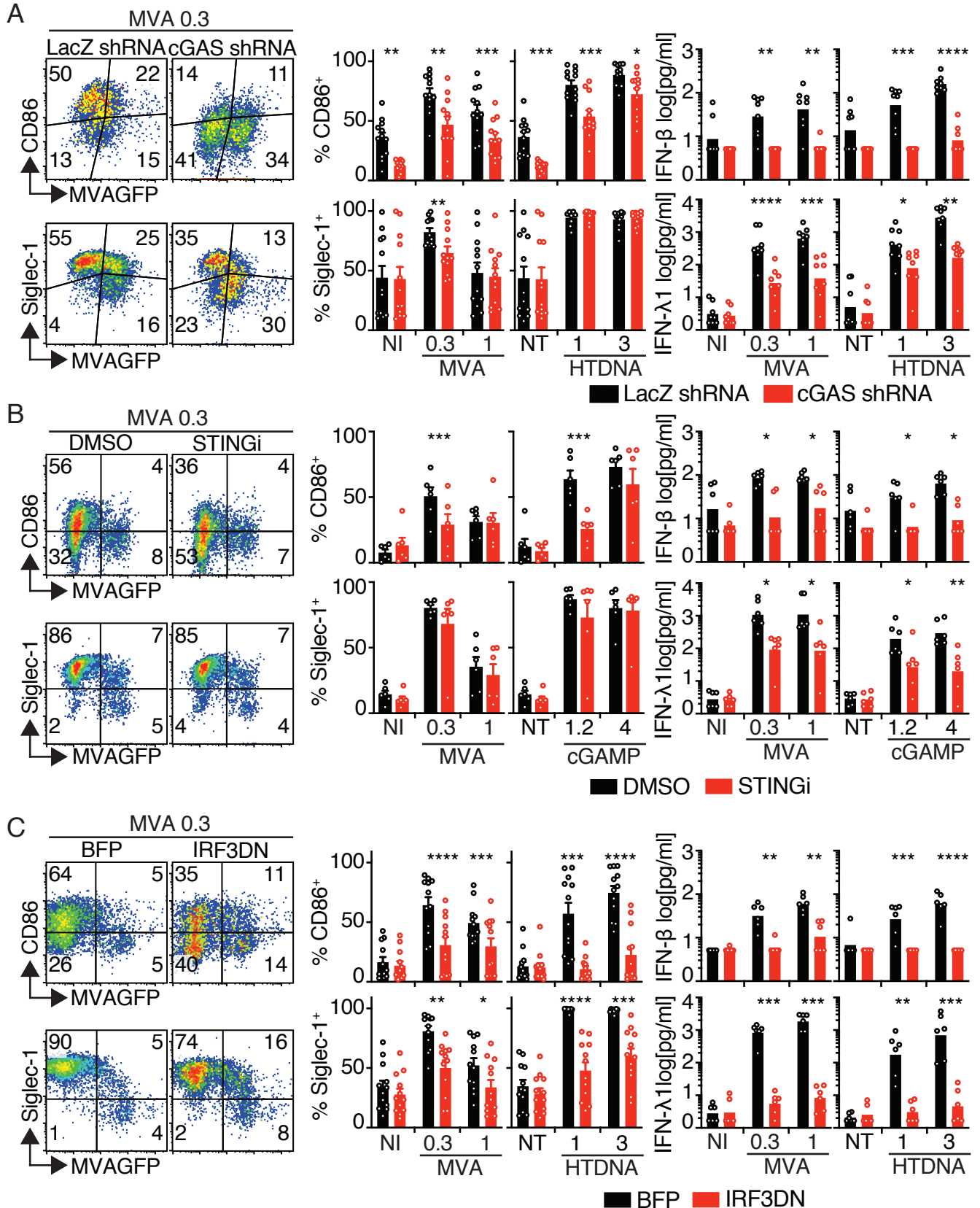
A
MVA 0.3
LacZ shRNA
cGAS shRNA
CD86
MVAGFP
Siglec-1
% CD86+
% Siglec-1+
IFN-β log[pg/ml]
IFN-λ1 log[pg/ml]
NI
0.3
1
NT
3
MVA
HTDNA
LacZ shRNA
cGAS shRNA
B
DMSO
STINGi
1.2
4
cGAMP
C
BFP
IRF3DN

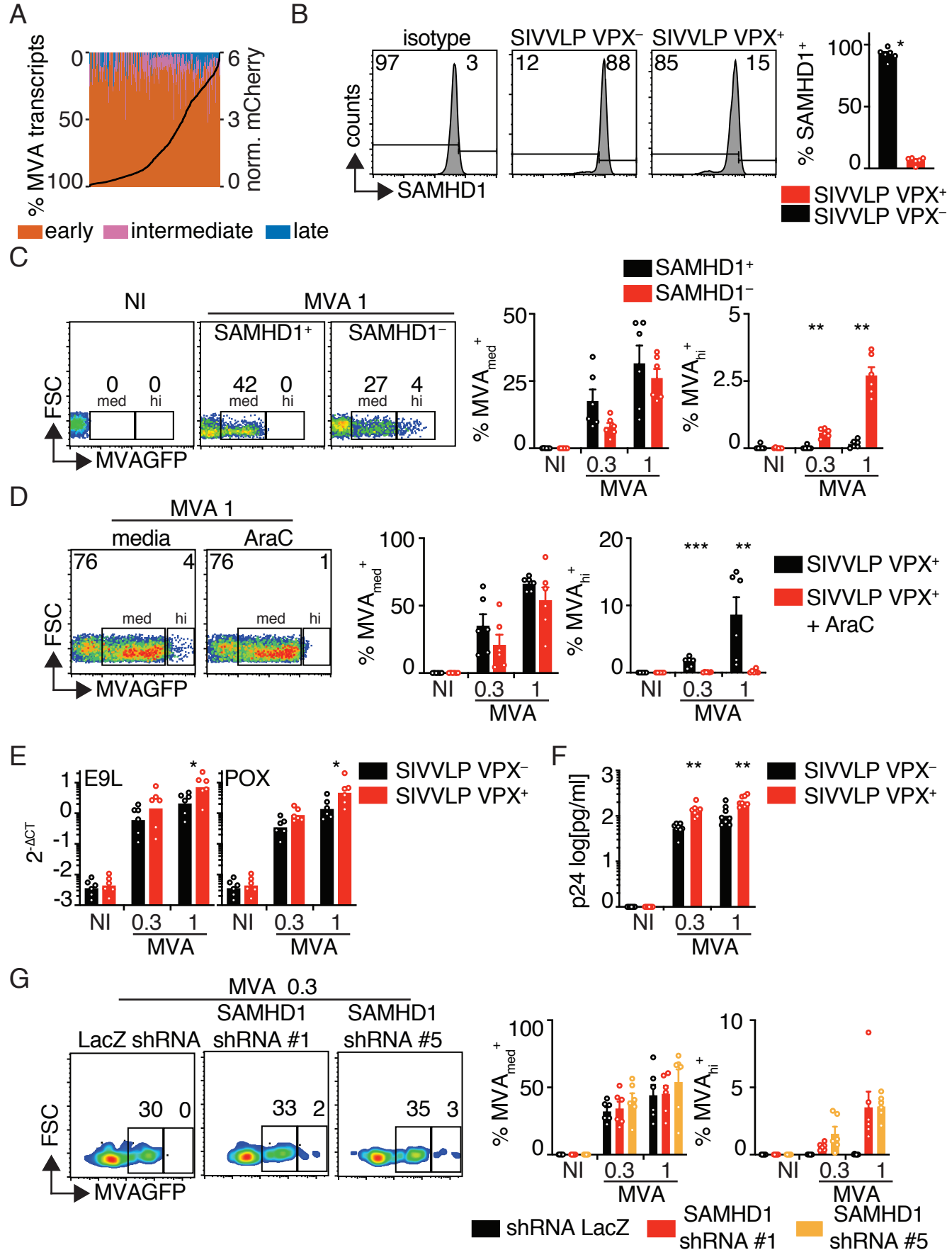
A
% MVA transcripts
norm. mCherry
early
intermediate
late
B
isotype
SIVVLP VPX⁻
SIVVLP VPX⁺
counts
SAMHD1
% SAMHD1⁺
SIVVLP VPX⁺
SIVVLP VPX⁻
C
NI
MVA 1
SAMHD1⁺
SAMHD1⁻
FSC
MVAGFP
med
hi
% MVA⁺med
% MVA⁺hi
MVA
D
media
AraC
SIVVLP VPX⁺
SIVVLP VPX⁺ + AraC
E
E9L
POX
2-ΔCT
F
p24 log[pg/ml]
G
LacZ shRNA
SAMHD1 shRNA #1
SAMHD1 shRNA #5
shRNA LacZ

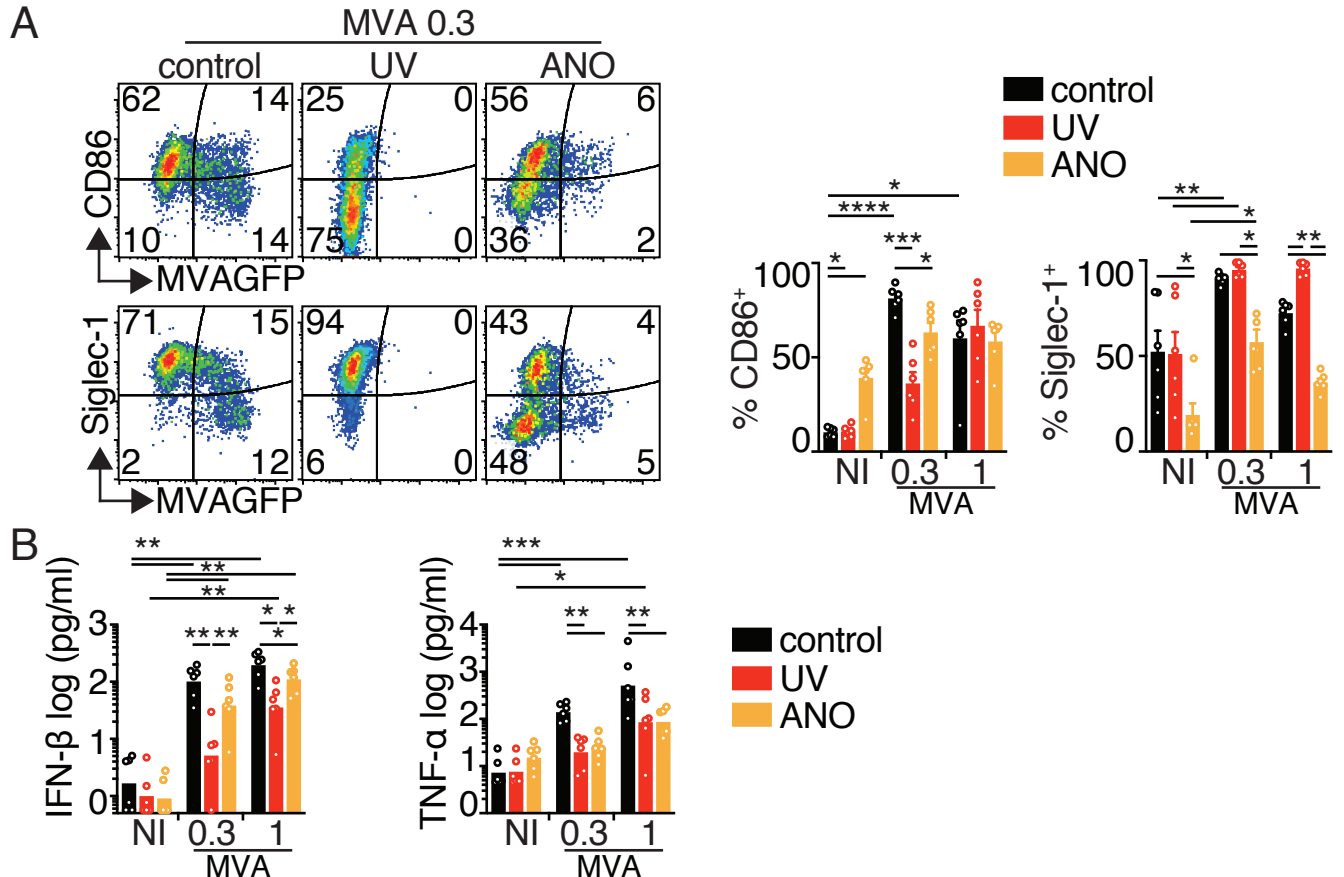
A
MVA 0.3
control
UV
ANO
CD86
MVAGFP
62
14
10
14
25
0
75
0
56
6
36
2
Siglec-1
71
15
2
12
94
0
6
0
43
4
48
5
control
UV
ANO
% CD86+
% Siglec-1+
NI
0.3
1
MVA
B
IFN-β log (pg/ml)
TNF-α log (pg/ml)

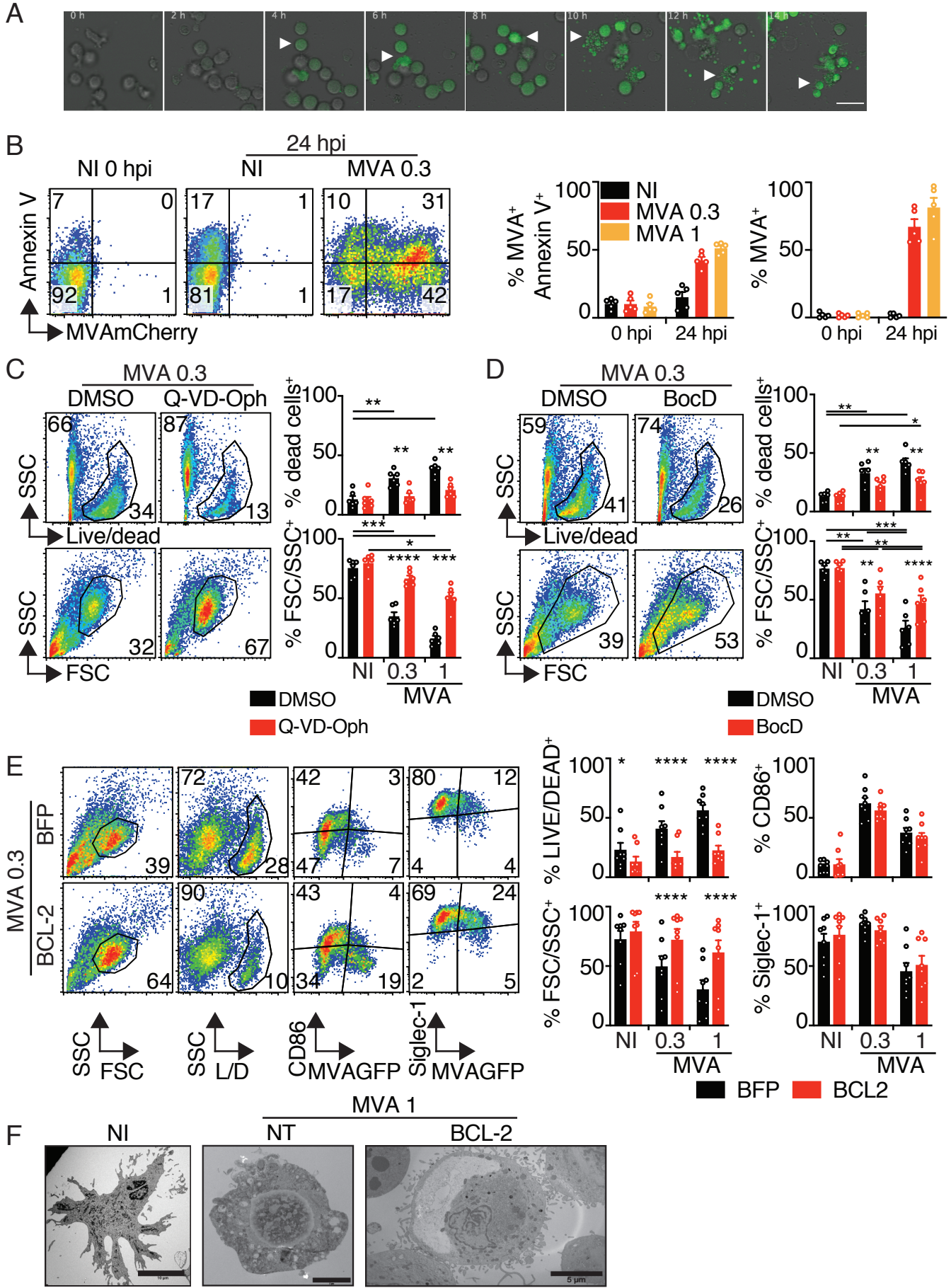
A
0 h
2 h
4 h
6 h
8 h
10 h
12 h
14 h
B
24 hpi
NI 0 hpi
NI
MVA 0.3
Annexin V
MVAmCherry
7
0
92
1
17
1
81
1
10
31
17
42
% MVA+ Annexin V+
NI
MVA 0.3
MVA 1
0 hpi
24 hpi
% MVA+
C
MVA 0.3
DMSO
Q-VD-Oph
SSC
Live/dead
FSC
66
34
87
13
32
67
% dead cells+
% FSC/SSC+
NI
0.3
1
MVA
DMSO
Q-VD-Oph
D
MVA 0.3
DMSO
BocD
59
41
74
26
39
53
BocD
E
MVA 0.3
BFP
BCL-2
72
39
28
42
3
47
7
80
12
4
4
90
64
10
43
4
34
19
69
24
2
5
SSC
FSC
L/D
CD86
MVAGFP
Siglec-1
% LIVE/DEAD+
% CD86+
% Siglec-1+
BFP
BCL2
F
MVA 1
NI
NT
BCL-2

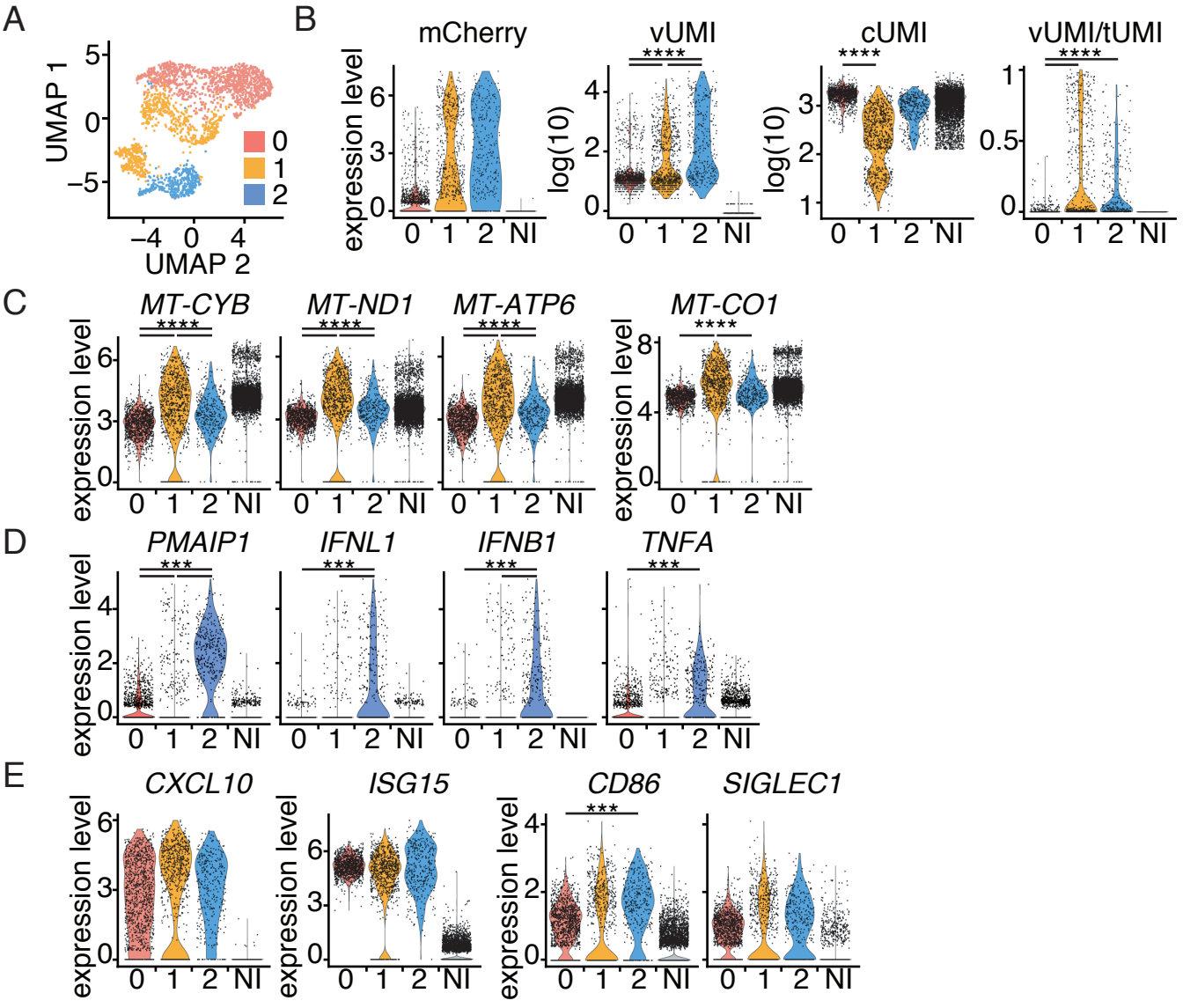
A
UMAP 1
UMAP 2
0
1
2
B
mCherry
vUMI
cUMI
vUMI/tUMI
expression level
log(10)
****
0 1 2 NI
C
MT-CYB
MT-ND1
MT-ATP6
MT-CO1
D
PMAIP1
IFNL1
IFNB1
TNFA
***
E
CXCL10
ISG15
CD86
SIGLEC1

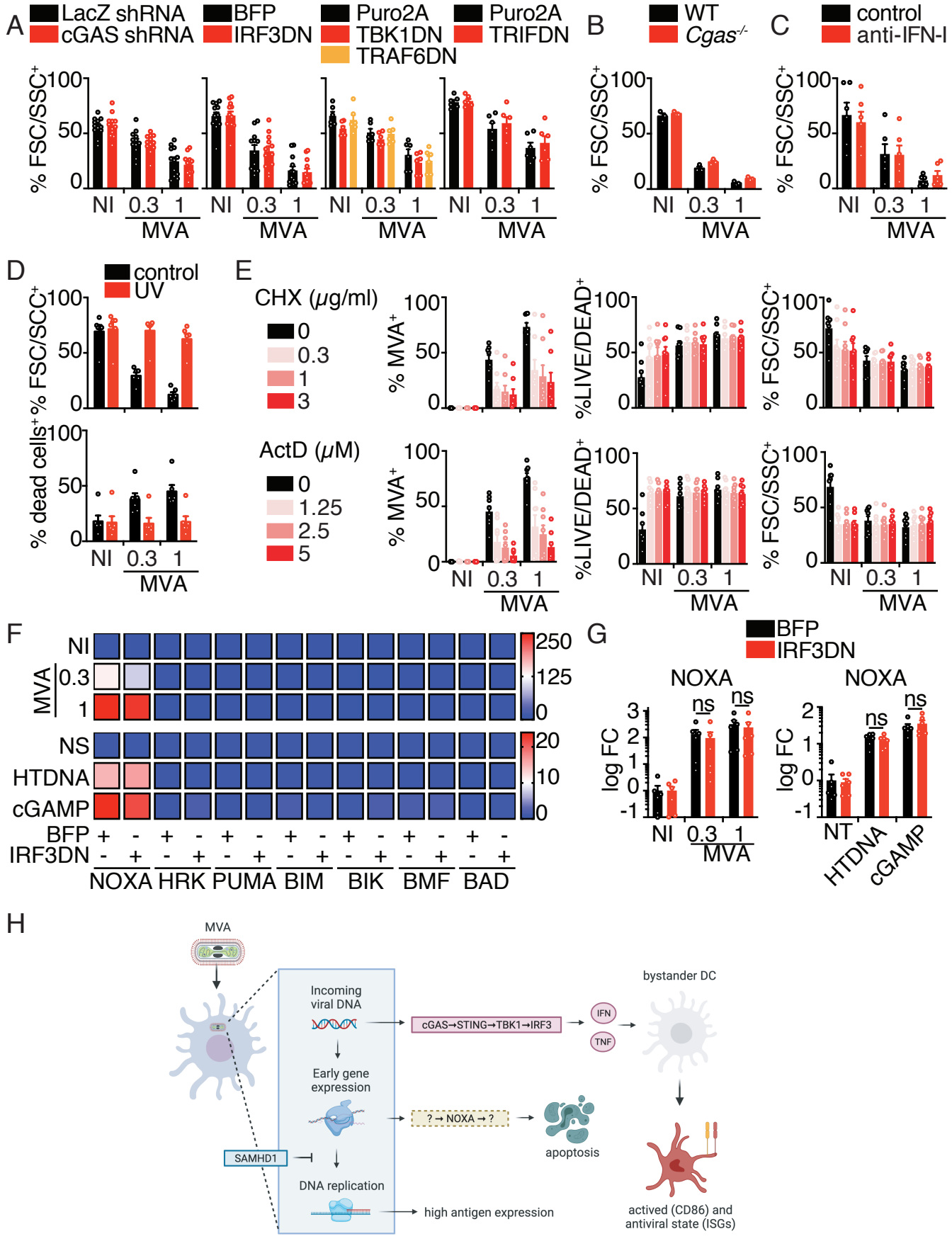
A
LacZ shRNA
cGAS shRNA
BFP
IRF3DN
Puro2A
TBK1DN
TRAF6DN
Puro2A
TRIFDN
% FSC/SSC+
NI
0.3
1
MVA
B
WT
Cgas-/-
C
control
anti-IFN-I
D
control
UV
% dead cells+
E
CHX (μg/ml)
0
0.3
1
3
ActD (μM)
0
1.25
2.5
5
% MVA+
%LIVE/DEAD+
F
MVA
NS
HTDNA
cGAMP
BFP
IRF3DN
NOXA
HRK
PUMA
BIM
BIK
BMF
BAD
G
BFP
IRF3DN
NOXA
log FC
ns
NT
H
MVA
Incoming viral DNA
cGAS→STING→TBK1→IRF3
IFN
TNF
bystander DC
Early gene expression
? → NOXA → ?
apoptosis
SAMHD1
DNA replication
high antigen expression
actived (CD86) and antiviral state (ISGs)

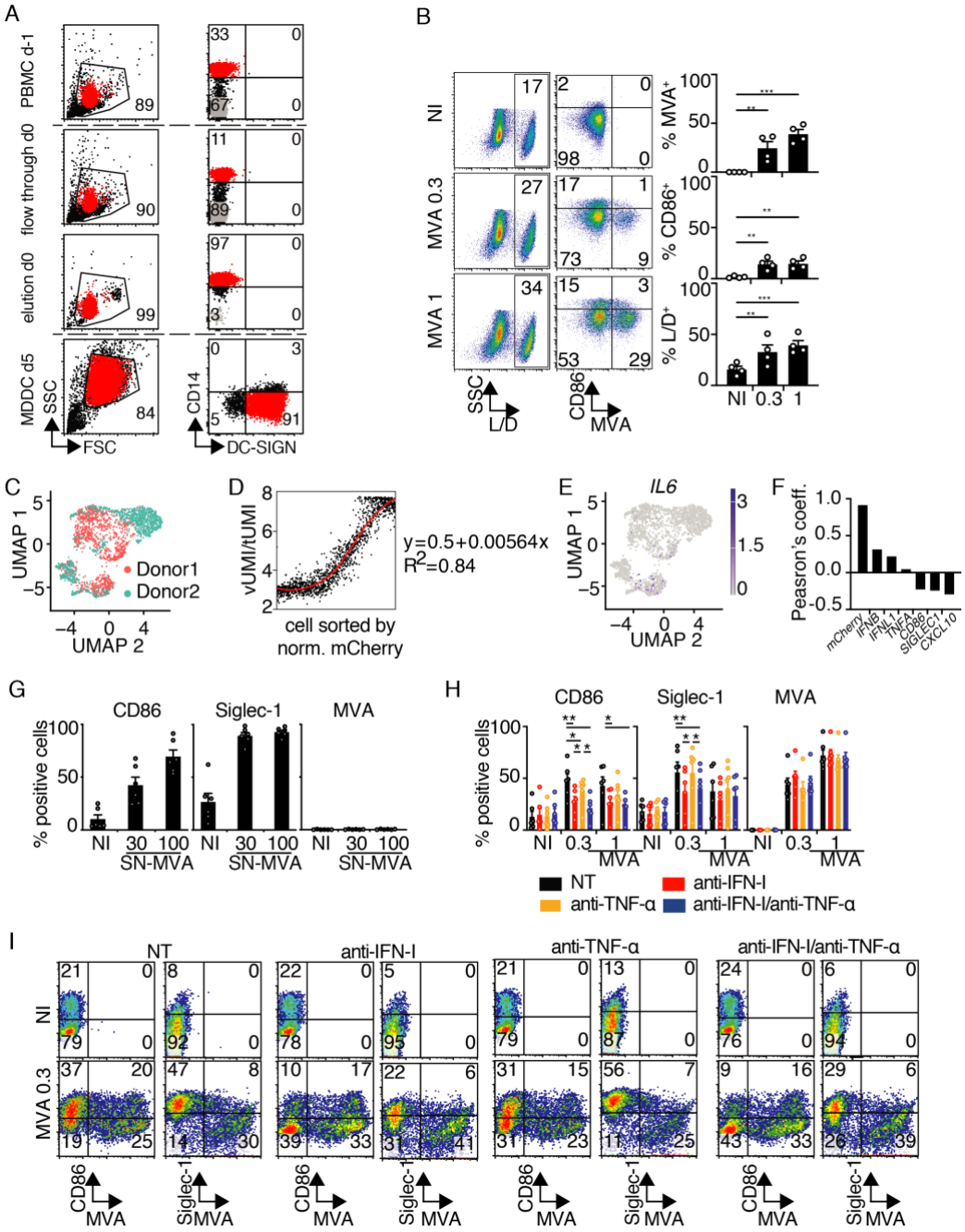

Fig. S1. Roles of TNF and IFN-I in activation of bystander cells. (A) Monocyte isolation from PBMCs on the basis of CD14 expression resulted in ~97% pure monocytes, and ~94% pure MDDC cultures. Representative data set from routinely performed immunostainings to assess purity of monocytes. **(B)** Side scatter, live/dead (L/D), CD86 and GFP expression (MVA) in cDC2s uninfected or infected with MVAGFP at MOI 0.3 or 1 (n=4 donors from 2 independent experiments, one-way ANOVA with Tukey test) **(C)** UMAP of the MNN reduction of two infected samples depicting the distribution of both donors across the three clusters. The UMAP was computed with default parameters of the Seurat function. **(D)** Polynomial smoothing of the vUMI/tUMI sorted by normalized mCherry expression depicting every cell. **(E)** Feature plot depicting log-normalized gene expression of IL6 in UMAP of the MNN reduction. **(F)** Pearson's coefficient for the co-expression of MVA genes (vUMI/tUMI) and indicated marker genes. **(G)** CD86, Siglec-1 and GFP expression (MVA) in fresh MDDCs treated with 30 µl or 100 µl filtered supernatant (SN) from MDDCs that were previously uninfected or infected with MVAGFP at MOI 1 for 24 hours. **(H)** Pseudocolor plots depicting CD86, Siglec-1, and MVAGFP expression of MDDCs infected with MVA (MOI 0.3 or 1) in the presence of neutralizing antibody cocktails against type I IFN, TNF-α or both 24 hpi. **(I)** Statistical analysis of single or combination treatment of MDDCs (n=6 donors from three independent experiments). In all graphs 0.3 and 1 indicate MOI of MVA. NI = non-infected; NT = non-treated. *p<0.05, **p<0.01, ***p<0.005 by analysis of variance (see *Methods*).

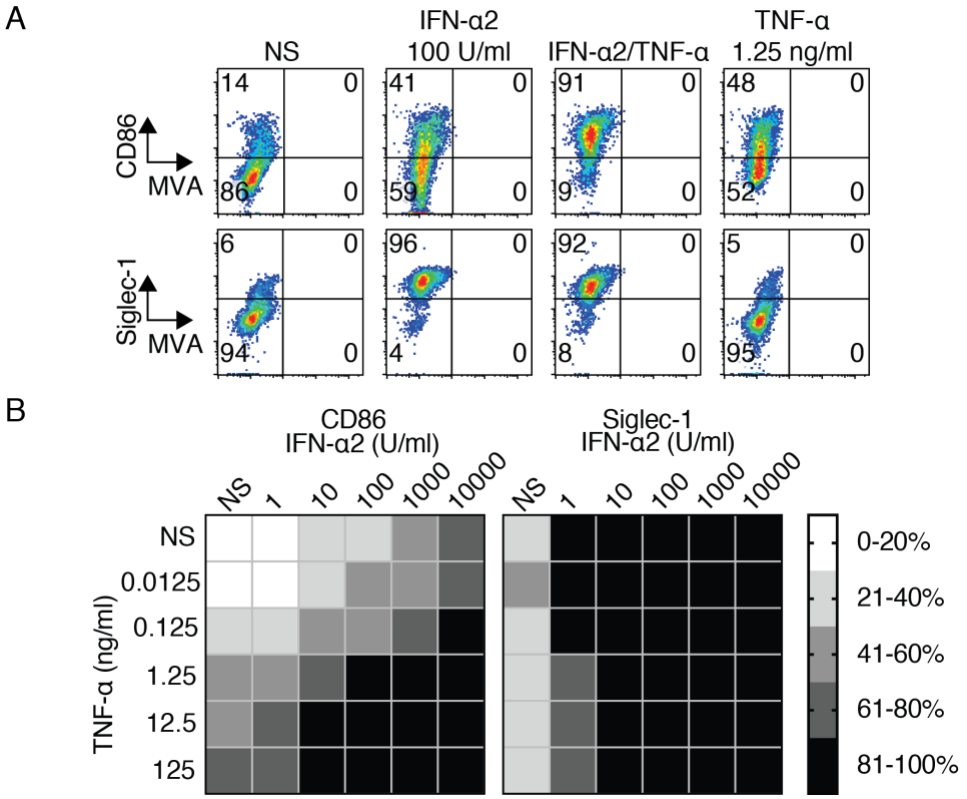

Fig. S2. Response of MDDCs to TNF and IFN-I. (A) Pseudocolor plots of CD86 (upper panel) and Siglec-1 (lower panel) expression of MDDCs stimulated with IFN-α2 (100 u/ml) and/or TNF-α (1.25 ng/ml). **(B)** Black and white heat map for CD86 (left panel) and Siglec-1 (right panel) expression of MDDC stimulated with increasing concentrations of IFN-α2 and/or TNF-α. n=7 donors from two independent experiments. Of note the stimulation with concentrations of IFN-α2 and TNF-α that would on their own not induce comparable CD86 expression synergistically induce higher CD86 expression. NS = non-stimulated.

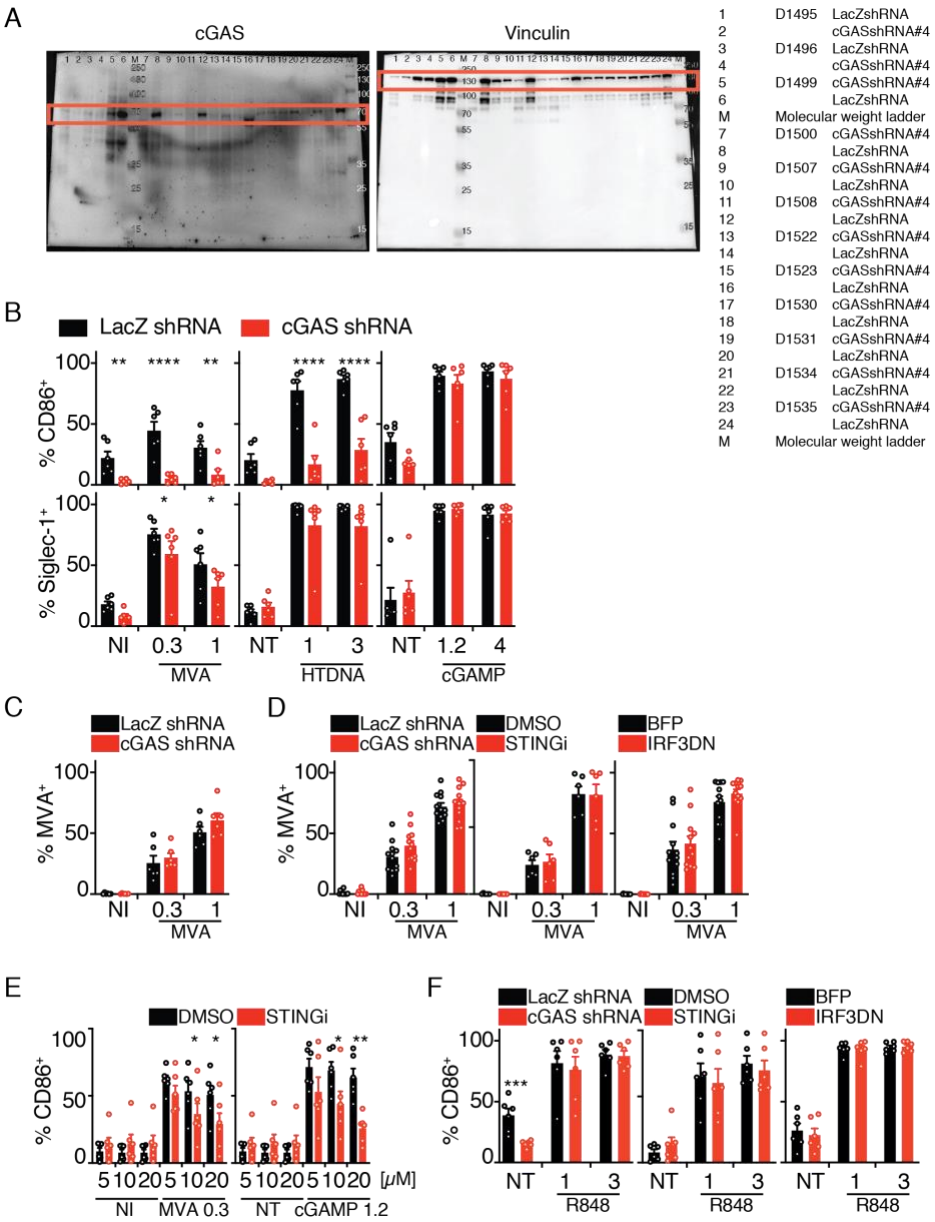

Fig. S3. Impeding with the cGAS/STING/IRF3 axis does not affect MDDC susceptibility to MVA. (A) cGAS expression in MDDCs transducted with LacZ- or cGAS-targeting shRNA (left) and their respective vinculin expression as loading control (middle). Legend to the right. **(B)** CD86 and Siglec-1 expression of cGAS KD or control MDDCs 24 hpi with MVA (left), stimulated with HTDNA (HT, middle panel), or stimulated with 2'3'-cGAMP (cG, right). **(C)** MVAGFP expression of MDDCs in (B). In (B) and (C), n=6 donors from three independent experiments. **(D)** MVAGFP expression of cGAS KD or control MDDCs (left, n=12 donors from six independent experiments), of STINGi treated MDDCs (middle, n=6 donors from three independent experiments), of IRF3DN expressing MDDCs (right, n=12 donors from 6 independent experiments). **(E)** CD86 expression in MDDCs treated with increasing amounts (5, 10, 20 µM) of STINGi upon MVA MOI 0.3 infection or upon stimulation with cGAMP 1.2 µg/ml. n=6 donors from three independent experiments **(F)** CD86 and Siglec-1 expression of cGAS KD or control MDDCs (left), of STINGi treated MDDCs (middle), of IRF3DN expressing MDDCs (right) 24 hps with R848. n=6 donors from three independent experiments. In all graphs 0.3 and 1 indicate MOI of MVA and PRR ligand concentrations are in µg/ml. NI = non-infected, NT = non-treated. *p<0.05, **p<0.01, ****p<0.0001 by analysis of variance (see *Methods*).

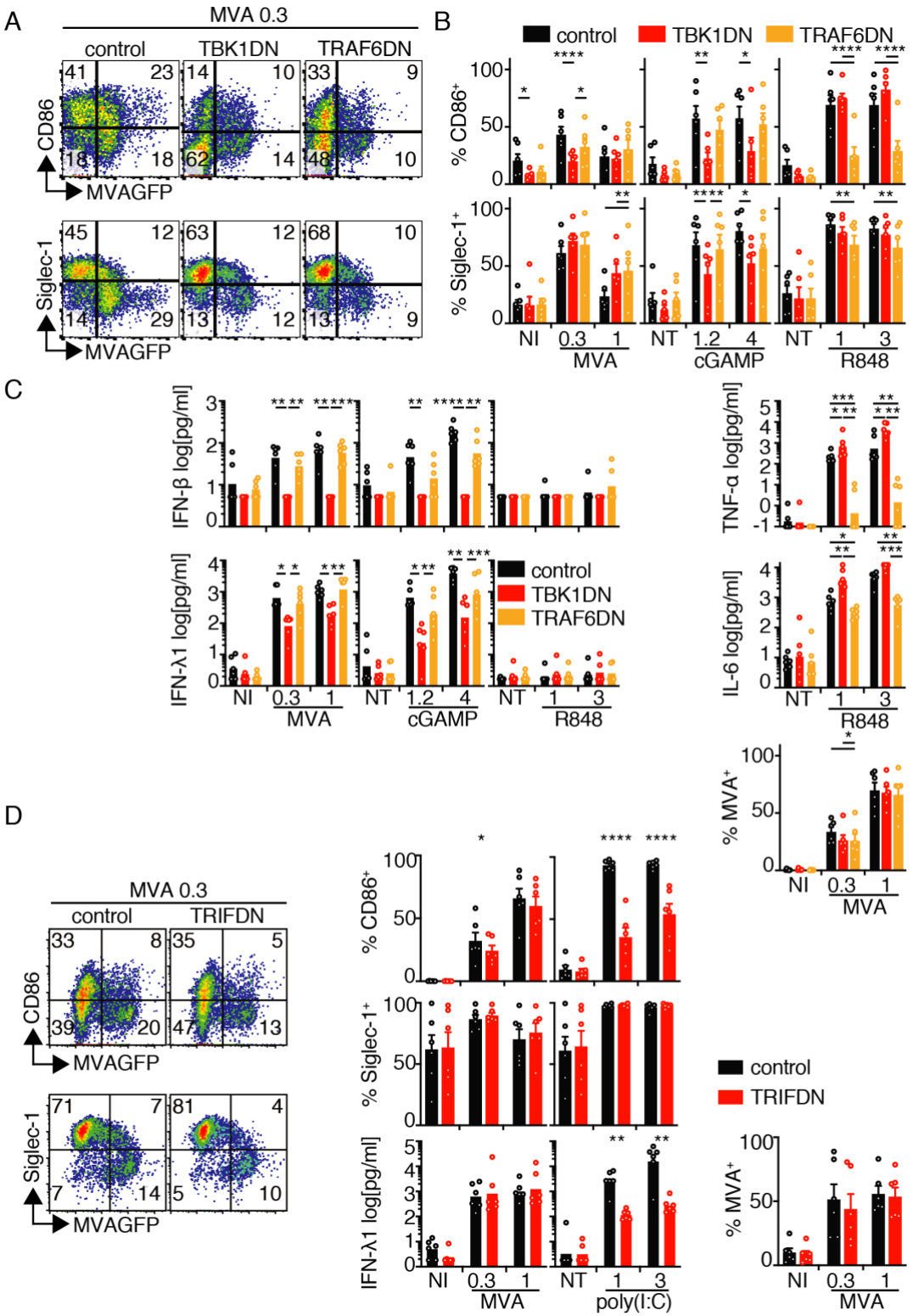

Fig. S4. TBK1 mediates signaling of MVA recognition in MDDCs, while TRAF6 and TRIF are dispensable. (A and B) CD86 and Siglec-1 expression of MDDCs transduced with control, TBK1DN, or TRAF6DN lentivectors 24 hpi with MVA or upon stimulation with either cGAMP or R848. **(C)** IFN-β and IFN-λ1, TNF-α and IL-6 secretion as well as MVAGFP expression of MDDCs in (A). **(D)** CD86 and Siglec-1 expression of MDDCs transduced with control or TRIFDN lentivectors 24 hpi with MVA or upon stimulation with poly(I:C). All panels: n=6 donors from three independent experiments; 0.3 and 1 indicate MOI of MVA; PRR ligand concentrations are µg/ml. NI = non-infected. *p<0.05, **p<0.01, ***p<0.005, ****p<0.0001 by analysis of variance (see *Methods*).

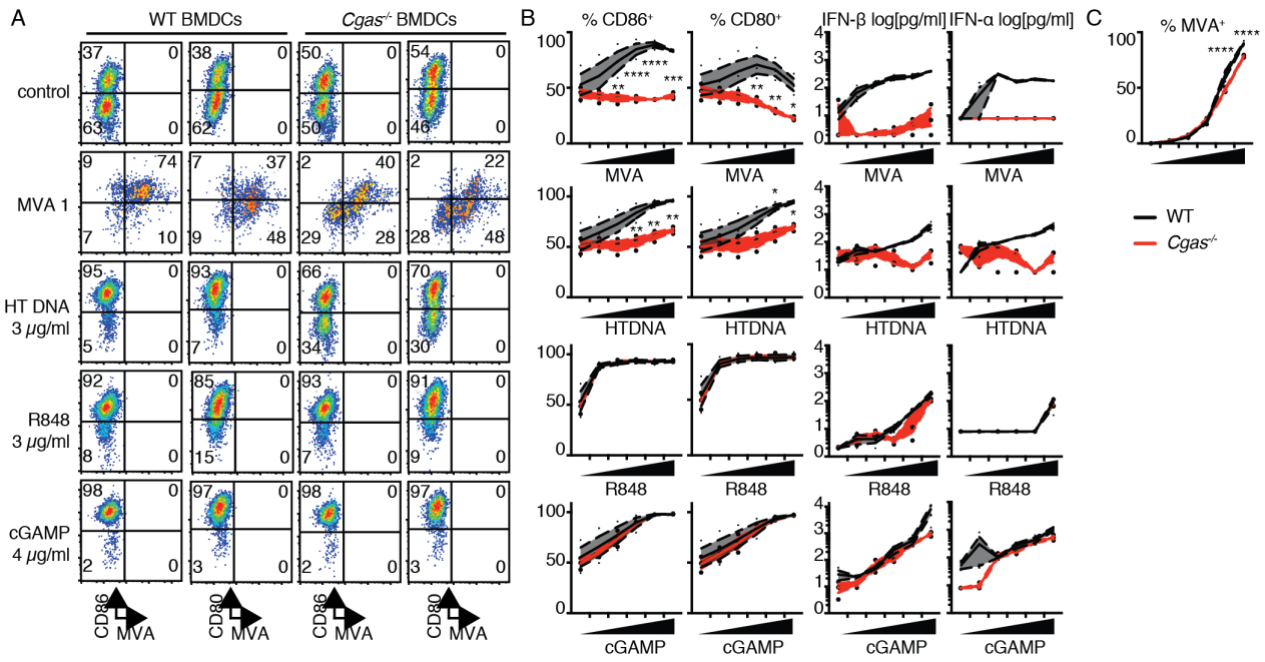

Fig. S5. BMDCs derived from *Cgas*$^{-/-}$ mice do not mount CD86/80 expression nor type I IFN responses upon MVA infection. (A) CD80, CD86, and MVAGFP expression of BMDCs 24 hpi with MVA. **(B)** Statistical analysis of CD80/86 expression, and of type I IFN expression by WT (black line) or *Cgas*$^{-/-}$ (red line) mice. BMDCs were infected with increasing amounts of MVA (MOI 0.01 to 1), or stimulated with increasing concentrations of HTDNA (0.03 to1 µg/ml), R848 (0.03-1 µg/ml), and cGAMP (0.04 to 4 µg/ml). **(C)** MVAGFP expression of WT and *Cgas*$^{-/}$ BMDCs. RM two-way ANOVA with Sidak's correction for multiple comparison. n=3 mice. *p<0.05, **p<0.01, ***p<0.005, ****p<0.0001 by analysis of variance (see *Methods*).

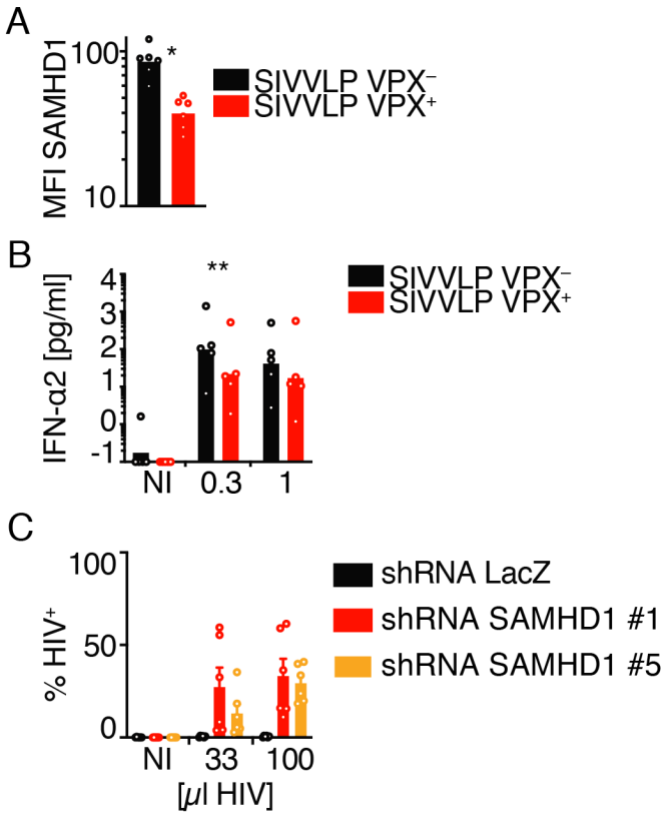

Fig. S6. Supplementary data for the analysis of SAMHD1. (A) MFI for SAMHD1 expression of MDDCs treated with empty (black bar) or VPX (red bar) containing VLPs. Wilcoxon matched-pairs signed rank test. **(B)** IFN-α2 secretion of MDDCs treated with empty (black bar) or with VPX-containing VLPs (red bar) 24 hpi with MVA. **(C)** Percent HIVGFP expressing MDDCs upon SAMHD1 KD with two different shRNAs 48 hpi with HIGGFP. In all graphs n=6 donors from three independent experiments, symbols represent single donors, and bars show mean + SEM, or geometric mean for logarithmic scales. *p<0.05, **p<0.01 by analysis of variance (see *Methods*).

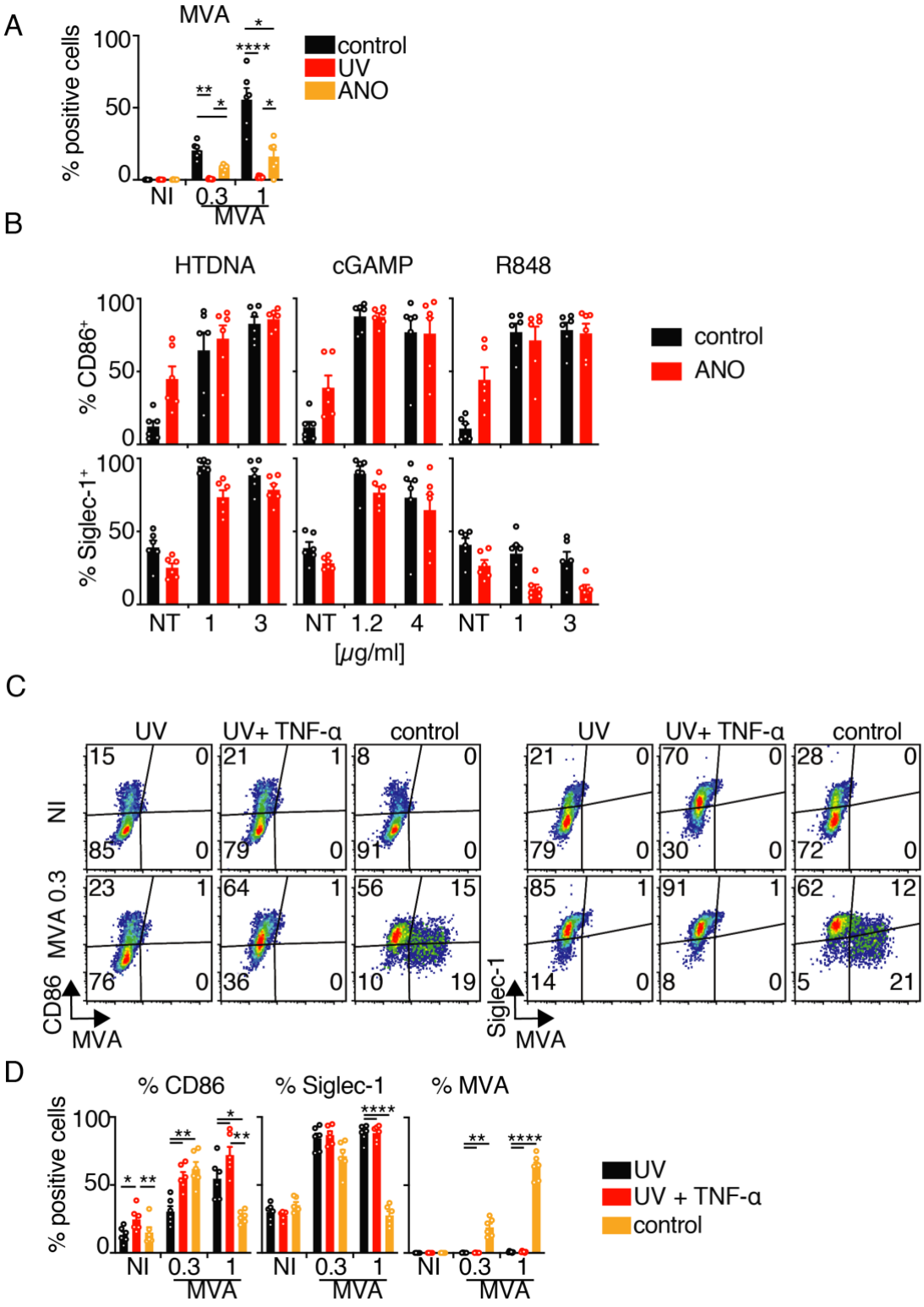

Fig. S7. Supplementary data for the analysis of the role of MVA early gene expression and TNF-α. (A) Percent of MVAGFP expression of MDDCs upon infection with MVA (control), UV irradiated MVA (300 mJ/cm^2 UV) and MVA infection in the presence of adenosine N_1-oxide (3 µg ANO). **(B)** CD86 (upper panel) and Siglec-1 (lower panel) expression of MDDCs stimulated with HTDNA, cGAMP or R848 in the presence of adenosine N_1-oxide (3 µg ANO, red bar). **(C)** CD86 (left panel) and Siglec-1 (right panel) expression of MDDCs treated with MVAUV or MVAUV+ TNF-α or MVA 24 hpi. **(D)** Statistical analysis of (C). In all graphs n=6 donors from three independent experiments, symbols represent single donors, and bars show mean + SEM. RM two-way ANOVA with Geisser-Greenhouse and Sidak's correction for multiple comparison. In all graphs 0.3 and 1 indicate MOI of MVA and PRR ligand concentrations are in µg/ml. NI = non-infected; NT = non-treated.

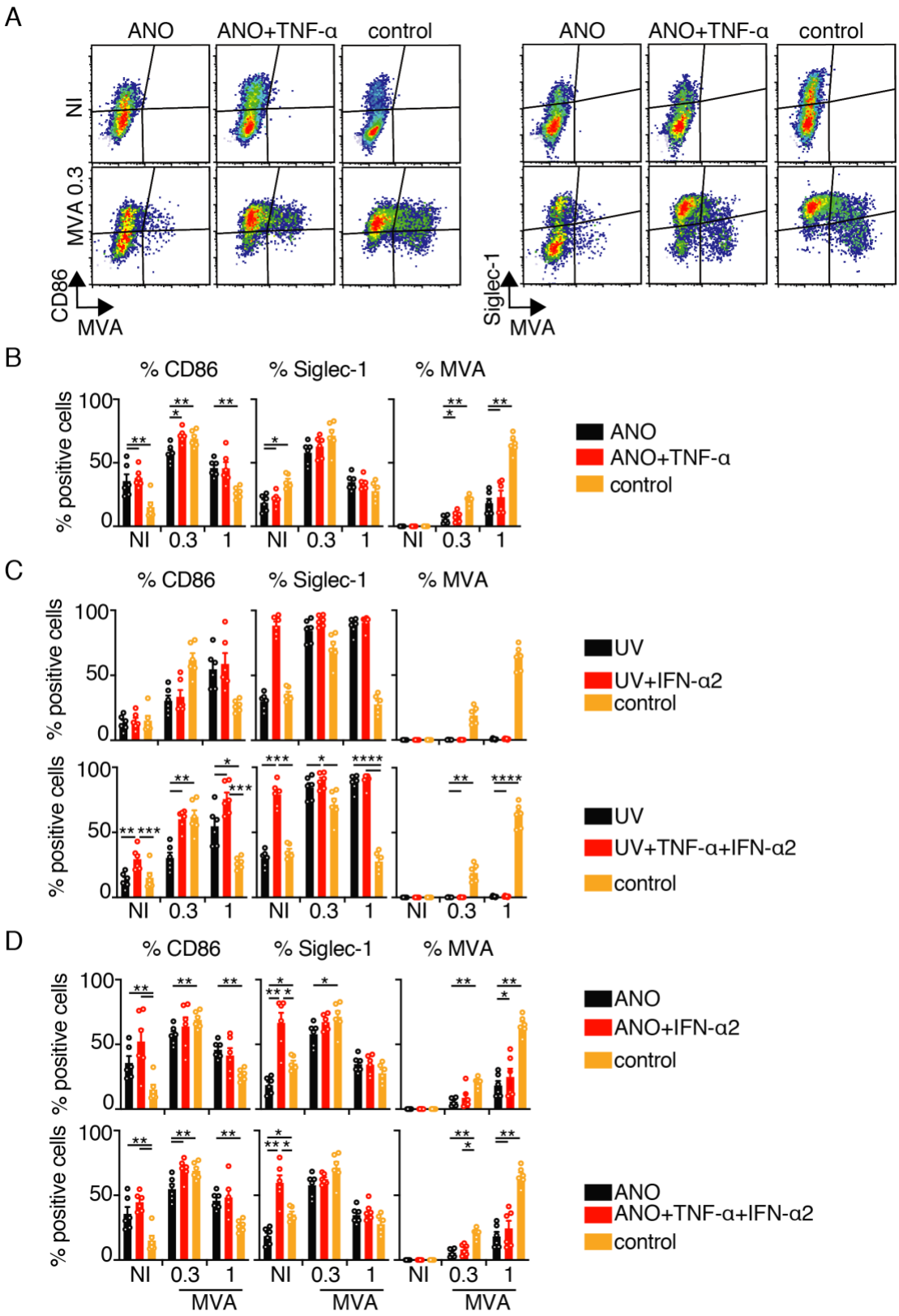

Fig. S8. Supplementary data for the analysis of the roles of MVA early gene expression, TNF-α and interferon. (A) CD86 (left panel) and Siglec-1 (right panel) expression of MDDCs treated with ANO or ANO+ TNF-α 24 hpi with MVA. **(B)** Statistical analysis of (A). **(C)** CD86, Siglec-1, and MVAGFP expression of MDDCs treated with IFN-α2 or TNF-α+IFN-α2 24 hpi with MVA (control) or MVAUV (UV). **(D)** CD86, Siglec-1, and MVAGFP expression of MDDCs treated with ANO, ANO+IFN-α2, or ANO+TNF-α+IFN-α2 during 24 hpi with MVA. In all graphs n=6 donors from three independent experiments. In all graphs 0.3 and 1 indicate MOI of MVA. NI = non-infected.

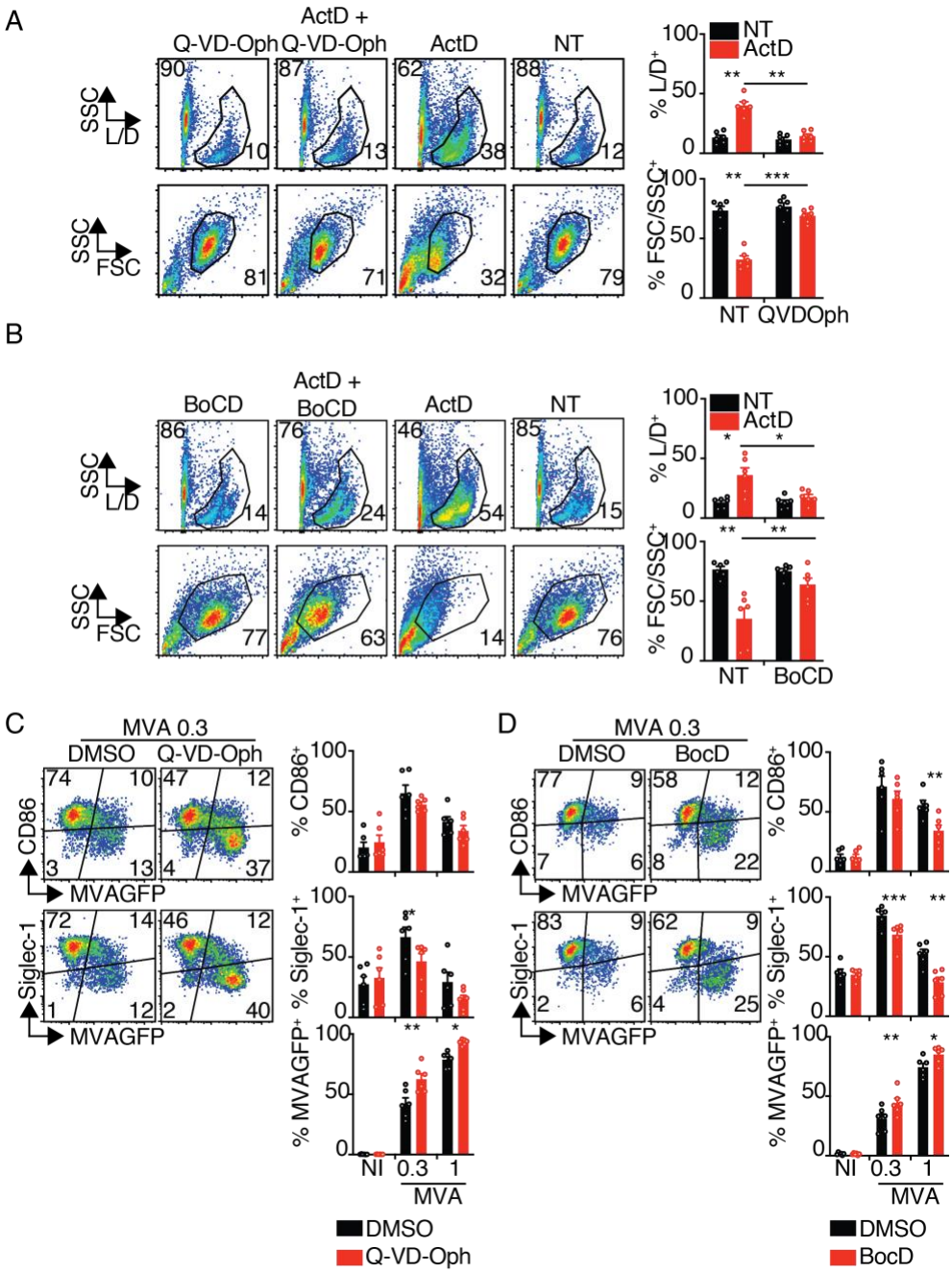

Fig. S9. The effect of caspase inhibitors on MVA infection and activation of MDDCs. (A) LIVE/DEAD labeling (upper panel) and FSC/SSC characteristics (lower panel) of MDDCs upon treatment with actinomycin D (ActD, 0.03 nM) in the presence of Q-VD-Oph (25 μM), statistical analysis on the right. **(B)** LIVE/DEAD labeling (upper panel) and FSC/SSC characteristics (lower panel) of MDDCs upon treatment with actinomycin D (ActD, 0.03 nM) in the presence of BoCD (25 μM), statistical analysis on the right. **(C)** CD86 (upper panel) and Siglec-1 (lower panel) expression of MDDCs 24 hpi with MVA in the absence (black bar) or presence (red bar) of the pan caspase inhibitor Q-VD-Oph. MVAGFP expression and statistical analysis on the right. **(D)** CD86 (upper panel) and Siglec-1 (lower panel) expression of MDDCs 24 hpi with MVA in the absence (black bar) or presence (red bar) of the pan caspase inhibitor BoCD. MVAGFP expression and statistical analysis on the right. In all graphs n=6 donors from three independent experiments. In all graphs 0.3 and 1 indicate MOI of MVA. NI = non-infected; NT = non-treated.

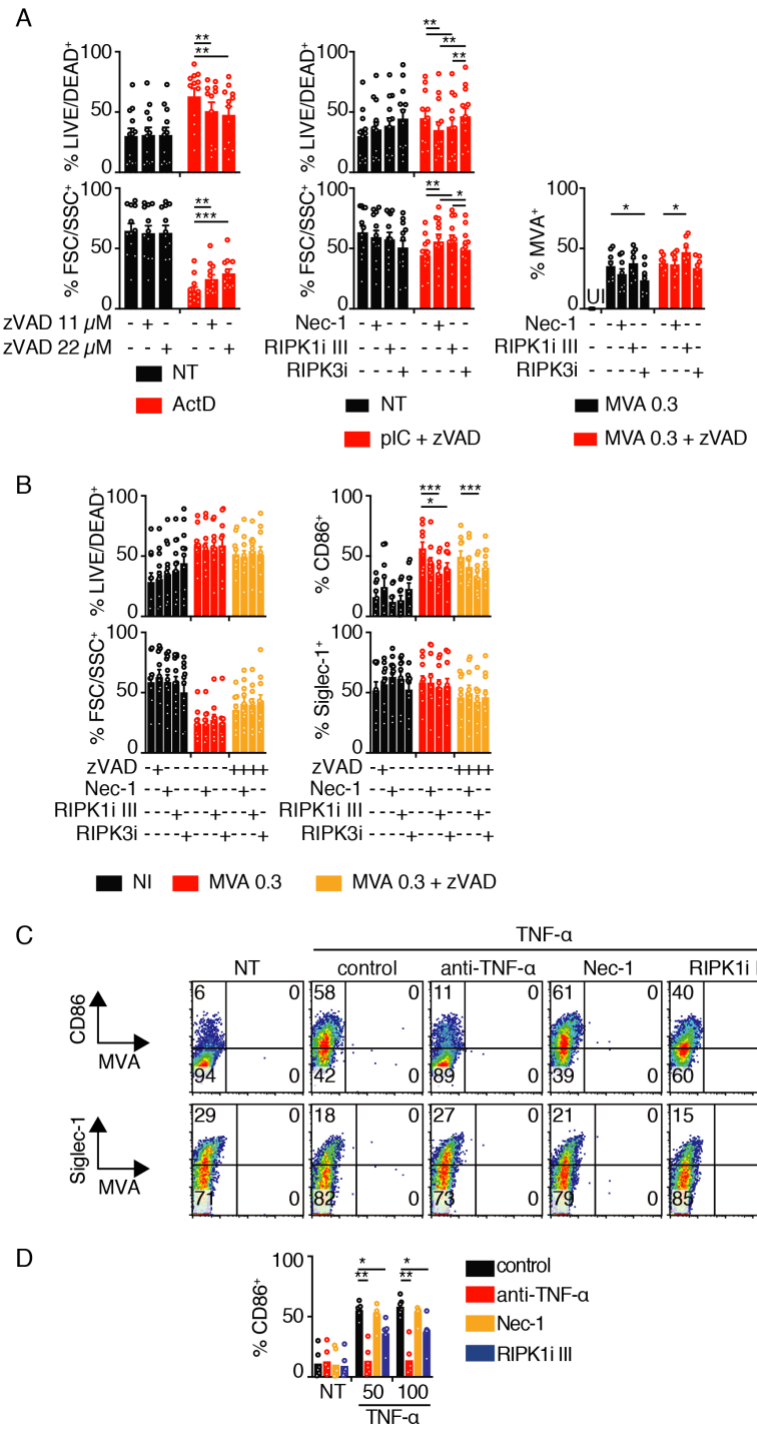

Fig. S10. The effect of necroptosis inhibitors on MVA infection and activation of MDDCs. (A) Statistical analysis of LIVEDEAD labeling and FSC/SSC characteristics upon actinomycin D induced apoptosis in MDDCs in the presence of two different concentrations of zVAD (left panel), upon activation-induced necroptosis (poly(I:C)+zVAD) in the presence of necrostatin-1 (Nec-1, 40 μM), RIPK inhibitors (RIPK1 inhibitor III 2 μM and RIPK3 inhibitor 12 μM) (middle panel), and MVAGFP expression of MDDCs 24 hpi with MVA. n=12 donors from 6 independent experiments. **(B)** LIVE/DEAD labeling, FSC/SSC position as well as CD86 and Siglec-1 expression of MDDCs infected with MVA or MVA+zVAD (22 μM) in the presence of RIPK inhibitors. n=10 donors from 5 independent experiments. **(C)** Pseudocolor plots of CD86 (upper panel) and Siglec-1 (lower panel) expression of MDDCs stimulated TNF-α (50 ng/ml) either in the presence of a TNF neutralizing antibody cocktail, or the RIPK1 inhibitors Necrostatin-1 (Nec-1) or RIPK1iIII. **(D)** Statistical analysis of the CD86 expression of MDDCs in (C). n=6 donors from three independent experiments. In all graphs 0.3 indicate MOI of MVA. NI = non-infected; NT = non-treated.

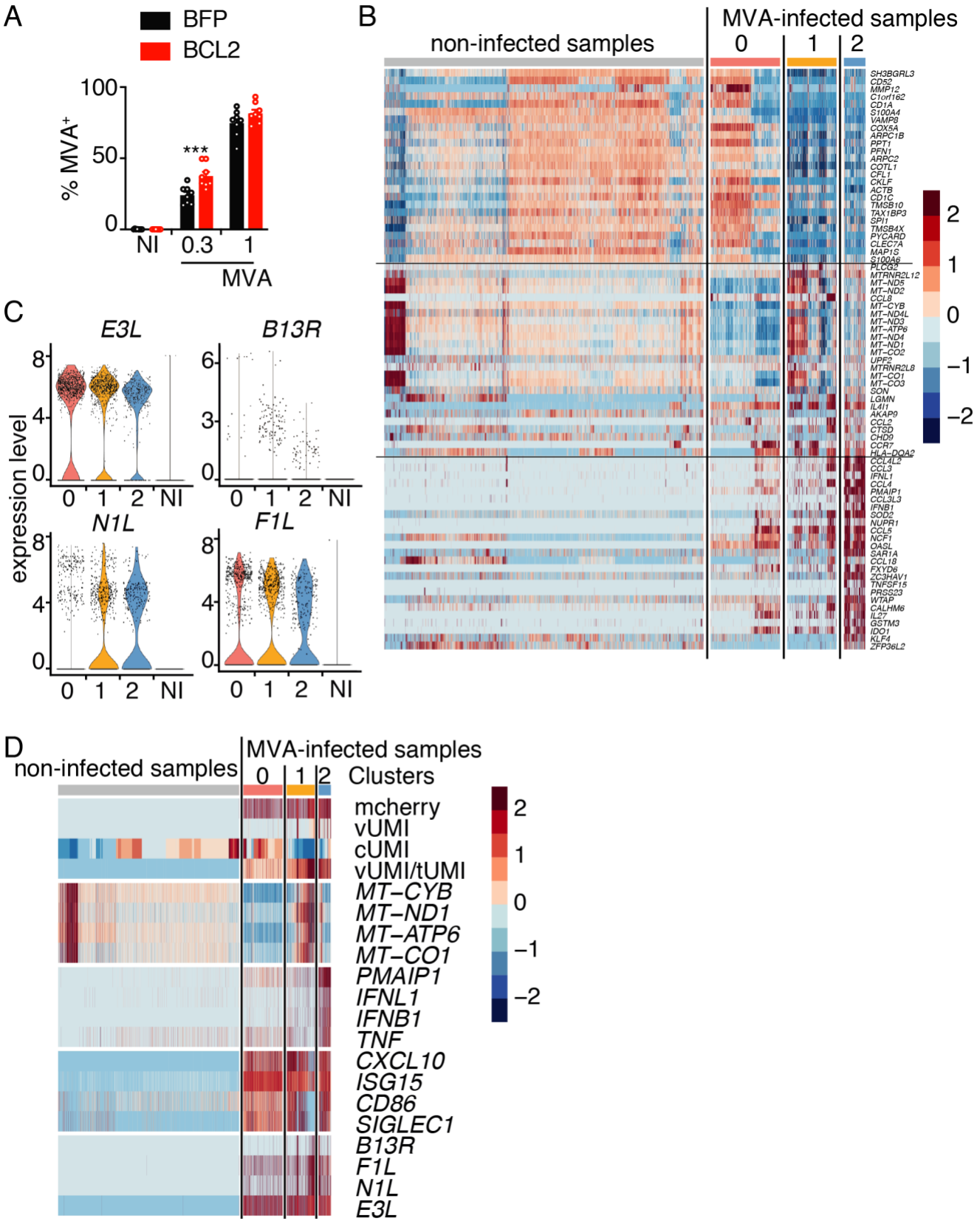

Fig. S11. Supplementary data for the analysis of MVA replication and cell death. (A) MVAGFP expression of control (BFP, black bar) or BCL2 expressing MDDCs (BCL2, red bar) 24 hpi with MVA (MOI 0.3 or 1) (n=8 donors from 4 independent experiments). **(B)** Heat map depicting the top 25 induced differentially expressed genes for each cluster obtained by comparing one cluster to the other two. (**C**) Expression of genes known to be found in apoptotic cells for each cluster. Artificially high values of some viral features in NI are the result of the normalization method (see methods). **(D)** MVA transcripts in each cluster.

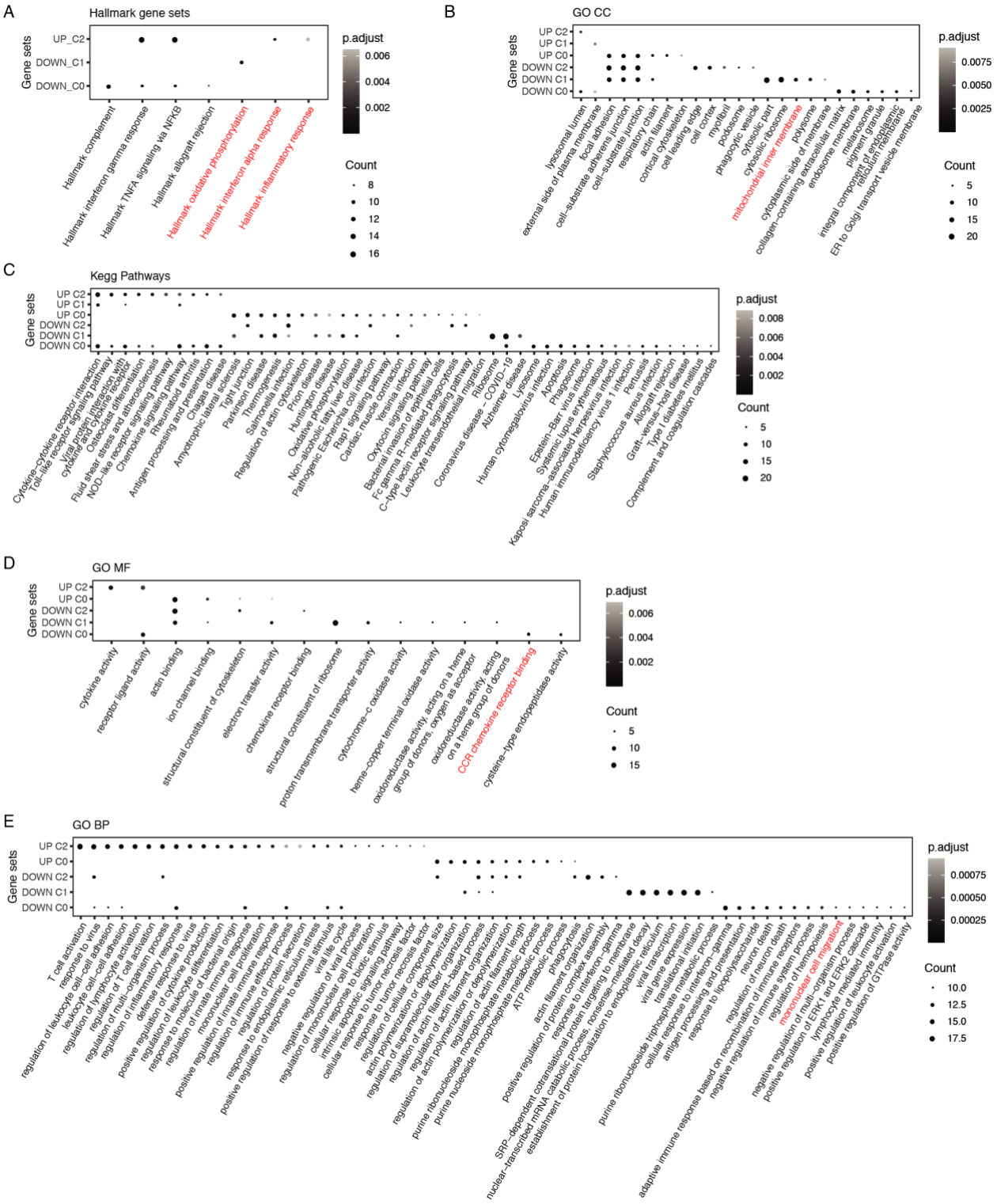

Fig. S12. Differentially enriched pathways and annotation terms. (A) Hallmark genesets from MSigDB. **(B)** Gene ontology cellular component (GO CC) annotation. **(C)** KEGG pathways. **(D)** Gene ontology molecular function (GO MF) annotation. **(E)** Gene ontology biological process (GO BP) annotation. Red indicates pathways highlighted in main text.

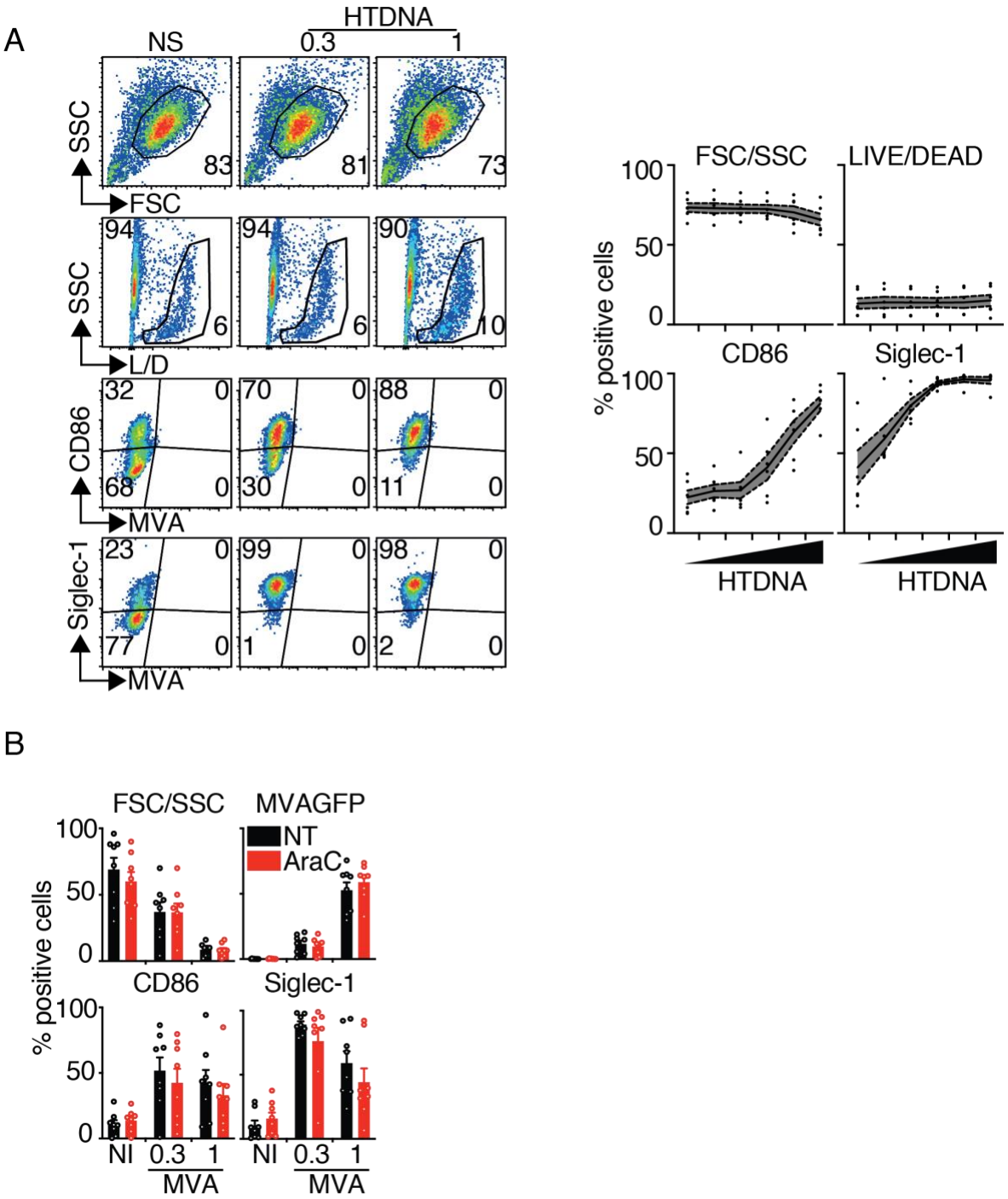

Fig. S13. Response of MDDCs to HTDNA stimulation viral DNA synthesis. (A) Forward and side scatter (FSC, SSC), viability (L/D), CD86 and Siglec-1expression of MDDCs stimulated with HTDNA. Left, representative plots with 0.3 and 1 µg/ml HTDNA. Right, quantification with serial dilutions of HTDNA from 0.01 to 1 µg/ml (n=6 donors from 3 independent experiments). **(B)** FSC/SSC characteristics, CD86/Siglec-1, and MVAGFP expression of non-treated (NT, black bar) or AraC-treated (AraC, 10 µM, red bar) MDDCs 24 hpi with MVA (MOI 0.3 or 1) (n=8 donors from 4 independent experiments, NI = non-infected).

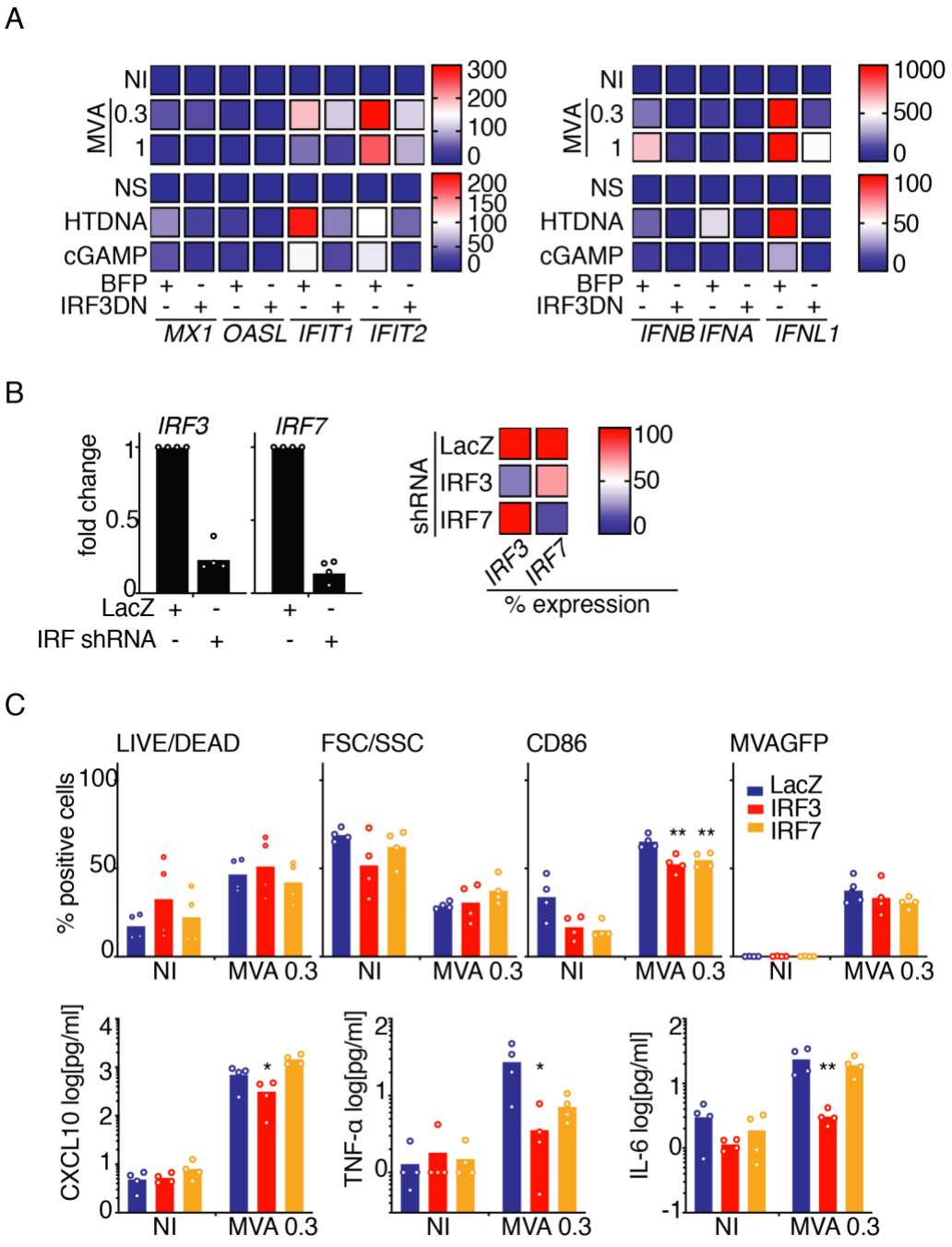

Fig. S14. Impact of IRF3 and IRF7 on induction of cytokines and ISGs in MDDCs upon cGAS or STING stimulation or MVA infection. (A) Heat map depicting the fold change of the expression of Mx1, OASL, IFIT1, and IFIT2 upon infection with MVA MOI 0.3 and 1 or stimulation with 1 µg/ml HTDNA and 1.2 µg/ml cGAMP (left panel). Heat map depicting the fold change of the expression type I and III IFN upon infection with MVA MOI 0.3 and 1 or stimulation with HTDNA or cGAMP (right panel). Heat maps were calculated with RT-qPCR data derived from 6 donors obtained in three independent experiments. **(B)** Expression levels of IRF3 and IRF7 in MDDCs upon KD of each particular IRF with a pool of 5 shRNAs assessed by RT-QPCR (left panel). Normalized IRF expression matrix depicting the impact of KD on the other IRF (right panel) (n=4 donors from two independent experiments). **(C)** LIVE/DEAD staining, FSC/SSC characteristics, CD86 and MVAGFP expression of IRF KD MDDCs 24 hpi with MVA MOI 0.3 (upper panel). CXCL10, TNF-α, and IL-6 secretion of IRF KD MDDCs 24 hpi with MVA MOI 0.3 (lower panel). n=4 donors from two independent experiments. RM two-way ANOVA with Geisser-Greenhouse and Dunnet's correction for multiple comparisons. NI = non-infected.

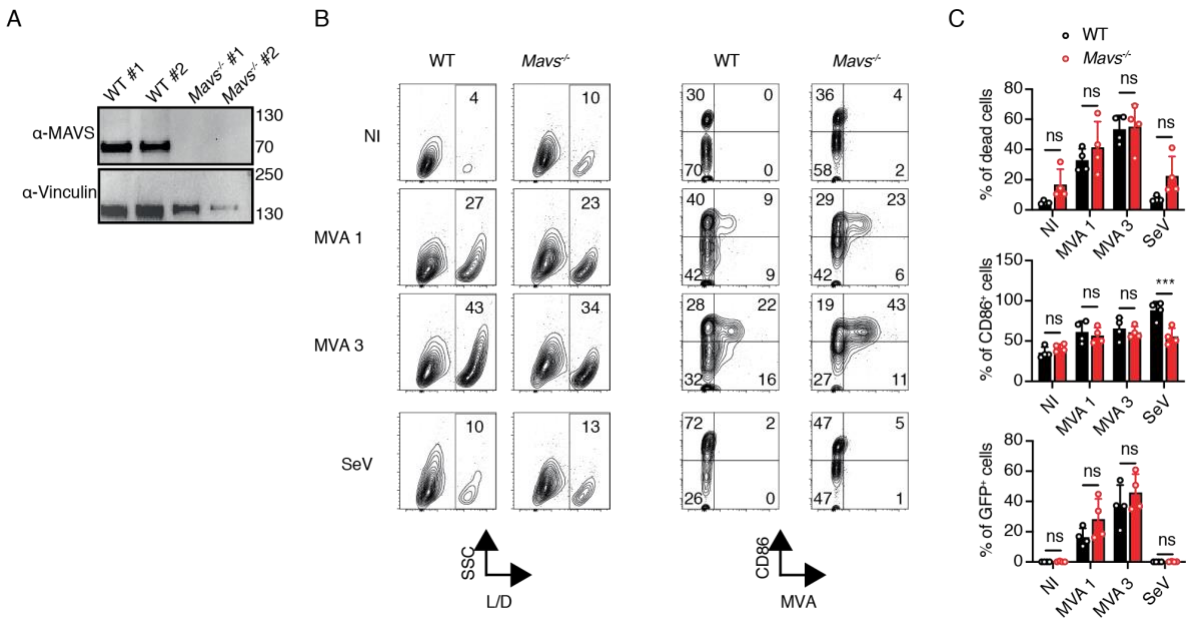

Fig. S15. Infection of *Mavs*$^{-/-}$ BMDCs with MVA. (A) MAVS and vinculin protein expression in lysates of BMDCs (2 mice each, representative of 2 independent experiments). **(B)** Side scatter, viability staining (L/D), MVAGFP expression (MVA), and CD86 expression in BMDCs uninfected (NI) of infected with MVAGFP (MOI 1 or 3) or Sendai virus (SeV) for 24 hours. Left, representative plots. Right, statistical analysis (n=4 mice from 2 independent experiments, one-way ANOVA with Sidak post-test).

A

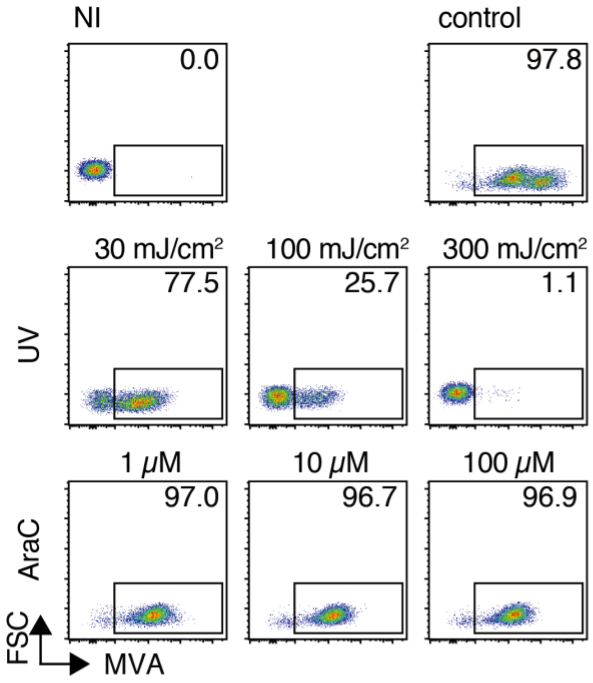

B

Sample	Mean Reads/Cell	Number of Reads	Sequencing saturation	Amount of cells targeted
NI-rep1	69603	197742309	72.5%	2000
NI-rep2	74180	182779722	65.6%	2000
MVA-rep1	136105	177073088	80.5%	1000
MVA-rep2	168275	178371303	82.0%	1000

C

Sample	Number of cells with CellRanger + EmptyDrops	Number of cells with CellRanger
NI-rep1	2752	2841
NI-rep2	2419	2464
MVA-rep1	1235	1301
MVA-rep2	1035	1060

D

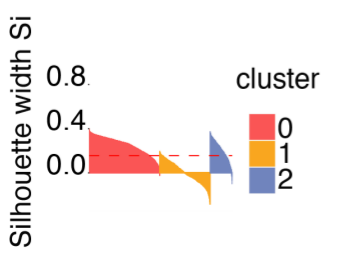

E

Fig. S16. **Supplementary data for the Materials and Methods. (A)** Increasing UV irradiation of MVA preparations revealed that by low UV exposure MVA replication was blocked in HeLa cells, while high amounts abrogated MVA gene expression completely. Increasing amounts of Arac only inhibited MVA replication and showed no effect on MVA gene expression in HeLa cells. Data representative of one experiment. **(B)** Analysis of library coverage for scRNA-seq of MVA infected MDDCs. **(C)** Cell calling by the combination of CellRangerV2 and EmptyDrops packages. NI = non-infected. **(D)** Silhouette scores for each cluster. **(E)** Donor contribution to each cluster.

Gene	Comparison	Adjusted p-value
vUMI	0_VS_2	7.36E-93
	0_VS_1	4.31E-45
	2_VS_1	6.53E-23
cUMI	0_VS_1	<5.00E-324
vUMI/tUMI	0_VS_2	9.62E-152
	0_VS_1	4.15E-184
MT-CYB	0_VS_2	1.67E-63
	0_VS_1	1.08E-267
	0_VS_NI	<5.00E-324
	2_VS_1	4.36E-28
	2_VS_NI	1.29E-111
MT-ND1	0_VS_2	1.03E-46
	0_VS_1	2.56E-282
	0_VS_NI	8.40E-148
	2_VS_1	1.70E-37
	1_VS_NI	9.03E-208
MT-ATP6	0_VS_2	7.58E-50
	0_VS_1	1.12E-270
	0_VS_NI	<5.00E-324
	2_VS_1	1.52E-32
	2_VS_NI	1.91E-78
MT-CO1	0_VS_1	5.48E-184
	0_VS_NI	3.26E-243
	2_VS_1	5.18E-16
PMAIP1	0_VS_2	8.45E-188
	0_VS_1	3.47E-96
	0_VS_NI	1.43E-227
	2_VS_1	6.32E-101
	2_VS_NI	<5.00E-324
IFNL1	0_VS_2	3.77E-65
	2_VS_1	2.94E-37
	2_VS_NI	8.05E-160
IFNB1	0_VS_2	2.66E-70
	2_VS_1	1.09E-42
	2_VS_NI	6.04E-238
TNF	0_VS_2	4.05E-33
	2_VS_NI	5.98E-154
CD86	0_VS_2	1.19E-37

Table S1. Adjusted p-values for volcano plots. 0, 1 and 2 indicate the cluster of infected samples. NI = non-infected sample.

REAGENT or RESOURCE	SOURCE	IDENTIFIER
Antibodies		
CD86 (Clone IT2.2)	Thermo Fisher Scientific	Cat#12-0869-42, RRID: AB_10732345
SIGLEC1 (Clone 7-239)	Miltenyi Biotec	Cat# 130-098-645, RRID: AB_265554
DC-SIGN/CD209 (Clone 120507)	R&D Systems	Cat# FAB161P-100 RRID: AB_357064
CD14 (Clone M5E2)	BD Biosciences	Cat# 557153 RRID: AB_396589
HLA-DR (Clone LN3)	eBiosciences	Cat# 47-9956-42 RRID: AB_1963603
CD1c (Clone L161)	eBiosciences	Cat# 46-0015-42 RRID: AB_10548936
CD123 (Clone AC145)	Miltenyi Biotec	Cat# 130-113-892 RRID: AB_2726384
CD45RA (Clone T6D11)	Miltenyi Biotec	Cat# 130-113-360 RRID: AB_2726132
CD33 (Clone WM53)	BD Biosciences	Cat# 555450 RRID: AB_395843
Clec-9A (Clone 3A4)	BD Biosciences	Cat# 563488 RRID: AB_2738237
AXL (Clone 108724)	Bio-Techne	Cat# FAB154P RRID:
CD19 (Clone LT19)	Miltenyi Biotec	Cat# 130-113-168 RRID: AB_2725996
CD3 (HIT3a)	BD Biosceinces	Cat# 555339 RRID: AB_395745
CD14 (Clone M5e2)	BD Biosciences	Cat# 555397 RRID: AB_395798
CD16 (Clone CLB/FcGran1)	BD Biosceinces	Cat# 656146 RRID: AB_2870395
CD34 (Clone 581)	BD Biosciences	Cat# 555821 RRID: AB_396150
cGAS (Clone D1D3G)	Cell Signaling Technology	Cat# 15102, RRID:AB_2732795
Vinculin (Clone hVIN-1)	SIGMA	Cat# V9264, RRID: AB_10603627
TNFRI/TNFRSF1A (Clone 16805)	R&D Systems	Cat# MAB625 RRID: AB_2204149
Human TNFRII/TNFRSF1B (Clone 22210)	R&D Systems	Cat# MAB726 RRID: AB_2206656
TNF-α MAb (Clone 1825)	R&D Systems	Cat# MAB210 RRID: AB_2240620
IFN-α monoclonal Antibody (Clone EBI-1)	Thermo Fisher Scientific (eBiosciences)	Cat# BMS160 RRID: AB_10597749
IFN-β (Clone A1)	Thermo Fisher Scientific (eBiosciences)	Cat# 16-9978-81 RRID: AB_1210676
IFN-α/β receptor chain 2 (Clone MMHAR-2)	Millipore	Cat# MAB1155 AB_11214312
anti-Annexin V	Miltenyi Biotec	130-093-060
MAVS antibody (rabbit specific)	Cell Signaling	Cat# 4983S

Table (S2) continues next page.

Mouse CD11b (Clone M1/70)	Thermo Fischer Scientific	Cat# A15390 RRID: AB_2534404

Mouse CD11c (Clone N418)	eBiosciences	Cat# 25-0114-82 RRID: AB_469590
Mouse CD80 (Clone 16-10A1)	BD Biosciences	Cat# 553769 RRID: AB_395039
Mouse CD86 (Clone GL1)	BD Biosciences	Cat# 558703 RRID: AB_2075114
Bacteria and viruses		
MVAGFP	ANRS	15938
MVAmCherry	ANRS	18108
NEB 10-beta competent *E. coli*	New England Biolabs	C3019I
Sendai virus	Charles River Laboratories	10100774 / Lot: 7Y131001
Chemicals, Peptides, and Recombinant Proteins		
Vaccinia Virus B18R Carrier-Free Recombinant Protein	Thermo Fisher Scientific (eBiosciences)	Cat# 34-8185-86
Human IL-4	Miltenyi Biotec	Cat# 130-093-922
Human GM-CSF	Miltenyi Biotec	Cat# 130-093-867
R848	Invivogen	Cat# tlrl-r848 CAS: 144875-48-9
2'-3'cGAMP	Invivogen	Cat# tlrl-nacga23-02 CAS: 1441190-66-4
DNA sodium salt from herring testes (HTDNA)	SIGMA	Cat# D6898 CAS: 438545-06-3
Poly(I:C) HMW	Invivogen	Cat# tlrl-pic CAS: 31852-29-6
TransIT®-293 Transfection Reagent	Euromedex	Cat# MIR2706
Lipofectamine 2000	Thermo Fisher Scientific	Cat# 10696153
rh IFN-α2a	Immunotools	Cat# 11343506
Puromycin	Invivogen	Cat# ant-pr-1 CAS: 58-58-2
Protamine sulfate salt from salmon	SIGMA	Cat# P4020-1G CAS: 53597-25-4
fetal bovine serum, Eurobio	Eurobio	Cat# CVFSVF0001
fetal bovine serum, Gibco	Thermo Fisher Scientific	Cat# 10270-106
fetal bovine serum, Corning	Thermo Fisher Scientific	Cat# 15377636
Penicillin-Streptomycin	Thermo Fisher Scientific	Cat# 15140122
Ficoll-Paque PLUS	Dutscher	Cat# 17-1440-03
Gentamicin (50 mg/ml)	Thermo Fisher Scientific	Cat# 15750037 CAS: 1405-41-0
HEPES (1M)	Thermo Fisher Scientific	Cat# 15630080
DMEM, high glucose, GlutaMAX™ supplement	Thermo Fisher Scientific	Cat# 61965026
RPMI 1640 Medium, GlutaMAX™ supplement	Thermo Fisher Scientific	Cat# 61870010
cOmplete, EDTA-free, protease inhibitor cocktail	Roche	Cat# 11873580001
SUPERSCRIPT III	Thermo Fisher Scientific	Cat# 18080044
RNaseA	Thermo Fisher Scientific	Cat# EN0531

Table (S2) continued; continues next page.

MgCl2 (1 M)	Thermo Fisher Scientific	Cat# 15568025
Recombinant Human TNFα	R&D Scientific	Cat# 210-TA020
t-butoxycarbonyl-asp-fluormethylketone (BOCD)	MPBio	Cat# 03FK011 CAS: 634911-80-1
Q-VD-OPh hydrate	SIGMA	Cat# SML0063

Ruxolitinib	Invivogen	Cat# Tlrl-rux CAS: 1092939-17-7
z-VAD-fmk caspase inhibitor	R&D Systems	Cat# FMK001
RIP1 Kinase Inhibitor III	Millipore	Cat# 5327290001
Necrostatin-1	SIGMA	Cat# N9037 CAS: 4311-88-0
RIPK3 Inhibitor GSK'872	Millipore	Cat# 530389
STING inhibitor H-151	ProbeChem	Cat# PC-3531 CAS: 941987-60-6
Cytarabine	Tocris/Bio-Techne	Cat# 4520 CAS: 147-94-4
Adenosine N1-oxide	ALFA Chemistry	Cat# ACM146929 CAS: 146-92-9
Cycloheximide solution	SIGMA	Cat# C4859 CAS: 66-81-9
ActinomycinD	SIGMA	Cat# A1410 CAS: 50-76-0
Critical Commercial Assays		
Purelink HiPure Plasmid Midiprep Kit	Thermo Fisher Scientific	Cat# K210015
Nucleospin Gel and PCR Clean-Up kit	Macherey-Nagel	Cat# 740609.50
NucleoSpin RNA	Macherey-Nagel	Cat# 740955.50
NucleoSpin Tissue	Macherey-Nagel	Cat# 740955.50
CD14 MicroBead human	Milteny Biotec	Cat# 130-050-201
LS columns	Milteny Biotec	Cat# 130-042-401
LightCycler480 SYBR Green I Master	Roche	Cat# 4887352001
HIV-1 p24 ELISA Kit	XpressBio	Cat# XB-1010
Human IP-10 Flex Set	BD	Cat# 558280
LEGENDplex Human Type 1/2/3 Interferon Panel (5-plex)	BioLegend	Cat# BLE740396B
QIAquick PCR purification kit	Qiagen	Cat# 28104
BD™ Cytometric Bead Array (CBA) Human Inflammatory Cytokine Kit	BD Biosciences	Cat# 551811
Experimental Cell Lines		
293FT	Thermo Fisher Scientific	Cat# R70007 RRID: CVCL_6911
HeLa	Laboratory of Dan Littman, New York University	N/A RRID: CVCL_0030
Oligonucleotides		
bactin737f	GGACTTCGAGCAAGAGATGG	
bactin970r	AGCACTGTGTTGGCGTACAG	
oas1-f	GAGCTCCAGGGCATACTGAG	
oas1-f	CCAAGCTCAAGAGCCTCATC	
IFIT1-143f	CAACCATGAGTACAAATGGTG	
IFIT1-425r	CTCACATTTGCTTGGTTGTC	
IFIT2-f	AGGTCTCTTCAGCATTTATTGG	
IFIT2-r	TATTGTTCTCACTCATGGTTGC	
CXCL10-116f	TGGCATTCAAGGAGTACCTC	
CXCL10-261r	TTGTAGCAATGATCTCAACACG	
IFNa-f	GGACTCCATYYTGRCTGTGA	

Table (S2) continued; continues next page.

IFNa-r	GATTTCTGCTCTGACAACCTCCC	
IFNb-f	GTCTCCTCCAAATTGCTCTC	
IFNb-r	ACAGGAGCTTCTGACACTGA	
IFNL1-f	AACTGGGAAGGGCTGCCACATT	
IFNL1-r	GGAAGACAGGAGAGCTGCAACT	
NOXA-f	GCTGGAAGTCGAGTGTGCTA	
NOXA-r	CCTGAGCAGAAGAGTTTGGA	
HRK-f	AGCAACAGGTTGGTGAAAACC	
HRK-r	TTTCTACGATCGCTCCAGGC	
PUMA-f	TGCCAGATTTGTGGTCCTCAG	
PUMA-r	CTCGTACTGTGCGTTGAGGT	
BIM-f	ACCAGATCCCCGCTTTTCAT	
BIM-r	GAAGAGGCATCCTCCTTGCATA	
BIK-f	ACCATGGAGGTTCTTGGCAT	
BIK-r	CCAGCACTATCTCGGGGTTT	
BMF-f	TCCCTCCTTCCCAATCGAGTC	
BMF-r	TTTTGGTTCTGCTGGTGTTGC	
BAD-f	CTTGGGCCCAGAGCATGT	
BAD-r	GGCGAGGAAGTCCCTTCTTA	
E9L-f	CGGCTAAGAGTTGCACATCCA	
E9L-r	CTCTGCTCCATTTAG TACCGATTCT	
POX-f	GCCAGAGATATCATAGCCGCTC	
POX-r	CAACGACTAACTAATTTGGAAAAAAAGAT	
HPRT-f	ACCCTTTCCAAATCCTCAGC	
HPRT-r	GTTATGGCGACCCGCAG	
RPL34-f	CTCTGTGCTTGTGCCTTCAA	
RLP34-r	TATGGTGGTTCCATGTGTGC	
Recombinant DNA		
CMV-VSVG	Manel *et al*., 2010 (*59*)	N/A
psPAX2	Manel *et al*., 2010 (*59*)	N/A
pLKO.1puro	Manel *et al*., 2010 (*59*)	N/A
pSIV3+	Manel *et al*., 2010 (*59*)	N/A
pTRIP-SFFV-mtagBFP-2A		
pLKO1puro-cGAS-sh4	CAACTACGACTAAAGCCATTT	
pLKO1puro-SAMHD1-sh1	GCAGATGACTACATAGAGATT	
pLKO1puro-SAMHD1-sh5	GCAGTGGTAAAGGCAAAGTAT	

Table (S2) continued; continues next page.

pTRIP-CMV-puro-2A-TRIFDN-CFLAG	
pTRIP-CMV-puro2A	
pTRIP-CMV-puro-2A-FLAG-TRAF6 DN	
pTRIP-CMV-Puro2A-hTBK1 DN	
pTRIP-SFFV-tagBFP-2A-BCL2	
pLKO1-puro-shLacZ	GCGATCGTAATCACCCGAGTG
pLKO1puro-IRF3-sh1	CTGCCTGGATGGCCAGTCACAC
pLKO1puro-IRF3-sh2	CATTGTAGATCTGATTACCTTC
pLKO1puro-IRF3-sh3	GCCACACATACTGGGCAGTGAG
pLKO1puro-IRF3-sh4	GCCTCAGGGCCTTGGTAGAAAT
pLKO1puro-IRF3-sh5	TACCCAGGAAGACATTCTGGAT

pLKO1puro-IRF7-sh1	CCCGAGCTGCACGTTCCTATA	
pLKO1puro-IRF7-sh2	GCTGGACGTGACCATCATGTA	
pLKO1puro-IRF7-sh3	CTATACCATCTACCTGGGCTT	
pLKO1puro-IRF7-sh4	CTGTTCGGAGAGTGGCTCCTT	
pLKO1puro-IRF7-sh5	CGCAGCGTGAGGGTGTGTCTT	
Software and Algorithms		
GraphPad Prism 7 – Version 7.0d/8.4.2	GraphPad	https://www.graphpad.com/
Flow-Jo Version – Version X	FlowJo	https://www.flowjo.com
LEGENDplex Software – Version 8.0	LEGENDplex	http://www.vigenetech.com/LEGENDplex7.htm
FCAP Array – Version 3.0.14.1993	BD	http://www.bdbiosciences.com/us/applications/research/bead-based-immunoassays/analysis-software/fcap-array-software-v30/p/652099
Image Lab software – Version 5.2.1	BioRad	http://www.bio-rad.com/fr-fr/product/image-lab-software?ID=KRE6P5E8Z
BioRender		Fig. 7H created with BioRender.com

Table S2. Reagents and resources used in the study. (*Table extends over multiple pages above*)

Data file S1: Gene expression data. Gene expression analysis in each differentially expressed gene (DEG) cluster, provided in an Excel file in the online supplementary material.